U.S. DEPARTMENT OF COMMERCE
National Technical Information Service

PB-272 922

Study on the Feasibility and Design of Automatic Particulate Size Distribution Analyzer for Source Emissions

GCA Corp, Bedford, Mass GCA Technology Div

Prepared for

Municipal Environmental Research Lab, Cincinnati, Ohio

Aug 77

PB 272 922

EPA-600/2-77-050
August 1977

Environmental Protection Technology Series

UNITED STATES
ENVIRONMENTAL PROTECTION AGENCY

REPRODUCED BY
NATIONAL TECHNICAL
INFORMATION SERVICE
U. S. DEPARTMENT OF COMMERCE
SPRINGFIELD, VA. 22161

TECHNICAL REPORT DATA

(Please read Instructions on the reverse before completing)

1. REPORT NO.
EPA-600/2-77-050

2.

3. RECIPIENT'S ACCESSION NO.
PB272922

4. TITLE AND SUBTITLE
STUDY ON THE FEASIBILITY AND DESIGN OF AUTOMATIC PARTICULATE SIZE DISTRIBUTION ANALYZER FOR SOURCE EMISSIONS

5. REPORT DATE
August 1977 (Issuing Date)

6. PERFORMING ORGANIZATION CODE

7. AUTHOR(S)
Pedro Lilienfeld; Daniel P. Anderson; Douglas W. Cooper

8. PERFORMING ORGANIZATION REPORT NO.
GCA-TR-76-22-G

9. PERFORMING ORGANIZATION NAME AND ADDRESS
GCA Corporation
GCA/Technology Division
Burlington Road
Bedford, Massachusetts 01730

10. PROGRAM ELEMENT NO.
1NB458

11. CONTRACT/GRANT NO.
68-03-2154

12. SPONSORING AGENCY NAME AND ADDRESS
Municipal Environmental Research Laboratory--Cin., OH
Office of Research and Development
U.S. Environmental Protection Agency
Cincinnati, Ohio 45268

13. TYPE OF REPORT AND PERIOD COVERED
Final

14. SPONSORING AGENCY CODE
EPA/600/14

15. SUPPLEMENTARY NOTES Project Officer: John O. Burckle, SHWRD/MERL/ORD - This work was performed under a research agreement for the Industrial Environmental Research Laboratory/Research Triangle Park.

16. ABSTRACT

The objective of this program was to evolve a method for the automatic determination of the size distribution of particulates within stack gas effluent streams. This device was designed to cover the typical mass concentration range encountered upstream as well as downstream of emission control systems, and to segregate the particles by means of a cascaded virtual inertial impaction configuration to be inserted into the effluent stream. Several alternative particle detection techniques compatible with this size segregation method were investigated in the course of this program and a stage filter pressure drop sensing technique was selected. The prototype device was subjected to laboratory and stack testing showing very good correlation with an Andersen-type impactor. The salient advantages of this instrument are: capability for extended operation (of the order of hours), real-time indication of size distribution of particulates in the stack environment, relatively low cost, and simplicity of operation.

17. KEY WORDS AND DOCUMENT ANALYSIS

a. DESCRIPTORS	b. IDENTIFIERS/OPEN ENDED TERMS	c. COSATI Field/Group
Air Pollution Flue Dust Aerosols Particle Size Distribution Size Determination Detectors	Monitoring Source Emission Measurements Virtual Impactor Contact Change Sensing Drag Flow Sensing Light Extinction Sensing	13B

18. DISTRIBUTION STATEMENT Release to Public	**19. SECURITY CLASS (This Report)** Unclassified	**21. NO. OF PAGES** 115
	20. SECURITY CLASS (This page) Unclassified	**22. PRICE** PC A06 / MF A01

EPA Form 2220-1 (9-73)

U. S. GOVERNMENT PRINTING OFFICE 1977-757-056/6479 Region No. 5-11

EPA-600/2-77-050
August 1977

STUDY ON THE FEASIBILITY AND DESIGN OF AUTOMATIC PARTICULATE SIZE DISTRIBUTION ANALYZER FOR SOURCE EMISSIONS

by

Pedro Lilienfeld

Daniel P. Anderson

Douglas W. Cooper

GCA/Corporation
GCA/Technology Division
Bedford, Massachusetts 01730

Contract No. 68-03-2154

Project Officer

John O. Burckle
Solid and Hazardous Waste Research Division
Municipal Environmental Research Laboratory
Cincinnati, Ohio 45268

This study was sponsored by
Industrial Environmental Research Laboratory
Research Triangle Park, North Carolina 27711

MUNICIPAL ENVIRONMENTAL RESEARCH LABORATORY
OFFICE OF RESEARCH AND DEVELOPMENT
U.S. ENVIRONMENTAL PROTECTION AGENCY
CINCINNATI, OHIO 45268

DISCLAIMER

This report has been reviewed by the Municipal Environmental Research Laboratory, U.S. Environmental Protection Agency, and approved for publication. Approval does not signify that the contents necessarily reflect the views and policies of the U.S. Environmental Protection Agency, nor does mention of trade names or commercial products constitute endorsement or recommendation for use.

FOREWORD

The Environmental Protection Agency was created because of increasing public and government concern about the dangers of pollution to the health and welfare of the American people. Noxious air, foul water, and spoiled land are tragic testimony to the deterioration of our natural environment. The complexity of that environment and the interplay between its components require a concentrated and integrated attack on the problem.

Research and development is that necessary first step in problem solution and it involves defining the problem, measuring its impact, and searching for solutions. The Municipal Environmental Research Laboratory develops new and improved technology and systems for the prevention, treatment, and management of wastewater and solid and hazardous waste pollutant discharges from municipal and community sources, for the preservation and treatment of public drinking water supplies, and to minimize the adverse economic, social, health, and aesthetic effects of pollution. This publication is one of the products of that research; a most vital communications link between the researcher and the user community.

This study deals with exploratory research aimed at establishing the feasibility of a continuous monitor for the measurement of the particle size distribution of source emission aerosols. The approach was based on dividing the aerosol into several size ranges and detecting the amount of particles in the size ranges. Successful development of such a monitor will provide a valuable tool to aid in a better understanding of particulate source emissions and their control, especially with respect to the control of fine particulate emissions.

Francis T. Mayo, Director
Municipal Environmental
Research Laboratory

ABSTRACT

The objective of this program was to evolve a method for the automatic determination of the size distribution of particulates within stack gas effluent streams. This device was designed to cover the typical mass concentration range encountered upstream as well as downstream of emission control systems, and to segregate the particles by means of a cascaded virtual inertial impaction configuration to be inserted into the effluent stream. Several alternative particle detection techniques compatible with this size segregation method were investigated in the course of this program and a stage filter pressure drop sensing technique was selected. The prototype device was subjected to laboratory and stack testing showing very good correlation with an Andersen-type impactor. The salient advantages of this instrument are: capability for extended operation (of the order of hours), real-time indication of size distribution of particulates in the stack environment, relatively low cost, and simplicity of operation.

CONTENTS

Foreword iii
Abstract iv
Figures vi
Tables ix
Unit Conversion Table x
Acknowledgments. xi

1. Introduction 1
2. Summary 3
3. Conclusions 6
4. Recommendations 7
5. Theoretical Aspects 8
6. Particle Sensing and Detection Methods 26
7. Virtual Impactor Development 43
8. Particle Sensing Methods 56
9. Virtual Impactor-Pressure Drop Lab and Field Tests 65

References 95

Appendix

Token Flow Corrections to Virtual Impactor Data Collected in New Bedford 98

FIGURES

Number		Page
1	Schematic of a Virtual Impaction Stage	12
2	Penetration, or Response, Function for Ideal and Nonideal Instrument	17
3	Error Factor Versus Number of Geometrically Increasing Sizing Intervals for Impactor	19
4	"Figure of Negative Merit" as a Function of Size Interval Ratio and Number of Stages	20
5	Data, F_2*, and Input Distributions, F_i, Regained by Correcting That Data, for a Three-Stage Virtual Impactor With 10 Percent Secondary Flow	25
6	Optical Sensing Configuration	29
7	A Contact Electric Sensor Technique	33
8	Filter Pressure Drop Technique	33
9	Efficiency of Glass-Fiber Filters as a Function of Particle Size and Flow Rate	34
10	Measured Dependency of $\Delta\rho$ on Time (Three Successive Experiments)	35
11	Comparison of Collection Efficiency E and Pressure Drop ΔP in Gravel and Fiber Filters at Darcy Air Flow Velocity v_D = 2.0 cm/sec and Gravel Layer Thickness L = 30 cm	36
12	Resistance Increase as a Result of Solid Particle Accumulation in Tests 7 Through 10	37
13	Filter Resistance During Operation	38
14	Pressure Drop Versus Collection Density at Various Filter Face Velocities (GCA Data)	39
15	Pressure Drop as a Function of Time for Extended Operation at Nearly Constant Concentration (GCA Data)	40

FIGURES (Continued)

Number		Page
16	Expected Variation of Pressure Drop as a Function of Accumulation and Particle Size	42
17	Cross-Section of Initial Version of Virtual Impactor Breadboard	45
18	Various Orifice and Nozzle Designs	46
19	Redesigned Collection Nozzle	50
20	Collection Efficiency Versus Particle Size	54
21	Electronic Schematic	57
22	Optical Sensing System	58
23	Aerosol Number Concentration by Gravimetric Versus Optical Detection for Arizona Road Dust, Aerosol Particles Greater Than 3.5 μm	60
24	Aerosol Number Concentration by Gravimetric Versus Optical Detection for Arizona Road Dust, Aerosol Particles Less Than 3.5 μm But Greater Than 1.5 μm	60
25	Electrical Sensing Design	62
26	Electronic Sensing Data	63
27	Virtual Impactor Schematic	66
28	Final Version of Prototype Virtual Cascade Impactor, Desassembled	67
29	Final Version of Prototype Virtual Cascade Impactor, Assembled With Backup Filter	67
30	Data For Test 23	70
31	Test Number 27, Coal Dust	73
32	Test Number 29, Fly Ash	74
33	Test Number 32, Iron Oxide	75
34	Test Number 35, Arizona Road Dust	76
35	Cumulative Size Distribution for January 29, 1976	81
36	Virtual Impactor Pressure Drop Data for January 30, 1976	83

FIGURES (Continued)

Number Page

37 Cumulative Size Distribution Data for January 30, 1976 84

38 Pressure Drop Versus Time for Run No. 1, 24 March 1976 89

39 Pressure Drop Versus Time for Test in Which Concentration Was Varied 90

40 Pressure Drop Versus Time for Stage 1, 26 March 1976 92

41 Pressure Drop Versus Time for Stage 2, 26 March 1976 93

TABLES

Number		Page
1	Concentration Extremes to be Sensed	27
2	Approximate Signal Currents Resulting From an Electric Charge-Wire Sensor, 30 Lit/Min Total Flow Rate	31
3	Effects of Velocity and Particle Size on Filtration Mechanisms	32
4	Virtual Impactor Test Data (First Version)	47
5	Virtual Impactor Dimensional Data	47
6	Virtual Impactor Test Data (Second Version) With Monodisperse Aerosol	51
7	Impactor Losses	53
8	Cut Size Data	55
9	Virtual Impactor Dimensional Data for Tests 15 Through 23	68
10	Virtual Impactor Test Data (With Arizona Road Dust)	69
11	Virtual Impactor Data (Polydisperse Dusts)	71
12	Andersen In-Stack Impactor Data Obtained During In-Stack Tests at New Bedford	79
13	In-Stack Virtual Impactor Data Taken at New Bedford (Corrected for Token Flow Effect)	80
14	Virtual Impactor Filter Pressure Gain Compared With Loading as Reported by the Andersen Impactor	85
15	Virtual Impactor Data From Preliminary Field Test	85
16	Andersen In-Stack Data	87
17	Virtual Impactor Data	88
18	Virtual Impactor Pressure-Drop Drag Coefficients	94

UNIT CONVERSION TABLE

1 inch = 2.54 cm

1 inch H_2O = 248.6 Newtons/m^2

1 inch Hg = 3386 Newtons/m^2

1 psi = 6895 Newtons/m^2

1 cfm = 4.719×10^{-4} m^3/sec

1 ℓpm = 1.667×10^{-5} m^3/sec

ACKNOWLEDGMENTS

The collaboration and support of Bill Kuykendal of the U.S. Environmental Protection Agency and John Langley of GCA during laboratory and field tests are gratefully acknowledged.

Our thankful appreciation is due to Phil Morrow, Walter Park, and Gordon Park of the supervisor staff, as well as to the members of the electrical shop of New Bedford Power and Light, for their invaluable help during the performance of the field tests.

SECTION 1

INTRODUCTION

Monitoring of particulates flowing in stack gases is a challenging problem for the instrumentation scientist. Stack sampling and sizing of particulates has, in general, been performed by extracting a sample, under manually adjusted isokinetic flow conditions, and collecting the particles by filtration or by impaction. The collected material is then evaluated gravimetrically; i.e., by weighing before and after collection. The average mass concentration as a function of size is then calculated on the basis of the total volume of air sampled during the collection period. This method is tedious, inefficient and incompatible with the continuous recording, automatic data transmission and processing that are required to handle the increasing volume of information resulting from intensive air pollution monitoring programs. Furthermore, these manual methods do not provide real-time information, or the temporal resolution from which to determine emission variability both from the point of view of total emission as well as size distribution.

Presently available methods for recording or indicating type particulate monitoring are based on such indirect sensing principles as measuring certain parameters related to either particle area or particle number concentration. If light scattering or extinction are used, variations in particle size, shape and index of refraction, such as are found in the stack environment, can introduce serious particle sizing errors. A recently developed technique, based on piezoelectric mass detection, utilizes either electrostatic precipitation or inertial impaction to deposit particulates on a quartz crystal whose oscillation frequency is a function of the collected mass. Operational difficulties, and the basic incompatibility of this technique with prolonged unattended operation, have restricted its use to certain laboratory applications.

The generally preferred solution to the problem of automated mass measurement of particulates from stack gases is based on beta radiation absorption sensing of material collected, within the stack, on a suitable substrate. This method when applied to particle sizing, however, results in instrumentation with significant mechanical and electronic complexity as exemplified by the seven-stage automatic beta-cascade impactor recently completed by GCA/Technology Division under another EPA contract.

The objective of the program reported herein was to determine the feasibility of the development of an instrument capable of rapid, real-time determination of the relative size distribution up and downstream of a particulate control device in typical stationary source environments. Cost and simplicity of operation were essential objectives, as well as reliability and compatibility with typical stack gas conditions.

Two general aspects were considered within this development program: the particle sizing method, and the sensing technique of the segregated particle fractions. Inertial sizing by virtual impaction was selected for the first of these aspects. Only inertial sizing methods are intrinsically and reliably related to particle dynamics and most of their interactions with the environment including health effects. Aerodynamic size provides the most useful particle characterization with the exception of visibility effects, although even there, particle persistence in the atmosphere and thus its temporal effect on visibility are related to aerodynamic properties.

The second and crucial aspect of this instrument development program was the method of sensing of the particulate fractions segregated by the inertial technique. This detection method had to be compatible with the measurement requirements as well as with the environmental constraints imposed by source conditions. Several candidate approaches to particle detection were investigated within this program; one of them—stage filter pressure drop sensing—was selected as the most promising technique.

SECTION 2

SUMMARY

The objective of this program was to perform a feasibility investigation consisting of the selection, development, fabrication and testing of a prototype instrument capable of providing a real-time or continual information on the size distribution of particulates contained in effluent stack gases. The basic measurement philosophy and criteria underlying this program were:

1. Particle sizing by inertial separation.

2. Particle collection and sensing within the stack itself (i.e., no sample extraction).

3. Particle sensing of the inertially separated fractions compatible with the stack environment and capable of providing continuously recordable signals to the outside of the stack.

4. Sensing technique had to be reliable and rugged.

At the outset of the program virtual cascade impaction was selected as the method of inertial particle size segregation. This technique was considered compatible with several candidate particle sensing approaches and presented several significant advantages over other inertial methods; e.g., large sample retention capability, relative simplicity and adequate size selectivity.

An initial theoretical effort was directed at the development of a mathematical approach for the optimization of the number of cascade sizing stages and the sizing separation between consecutive stages. This model took into consideration the nonideal size selectivity of typical virtual impaction stages and resulted in a "figure of merit" characterization indicating that a size interval ratio of about 2.5 provides an optimum compromise between selective size information and stage overlap effects. Another mathematical effort was directed at developing a data inversion approach to incorporate the effect of the secondary or token flow at each virtual impaction stage in the calculation of the actual particle size distribution. Both of these mathematical tools should prove very useful in the development and characterization of related devices and techniques.

During the initial phases of the program a three-stage virtual impactor prototype was designed and fabricated. This initial version was then subjected to a series of laboratory tests to determine and characterize particle selectivity as well as interstage particle losses. As a result of this experimental evaluation a second version was fabricated incorporating several modifications

and improvements designed to minimize particle losses and facilitate disassembly and replacement of various nozzles of different dimensions. This second version was then in turn subjected to laboratory testing using fluorescent particle aerosols, and the results, reported in detail within the body of this report, were entirely satisfactory.

In parallel with the virtual impactor development, four alternative particle sensing methods were investigated experimentally in order to select one of these techniques and incorporate it within the three-stage prototype virtual cascade impactor. These four sensing principles were:

1. Light extinction within each virtual impactor stage stagnation volume, using fiber optics as source and signal light carriers.

2. Impact momentum sensing of the particles entering the stagnation volumes, using a pressure sensitive transistor.

3. Triboelectric particle sensing by placing a detection electrode in a small constriction within each of the stage token flow lines.

4. Pressure drop sensing across a filter at each stage, resulting from the token flows through the accumulating dust layer.

The tests conducted with each of these methods indicated that of the first three techniques listed above, light extinction and triboelectric or contact charging appeared as feasible candidates although their implementation in a practical field-worthy system would entail considerable effort without guarantee of ultimate success. The latter technique; i.e., flow drag sensing across each stage filter, however, provided the most reliable results with a minimum of system complexity, and it was thus selected for integration into the virtual cascade impactor for subsequent field testing. This sensing method presented the further advantage of incorporating its own calibration reference since the total weight increment on each stage filter can be used to normalize the average slope of the pressure drop versus time signal obtained from each stage.

The three-stage virtual impactor (two inertial stages and a back-up filter, with 50 percent cutoff points of 7 and 2 μm for the first two stages) was modified incorporating pressure sensing taps, and hardened to withstand the elevated stack temperatures by using heat-resistant gasketing and tubing, and a series of tests were undertaken within a stack of an oil-fired power plant. Concurrent samples were taken with an Andersen in-stack cascade impactor and the results of these tests showed a reliable correlation between stage filter pressure drop slopes and stage collection, as well as excellent correlation between the stage filter collection of the virtual impactor and the reference Andersen jet-to-plate impactor.

Similar results were obtained during a subsequent test series performed at two different EPA wind-tunnel facilities with concurrent comparisons with Andersen and Brink cascade impactors. During these latter tests it was determined that collections of the order of 3000 mg on the first stage filter and

150 mg on the second stage filter could be collected without loss of pressure drop versus mass linearity.

The tests performed with the prototype cascade virtual impactor with individual stage pressure drop sensing demonstrated the following crucial aspects:

1. Mass concentrations and size distributions agreed remarkably well with concurrent measurements performed with an Anderson in-stack cascade impactor.

2. Sampling times of several hours in duration can be performed without sample retrieval or operator intervention.

3. Stage loads of the order of hundreds of milligrams can be collected without loss of pressure drop versus loading linearity with a device whose cross sectional dimensions are compatible with insertion through a 4-inch diameter port.

It is worth pointing out that the originally stipulated performance objectives of this program were in most cases either met or exceeded by this collector-sensor combination.

SECTION 3

CONCLUSIONS

The instrumental combination of a multiple-stage virtual impactor and pressure drop sensing across stage filters provides a relatively straightforward, simple and reliable method for the in-stack determination of the time dependent size distribution of particulates. Linear increase of filter pressure drop versus mass loading provides a reliable indication of both cumulative mass (average size distribution), as well as short term or nearly real-time concentration (instantaneous size distribution) with time resolutions in the range of 1 to 10 minutes.

Salient advantages and other characteristics of this instrumental approach to stack effluent particulate monitoring are:

1. Compatibility with high temperature and corrosive environments.
2. Compatibility with large cumulative collections and thus capability for extended measurement times without overloading.
3. Minimum maintenance requirements.
4. Self calibrating operation by gravimetry of stage filters.
5. Simplicity of read-out and signal transfer from stack.
6. Operation in a specific stack may require only occasional self-calibration checks. Transfer to other sources requires self-recalibration. Calibration against an independent reference method may prove to be unnecessary.
7. Adaptability to high and low source concentration levels (up and downstream of controls).

SECTION 4

RECOMMENDATIONS

The positive results of the laboratory and field tests performed with the cascade virtual impactor-pressure drop system, as well as the attractive simplicity and basic nature of the measurement principle applied therein strongly favor further development work on this instrumental approach with the specific objectives of more fully characterizing this type of in-stack particle sizing device, and principally to develop a practical and fully field-worthy instrument compatible with prevailing testing facilities and easily adaptable to the entire range of particulate concentrations encountered within source environments.

Additional refinements and improvements to be considered for such a follow-on development program are in the area of pressure drop signal recording and processing. The use of dial-type gauges and liquid manometers was justified within the reported program and may be acceptable for other research type measurements but for more routine and extensive measurement programs electric pressure transducers with continuous recording and slow-differentiation of the pressure drop-versus-time signal would provide more useful and less labor-intensive data retrieval.

Extensive field testing under a wide variety of source environments and emission characteristics should be an important phase of such follow-on activities.

SECTION 5

THEORETICAL ASPECTS

PARTICLE SIZING METHOD

Aerodynamic Particle Diameter

The aerodynamic fate of the emitted particulates and their effect on human health are the primary areas of concern on which control technologies must be based, and thus the sizing approach for the measurement of these particulates must be as representative as possible or as directly "coupled" as possible to those criteria. Particle sizing methods based on optical, electrical, acoustical, etc., techniques are not directly related to the aerodynamic behavior of particulates and to their mass. Inertial methods, on the other hand, provide a size selection mechanism that is based on the aerodynamic properties of the particles and is directly relared to the atmospheric transport and sedimentation characteristics, as well as to the respiratory tract deposition and clearance behavior of airborne particulates.[1-3] Thus the selected sizing method had to be based on the inertial separation of particles providing a measure of their aerodynamic diameter.

The aerodynamic diameter characterizes particle behavior under the force of gravity and under inertial acceleration in fluid flow fields, such as acceleration caused by curvature of the flow. The mechanisms of impaction and sedimentation and, indirectly, diffusion, depend on the aerodynamic diameter, and those are the predominant mechanisms in filtration and in lung deposition. Furthermore, the behavior of particles in such control devices as cyclones, Venturi scrubbers, electrostatic precipitators, filters, and settling chambers also depends directly or indirectly upon aerodynamic diameter. The aerodynamic diameter comes into play in the dispersion of particles in the atmosphere, controlling the sedimentation of particles, their capture by obstacles in a wind, and their scavenging by rain.

The optical equivalent diameter (or light scattering cross-section), on the other hand, is significant in the effect of particles on visibility.

Other measures of particle size have special contexts that are less directly related to particle behavior and are of interest for special and more restrictive particle studies.

The aerodynamic diameter of a particle of arbitrary shape is that diameter which would give the same terminal settling velocity for a sphere of unit density. Mathematically,

$$v_s = \left[\rho_o \, D_{ae}^2 \, C/18\mu\right] g$$

where v_s = terminal velocity

ρ_o = unit density

D_{ae} = aerodynamic diameter

C = Cunningham correction factor (calculated for D_{ae})

g = gravitational acceleration

μ = gas viscosity

The term in brackets, the "relaxation time" of the particle, governs the behavior of particles falling due to gravity (sedimentation) or crossing the streamlines of a gas to strike an obstacle deflecting the gas (impaction). The choices for separating particles on the basis of their aerodynamic diameters narrow down to: gravitational sedimentation, centrifugation and jet impaction. Of these alternatives, a variation of jet impaction (virtual impaction) was selected because, among other reasons, it provides a more controllable collection geometry and better size segregation selectivity as well as compatibility with several sensing techniques.

Sampling Considerations

The need for isokinetic sampling does not have to be re-emphasized here. The problems unique to inertial sizing devices, however, preclude flow rate adjustment as one of the means to match stack and sampler inlet velocities. The only method to obtain such sampling conditions without affecting the size segregation properties of an inertial separator is by changing inlet cross-sectional area; i.e., by selecting an inlet nozzle of proper size. This method, however, is not compatible with any straightforward automation, but remains at present the only feasible approach and was thus adopted for the instrumentation problem at hand.

The problem of sample extraction versus nonextractive in-stack sampling will now be discussed. The conclusions presented in a comprehensive GCA/Technology Division literature review on source testing instrumentation[4] will simply be restated verbatim:

"Most stack sampling devices used for routine measurements are based on the sample extraction approach; i.e., an isokinetic inlet nozzle followed by a duct, commonly called a 'probe' whose length is determined by the cross-sectional dimensions of the stack at the point of sampling. The particle-laden gas flows through this probe, and the particulate matter is collected on filters or other devices on the outside of the stack wall, through which the probe passes. This procedure is specified for stack sampling by the Environmental Protection Agency. This method has several drawbacks that are, although acceptable for manual operation, not compatible with the meaningful operation of an automated device, and in particular for a particle sizing instrument. These problem areas are (1) particulate losses along the probe or, extraction duct, and (2) condensation within the exterior section of the probe and at the collector exposed to lower temperatures than the stack environment (or conversely the need for heating of these elements, not only above the water dewpoint, but also above the acid mist condensation temperature).

"The first problem (i.e., particulate losses within the probe) is caused by the following mechanisms:

1. Impaction in tube bends.
2. Sedimentation due to gravity.
3. Electrostatic scattering due to mutual repulsion by charged particles.
4. Turbulent deposition.
5. Electrostatic precipitation due to image charges.
6. Diffusional loss to the tube wall.
7. Thermal precipitation due to temperature difference between gas and tube wall.

All of these loss mechanisms are dependent on particle size, thus changing not only the total concentration but also the shape of the size distribution. Such losses in stack tests have been shown to occur.[5] Further changes in the size distribution can come from:

1. Coagulation, enhanced by shear in the gas velocity profile and by vapor condensation.
2. Re-entrainment.
3. Condensation.

The approximate magnitude of such influences can be estimated from formulas available in the literature.[6,7] In any case these losses are unacceptable for an automated-recording type instrument for the obvious reason that the fraction deposited in the probe is not incorporated in the measurement. The EPA specified procedure for manual sampling includes the requirement for probe washout and addition of the mass of particulates retained in the probe to the collected mass on the filter. Such a procedure must be ruled out for an automated measurement system. No practical method has yet been found to eliminate the deposition of particulates in probes for size distributions with mass median diameters of 10 to 20 μm and σ_g between 2 and 5, typical of stack environments, and for probe lengths of the order of, or in excess of 4 meters required to sample representatively a stack with a flow duct area of up to about 50 m^2 (approximately 500 square feet). The only method by which probe deposition can be reduced, albeit not eliminated, is by increasing the flow velocity to very high values (of the order of 20 m/s or more) to produce re-entrainment of particles collected on the probe walls. This procedure may be marginally acceptable for total mass measurements, but not for accurate sizing purposes since particle agglomeration and clustering can be expected in any situation where re-entrainment plays a significant role.

No line losses are acceptable unless they constitute a known fraction of the inlet loading, a highly unlikely condition indeed. Obviously the conclusion is that since the probe length cannot be minimized if the collection-sensing device is exterior to the stack, the only rational solution is to place the device within the stack duct to be sampled. This method also resolves in large measure a second problem: the condensation of water and acid mist at the measurement site. By operating the sampler wholly at the source temperature, condensation can be precluded. At typical stack gas temperature of 150°C to 260°C (300°F to 500°F) all the water is in the vapor phase and if the collection-detection head is exposed to the same environment, no condensation will occur.

The measurement of particulate mass and especially of the size distribution by mass of stack emissions can only be determined meaningfully at two locations: (1) within the stack itself, or (2) downstream from the stack exit (stack plume). The first of these approaches can provide information on the particulate emissions as they are generated, and within the high temperature environment of the stack itself. The second approach would provide a measure of the particulates as they will eventually disperse in the atmosphere. Both of these approaches have their merit.

Sample extraction, by lengthy probes and requiring thermal control, is an approach that we believe is an unacceptable compromise between the two alternatives presented above, and it is especially incompatible with representative size measurements.

Cascade Virtual Impaction Advantages

Inertial particle separation by cascade impaction has been used extensively in a number of different configurations, and the literature on the subject of impaction and its application to sizing through the cascade arrangement is copious.[8-11] The use of cascade impaction in source testing has received increasing attention in the last few years and several versions of the multi-orifice (e.g., Andersen) configuration have been designed for direct insertion into the stack environment.[12] Such devices are merely size-selective collectors of particulates, and the evaluation of the collected material is performed subsequently by gravimetry, chemical analysis, etc.

All these devices, however, are based on the jet-to-plate configuration; i.e., particle interception by a solid (usually coated) collection surface. A variation on this generalized approach is the cascade centripeter, aerosol concentrator or virtual impactor. Figure 1 is a schematic of a virtual impactor stage.

The method of virtual impaction was originally developed by McGinn and MacWaters[13] and then by Hounam and Sherwood[14] who called the device a "cascade centripeter." Similar devices have been described by Conner[15] and Loo.[16] All

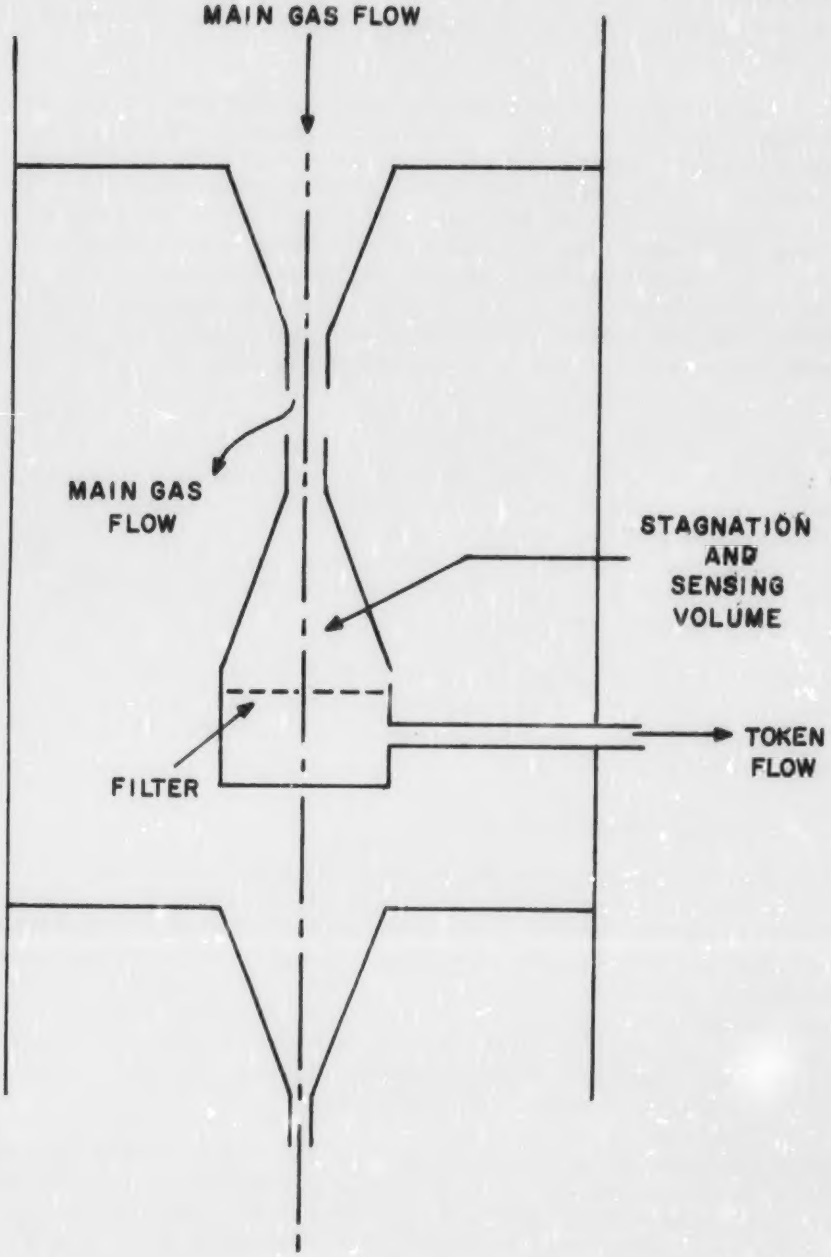
MAIN GAS FLOW
MAIN GAS FLOW
STAGNATION AND SENSING VOLUME
TOKEN FLOW
FILTER

Figure 1. Schematic of a virtual impaction stage.

these devices are based on "impaction" into a stagnation volume rather than onto a solid surface normal to the flow direction as in the case of jet-to-plate impactors. Particles larger than a characteristic cut-off dimension penetrate into the void due to their inertia, while the smaller particles are entrained by the air that circumvents the entrance to the void volume. Particles entering the void can then be collected on a filter, or detected as they are being extracted by means of a small secondary flow typically of the order of several percent of the primary sampling flow. This small flow rate can be obtained either by relying on the jet impact pressure or by a small diversion flow line from the vacuum pump.

The equation governing the collection of particles by means of an impactor, and thus equally applicable to a centripeter or virtual impactor, is

$$\psi^{1/2} = \left(\frac{C\rho_p \; v}{18\mu \; W_j} \right)^{1/2} D_p$$

where ψ is the impaction parameter (geometry dependent)

ρ_p is the particle density

v is the jet velocity

D_p is the particle diameter

μ is the coefficient of viscosity of the gas

W_j is the jet width

C is the Cunningham correction factor.

For the experimental set up of Conner,[15] $\psi^{\frac{1}{2}} = 0.6$, and for the experimental set up Hounam and Sherwood[14] $\psi^{\frac{1}{2}} = 0.73$, a value considerably higher than the typical round jet impactor value of about 0.3 cited by Mitchell and Pilcher,[9] but very close to the value reported by Lundgren[8] for a rectangular jet (slit) type impactor ($\psi^{\frac{1}{2}} = 0.6$).

The advantage of the virtual impaction method with respect to the usual impaction approach is the vastly increased mass which can be collected on each stage without overloading and concomitant re-entrainment. Particle bounce problems due to uncoated or poorly coated impaction surfaces[17] are eliminated. In addition, filter collection of each of the particulate size fractions is made possible because lower collection flow rates can be used; i.e., the small "token" extraction flow mentioned above, permitting large collection densities on such filters without excessive pressure drops, and thus extended sampling times between filter replacements become possible. Filter collection offers other advantages with respect to the usual impaction methods in that samples may be collected for subsequent physical or chemical analysis; or small samples may be collected, the filter material being rendered transparent by use of immersion oil, and the sample inspected using light transmission microscopy. Furthermore, for certain particle sensing techniques this method provides a significant and necessary enhancement of concentration within the stagnation volume wherein the particles are retained. For those sensing methods not requiring actual collection and retention of particulates (i.e., nonintegrating techniques), the virtual impaction approach obviates the need for any frequent and routine collection surface renewal or cleaning, as opposed to the usual type of impaction.

Theoretical Cascade Virtual Impactor Optimization

The resolution or size selectivity of a cascade impactor depends on the number of stages used to cover the desired total size interval to be assessed. In practice, however, because the retention characteristics of impactor stages are not ideal; i.e., they deviate significantly from true step functions, the resulting overlap between stages becomes the limiting factor tending to degrade the information as the size interval between successive stage is decreased.

A computer program was thus developed to characterize this cascade impactor behavior and provide the criteria for its optimization. This program was based on a cumulative log-normal stage retention curve with a geometric standard deviation of 1.4 as a reasonably close approximation to the collection efficiency curve found by Conner[15] for a cascade centripeter or virtual cascade impactor. This program provides a measure of the error amplification or degradation in the measurement accuracy, of a cascade separator of nonideal characteristics; i.e., with gradual particle-size cuts rather than a step-function. In fact, as a result of this deviation from ideal conditions, what is retained on any stage of a series of such stages is really the result of the interaction of that stage with those preceding it. This problem of cross sensitivities is obviously crucial in determining how closely spaced the impactor size intervals can be and yet contribute constructively to the size characterization of an aerosol.

There is an extensive literature concerning the solution of the integral equations which are typical of some data analysis problems:

$$F^*(a^*) = \int_0^\infty p(a^*,a)\, f(a)\, da$$

where $F^*(a^*)$ is the reading (or the penetration, transmission, etc.) which results when an instrument which has the reading or response $p(a^*,a)$ to a monodisperse distribution (a delta function) is used to measure a polydisperse distribution $f(a)$. By definition $\int_0^\infty f(a)\, da = 1$ and $p(a^*,a)$ and $F^*(a^*)$ are dimensionless and are in the range 0 to 1. This kind of formulation has been used by several authors in the aerosol analysis context[18-20] and occurs in many other fields as well. The method of solution is to convert this equation into a set of linear equations by approximating the integral by a summation.

Of the ways to convert the integral equation to a set of linear equations, we discuss only one, the use of a quadrature formula. A specific upper limit is chosen, a_∞ and a lower limit, a_0. The interval of integration is broken into segments in terms of the known kernel, $p(a^*,a)$, and the unknown function $f(a)$ evaluated at specific points within the segments:

$$\int_{a_0}^{a_\infty} p(a_i^*,a)\, f(a)\, da \doteq \sum_{j=1}^{N} p(a_i^*, \bar{a}_j)\, f(\bar{a}_j)\, \Delta a_j$$

or

$$F^*(a_i^*) = \sum_{j=1}^{N} P_{ij} \left[f\ \Delta a \right]_j$$

We have made the decision to evaluate the segments at their midpoints, $\bar{a}_j$, which means we are using a "midpoint quadrature," the error of which is known. Usually, the number of points at which the data are obtained (a_i^*) will be the same as the number of points at which the integral is evaluated (a_j). The last equation is conveniently written in vector-matrix notation as

$$\underset{\sim}{F}^* = P\underset{\sim}{\Delta F}$$

where the vector ΔF has components $f_j\ \Delta\ a_j$. If the set of linear equations, $\underset{\sim}{F}^* = P\underset{\sim}{\Delta F}$, is solved with a standard computer program the solutions can be expressed as

$$\underset{\sim}{\Delta F} = P^{-1}\underset{\sim}{F}^*$$

and the matrix P^{-1} is referred to as the inverse of P.

Twomey[21] used such a method to invert the data from a diffusion battery method and found that the solutions were highly oscillatory functions, even sometimes negative. Twomey[22] and Phillips[23] and others have tried to circumvent the oscillatory results by "smoothing" techniques, which solve the equations with the constraint that the solutions be as smooth as possible and still come within a prescribed error in giving results which match the data. Rust and Burrus[24] and Cooper,[19] among others, have discussed such methods at length; the choice of the degree of smoothing is formidable. The oscillations result from magnification of small errors which come from the formulation (approximating the integral) or from the data. The error in the solution, $\delta\ (\Delta F)$, due to a small error in the data $\delta\underset{\sim}{F}^*$ can be shown to be

$$\frac{\|\ \delta\ (\underset{\sim}{\Delta F})\ \|}{\|\ \underset{\sim}{\Delta F}\ \|} \leq \|\ P\ \| \cdot \|\ P^{-1}\ \| \left[\frac{\|\ \delta\underset{\sim}{F}^*\ \|}{\|\ \underset{\sim}{F}^*\ \|} \right]$$

where the notation $\| P \|$ indicates the magnitude or norm of P. One set of vector and matrix norms is defined as follows (the maximum norm):

$$\| \underset{\sim}{F}^* \| = \max |F_i^*|$$

$$\| P \|_\infty = \max_{1 \le j \le N} \sum_{i = 1}^{N} |P_{ij}|$$

The contribution of an error in the matrix, δP, is akin to that of the contribution of an error in the data. The product $\| P \| \cdot \| P^{-1} \|$ is referred to in the literature of linear equation solving as the condition number of P, cond (P). For the Lundgren impactor,[8] this cond(P) is about 25; and is very much larger for diffusion batteries, meaning that a few percent error in the data will be greatly magnified by attempts to improve the results by solving the linear equations. The condition number will get larger as the number of data points (subintervals or segments) increases or as the sharpness of size discrimination (e.g., d_{84}/d_{50}) decreases, as discussed elsewhere.[19]

The role of the condition number, dominated by $\| P^{-1} \|$, is examined in detail by Cooper[19] with respect to its influence on data inversion. What does not seem to have been realized previously is that $\| P^{-1} \|$ is important even in situations where the data are not to be inverted, but used directly.

Figure 2 shows an ideal cascade impactor response (unity within the assumed sizing interval and 0 outside) with a nonideal response function superimposed upon it. The nonideal instrument shows "cross-sensitivity," a response in a given channel to a particle size which is actually outside the bounds of that channel. A channel for a cascade impactor is simply the impactor stage, and the size associated with that stage is generally taken to be the difference between d_{50} for that stage and d_{50} for the stage upstream from it. Because the multi-channel interpretation of the impactor data is related to differences, the response of the i^{th} channel with respect to the j^{th} particle size is defined here as ΔP_{ij}.

If the impactor were ideal, that is if the response functions were step functions, then they would be characterized by the equations which characterize the ideal instrument shown in Figure 2; that is,

$$\Delta \underset{\sim}{F}^* = I \, \Delta \underset{\sim}{F}$$

where I is the identity matrix ($I_{ii} = 1$, $I_{ij} = 0$ for $j \neq i$). The difference between what is registered by the nonideal instrument and what is actually in the assumed size intervals associated with the stages is given by:

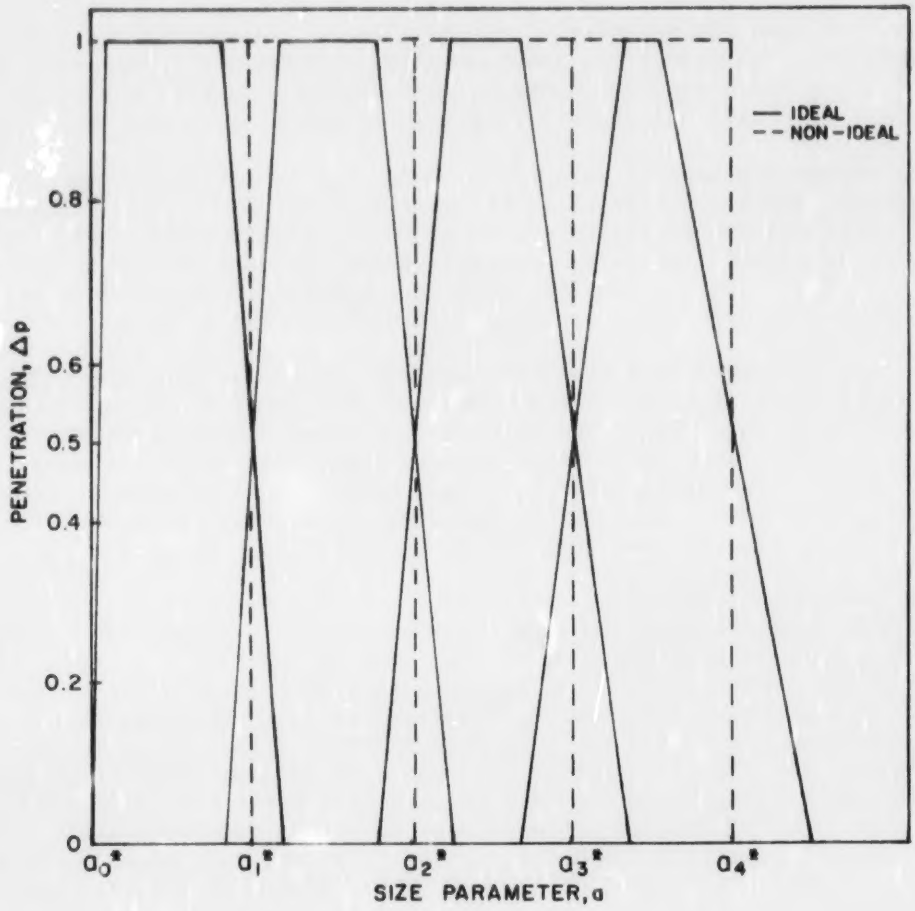

Figure 2. Penetration, or response, function for ideal and nonideal instrument.

$$\Delta \underset{\sim}{F}^* - \Delta \underset{\sim}{F} = (I - \Delta P^{-1})\, \Delta \underset{\sim}{F}^*$$

where ΔP^{-1} indicates the inverse. When impactor data are used directly, it is assumed that they represent the aerosol to be found within the limits associated with the i^{th} stage, but this assumption is incorrect by the factor of $(I - \Delta P^{-1})$, and thus, its magnitude is a measure of the error associated with the instrument. The linear equations were solved to obtain an error factor, $\| \Delta P^{-1} \|$, for several cases to show the severity of the problem or cross-sensitivity for a cascase impactor. Two points are important here: this is a factor related to instrument error which applies *whether or not* any data inversion techniques are tried; $\| \Delta P^{-1} \| \gg 10$ indicates that data inversion will be difficult.[19]

The integral equations were set up using the response function for a cascade virtual impactor ("cascade centripeter") given by Conner,[15] approximated by cumulative log-normal distributions with the medians (d_{50}) chosen to be the size interval demarkation (a_i*) and their geometric standard deviation chosen to be 1.4. The range for the impactor tests was $a_o = 0$ and $a_\infty = 1$, with the device assumed to have one stage a_∞ and in absolute filter at a_o.

One set of numerical experiments was done by subdividing the range into equal sizing intervals. For N measurements, there were N sizing intervals, each having a width of 1/N. Values of N from 2 to 10 were used, representing two-state measurements, three-stage measurements, etc. As N increases, the interval between the stages decreases and the degree of overlap of the response functions, the cross-sensitivities, increases. The values for cond (ΔP) and $\| \Delta P^{-1} \|$ are nearly the same (because $\| \Delta P \| \doteq 1$).

A second set of numerical experiments was made by dividing the range ($a_\infty - a_o = 1$) into segments which increased geometrically in size. The sizing intervals were chosen so that their boundaries were $a_i = A^{i-N}$ for i from 1 to N and $a_o = 0$,* A was chosen to be $2^{\frac{1}{2}}$, 2, 3, 10. As can be seen in Figure 3, this leads to error factors that tend toward an equilibrium value at large N, are smaller than the corresponding case for intervals sized at 1/N, and are not much larger than 1 except for the $A = 2^{\frac{1}{2}}$ case. To select an optimum value of A, the ratio between impactor stage cut-offs (d_{50} values), the error factor $\| \Delta P^{-1} \|$ should be combined with some measure of advantage to form a figure of merit. Generally, closely spaced data are desired (small A) and so are small values of $\| \Delta P^{-1} \|$. Figure 4 is a plot of the resulting "figure of negative merit" defined by the product of the sizing interval ratio A times the above mentioned error multiplication parameter $\| \Delta P^{-1} \|$ resulting from stage size separation overlap. This product $A \times \| \Delta P^{-1} \|$ is to be minimized for maximum size resolution and minimum overlap error. The variable N is the number of stages of the impactor such that the total range covered is equal to A^N:1.

It is obvious from Figure 4 that an optimum condition exists for a size interval ratio of about 2.5 for most values of N. For a typical total range of

---

*Where A is defined as the sizing interval factor; i.e., the ratio between adjacent particle size cuts.

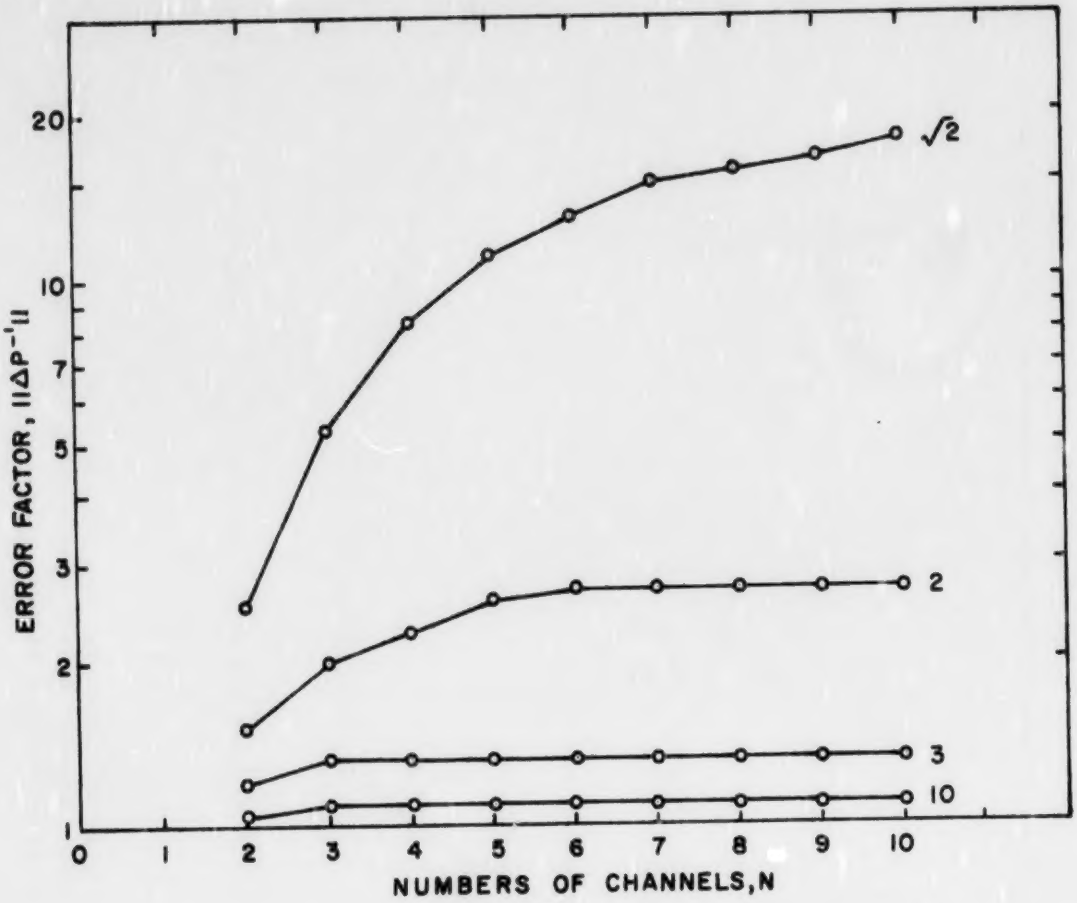

Figure 3. Error factor versus number of geometrically increasing sizing intervals for impactor.

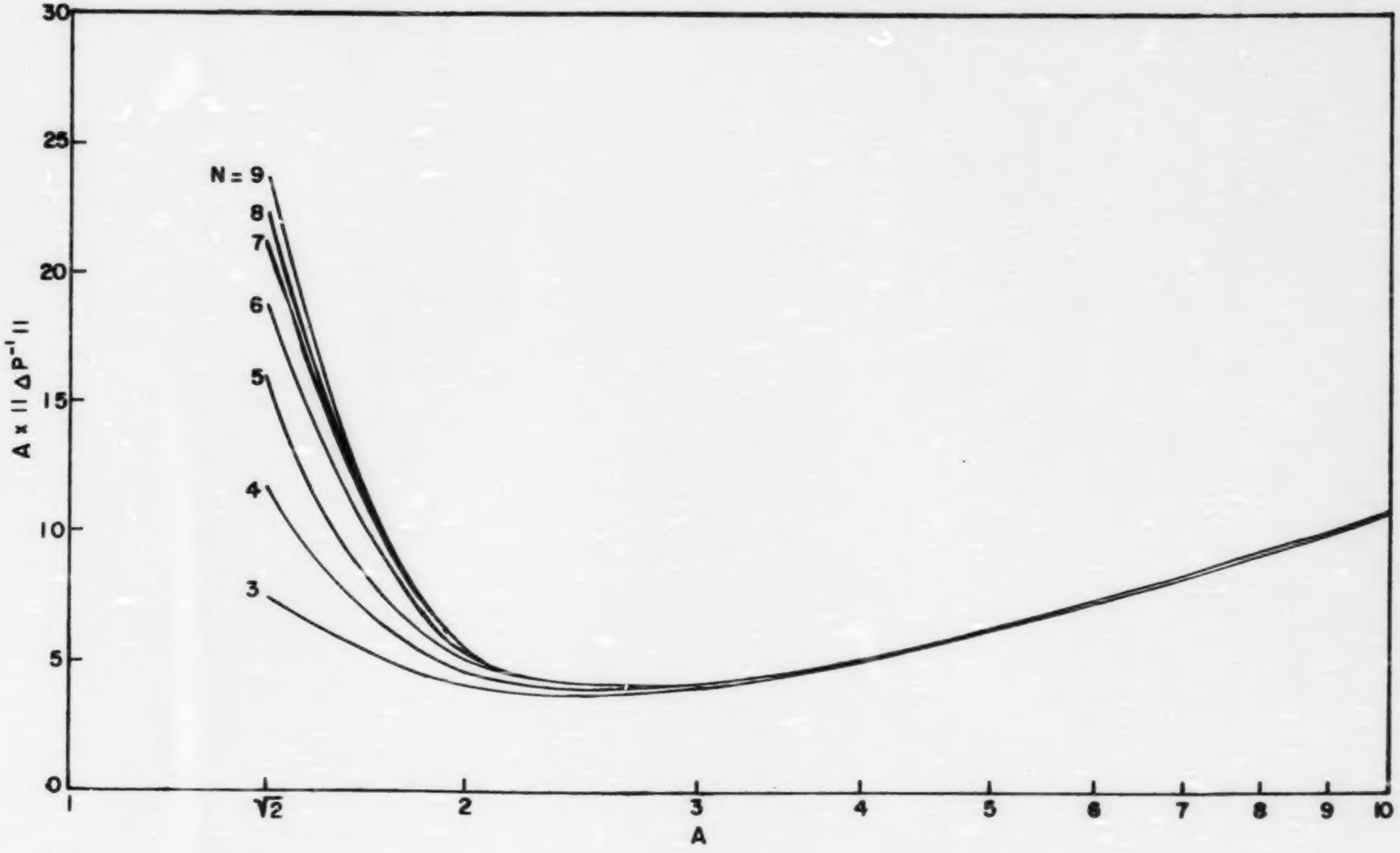

Figure 4. "Figure of negative merit" as a function of size interval ratio and number of stages. For a log-normal stage collection efficiency curve whose geometric standard deviation is equal to 1.4 (typical of virtual impactor stages).

20:1 (e.g., 0.5 μm to 10 μm) the corresponding number of stages would be 3.3. A somewhat more practicel value results by setting N = 4 which corresponds to A = 2.11, a value sufficiently close to that of the minimum product $A \times \|\Delta P^{-1}\|$. For N = 5, and a range of 20:1, A = 1.82 which corresponds to a higher "figure of negative merit;" i.e., a less advantageous measurement condition. A compromise between measurement, figure of merit and practical design considerations appears to be a four-stage configuration with a sizing interval ratio A = 2 and a corresponding total range of 16:1 (e.g., 0.5 μm to 8 μm) which could be extended by the addition of a fifth stage if so desired.

Data Inversion Incorporating Secondary Flow

As shown in Figure 1 (page 12), the aerosol enters the first impaction stage and virtually all particles with aerodynamic diameters larger than the cut-off particle diameter of that stage are captured by "impaction" into the nearly-stagnant volume of that stage. A small flow, the secondary flow, is removed to draw the particulate material to the filter, where its mass can be determined by several different techniques. The same process occurs at the subsequent stages, after which the remaining aerosol flows to and is captured by the final filter, the last sizing stage. During this program it was found that the losses of particulate matter in the impactor can be minimized if a fairly substantial secondary or token flow (as much as 10 percent of the main flow) is employed; this flow could cause a data analysis problem because it contains a sample of particles of all sizes not already captured upstream. It thus becomes necessary to develop a mathematical procedure in order to correct for this secondary flow contribution. This method should also be applicable to other particle sizing situations in which there is a constant fraction of the aerosol material either lost or added to a sizing stage.

If the centripeter worked like an ideal multichannel sizing device, each stage would have 100 percent collection efficiency for particles within its assumed sizing interval and 0 percent efficiency for particles outside this interval. Unfortunately, there are three nonideal aspects of the centripeter: (1) the secondary flow collects a fraction of all the particulate matter present in the gas stream approaching the nearly-stagnant region of each stage; (2) the series (cascade) nature of the centripeter means that succeeding stages have their effective capture efficiencies influenced by the preceeding stages; i.e., they cannot capture what does not reach them; (3) even without these two interferences, each centripeter stage does not change abruptly from 0 percent to 100 percent efficiency at the stage cut size. Correcting for the latter two factors has been the subject of the preceding section of this report and will not be discussed further here. We shall now assume that the secondary flow factor is a predominant error factor, which should be true for centripeters with secondary flows of more than a few percent and with sizing intervals large compared with the particle size differences needed to go from nearly 0 percent to nearly 100 percent impaction efficiency for the stages.

Let the fraction (by count, mass, etc.) of the aerosol which is truly in size range j be labeled F_j. Let the efficiency of the i^{th} sizing stage for particles which are in the j^{th} size range be E_{ij}. Then the fraction, F_i^*, of the total collected aerosol material which is collected on the i^{th} stage will be given by (for a device of k stages)

$$F_i^* = \sum_{j=1}^{k} E_{ij} F_j$$

In the case of a three-stage centripeter this becomes:

$$F_1^* = E_{11} F_1 + E_{12} F_2 + E_{13} F_3$$

$$F_2^* = E_{21} F_1 + E_{22} F_2 + E_{23} F_3$$

$$F_3^* = E_{31} F_1 + E_{32} F_2 + E_{33} F_3$$

If the secondary flow is a constant fraction, e, of the primary flow (secondary flow assumed to have same size distribution as primary flow), and if the capture efficiency of the stage is essentially 100 percent for particles larger than the cut size and essentially 0 percent for smaller particles, one has:

$$F_1^* = (1)\ F_1 + (e)\ F_2 + (e)\ F_3$$

$$F_2^* = (0)\ F_1 + 1(1-e)\ F_2 + e(1-e)\ F_3$$

$$F_3^* = (0)\ F_1 + (0)\ F_2 + 1(1-e(1-e)-e)\ F_3$$

The set of linear equations can also be written as the transformation of a vector by a matrix:

$$\vec{F}^* = \underset{\sim}{E}\ \vec{F}$$

where the vector $\vec{F}^*$ has as its components

$$\vec{F}^* = (F_1^*, F_2^*, F_3^*)$$

The matrix is just the array of the coefficients of the linear equations:

$$\underset{\sim}{E} = \begin{bmatrix} 1 & e & e \\ 0 & 1(1-e) & e(1-e) \\ 0 & 0 & 1(1-e(1-e)-e) \end{bmatrix}$$

One can solve the linear equations by the usual methods[24] to obtain (for $E_{21} = E_{31} = E_{32} = 0$):

$$F_3 = F_3^*/E_{33}$$

$$F_2 = (F_2^* - E_{23}F_3)/E_{22}$$

$$F_1 = (F_1^* - E_{12}F_2 - E_{13}F_3)/E_{11}$$

These equations show that the true distribution can be obtained by subtracting the material caught due to secondary flow and correcting for the loss of the material before it reaches the sizing stage ($E_{ii} < 1$). Another way of solving the system of equations is to obtain the inverse matrix, $\underset{\sim}{E}^{-1}$, and thus $\vec{F}$ from:

$$\vec{F} = \underset{\sim}{E}^{-1} \bar{F}^*$$

In this case the inverse matrix can be shown to be

$$\underset{\sim}{E}^{-1} = \begin{bmatrix} E_{11}^{-1} & (-E_{12}/E_{11}E_{22}) & (E_{12}E_{23}E_{22}^{-1} - E_{13})/E_{11}E_{33} \\ 0 & E_{22}^{-1} & -E_{23}/E_{22}E_{33} \\ 0 & 0 & E_{33}^{-1} \end{bmatrix}$$

which becomes:

$$E^{-1} = \begin{bmatrix} 1 & -(e^1 + e^2 + e^3 + \ldots) & -(e^1 + e^2 + e^3 + \ldots) \\ 0 & (1 + e^1 + e^2 + e^3 + \ldots) & -(e^1 + 2e^2 + 3e^3 + \ldots) \\ 0 & 0 & (1 + 2e^1 + 3e^2 + 4e^3 + \ldots) \end{bmatrix}$$

The equations presented above are sufficient to correct for the secondary flow effect for a three-stage device. For four or more stages, it is probably more convenient to use computer subroutines to obtain solutions to the linear equations (or to obtain the inverse matrix).

A number of simulations were performed to determine the magnitude of the corrections. Hypothetical distributions were "sampled" by the centripeter. (Actually, $\vec{F}^*$ was obtained from $\underset{\sim}{E}\,\vec{F}$.) The "data," F_i^* were then used to obtain, once again, the input distribution, F_i. (This is the same as obtaining F_i from $\underset{\sim}{E}^{-1}\,\vec{F}_i^*$.) The results are shown in Figure 5; the size cuts were shown for 2 μm and 7 μm (same as those obtained for the actual prototype to be described later), but the actual cut sizes are immaterial to this analysis. Figure 5 shows five comparisons between corrected and uncorrected data obtained by mathematical simulation for a three-stage centripeter ($e = 0.1$). The first case has an aerosol having all the particles actually within the first size range ($F_1 = 1$); the uncorrected and corrected data produced the same result. In the second case the aerosol is all within the second size range ($F_2 = 1$). The uncorrected data show aerosol in the first two sizing intervals, but the corrected data give the right result. The third case shows the uncorrected and corrected data for an aerosol simulated to be wholly within the smallest size range ($F_3 = 1$). (These three cases correspond to sampling aerosols with sufficiently narrow size distributions that each was wholly within one sizing interval.) The fourth case is for an aerosol equally divided between all three size intervals and the fifth has an aerosol which is split between the two smallest size intervals. In all cases but the first, the corrections are appreciable. In all cases, the true aerosol size distributions are recovered by using $\underset{\sim}{E}^{-1}$.

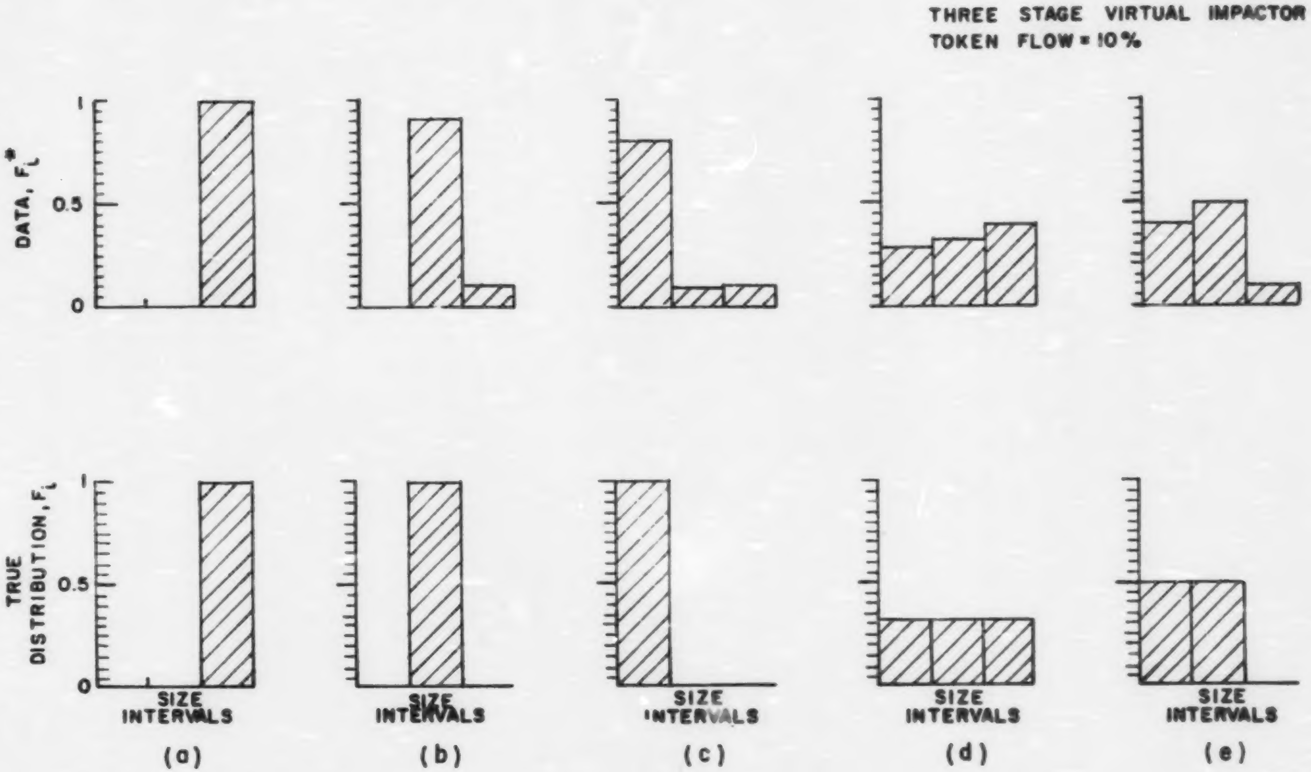

Figure 5. Data, F_2^*, and input distributions, F_i, regained by correcting that data, for a three-stage virtual impactor with 10 percent secondary flow, flow = 10 percent; (a) $F_1 = 1$, (b) $F_2 = 1$, (c) $F_3 = 1$, (d) $F_1 = F_2 = F_3 = 1/3$, (e) $F_2 = F_3 = 1/2$.

SECTION 6

PARTICLE SENSING AND DETECTION METHODS

Once inertial or aerodynamic size segregation of the particles has been effected, the objective of this instrument development program was to determine by some method of particle sensing or detection, the relative amounts in each size fraction and this information had to be made available as an output signal which can be displayed and/or recorded.

Several reviews of applicable techniques have been published, among them Dorsey and Burckle presented a comprehensive tabulation.[25]

The method of sensing the particulates in each size fraction had to fulfill several conditions which are dictated by the specifications of the pertinent RFP as well as by the overall utilization objectives of the instrument.

In reviewing some of these specifications, it became obvious that very few sensing techniques are available fulfilling these conditions. From Table 1, based on the original specification of the request for proposal, it becomes apparent that the required measurement range extends over about 4-1/2 decades; i.e., from about 0.07 mg/m^3 to as high as about 2000 mg/m^3.

If, in addition, one considers that the low limit must be detected within typically ±10 percent the overall sensing range becomes a staggering 5-1/2 decades, by no means a trivial objective. For a cumulative method; i.e., where the particulates are collected and the measurement is based on an integrating phenomenon, such as filter collection, the required range is further extended because of the stipulated time requirements of 10 minutes minimum resolution and 2 hours minimum operational time without servicing. Superimposed on this rather demanding range requirements were other very rigorous operational constraints, some of them stated specifically in the RFP and others, although not mentioned there, of an even more fundamental nature which have been discussed in a preceding section; i.e., the need for direct insertion of any sampling-sizing-sensing configuration into the stack or flue environment, with the attendant problems of temperature compatibility and corrosion resistance.

Last, but not least, the overriding requirement for low cost and simplicity introduce further severe limitations in the selection of a sensing method.

The combination of all the preceding conditions, specifications and qualitative objectives made the selection of a particle detection method exceedingly difficult. Thus, after careful review of all applicable techniques, it was decided to explore three of the most promising approaches within this program with the objective of making a final selection to be incorporated in the prototype device.

TABLE 1. CONCENTRATION EXTREMES TO BE SENSED

Outlet loading		Inlet loading	
Size interval, μm	Loading, mg/m^3	Size interval, μm	Loading, mg/m^3
>6.0	0.23	>3.4	1021
3.75-6.0	1.15	2.0-3.4	156
2.53-3.75	0.092	1.3-2.0	529
1.71-2.53	0.115	0.7-1.3	1992
1.09-1.71	0.069	0.43-0.7	1309
0.52-1.09	0.184	0.23-0.43	472
0.30-0.52	0.391	<0.23	577
0.18-0.30	0.391		
<0.18	1.265		

The detection methods that were studied during this program were:

1. Optical sensing.
2. Electrical sensing.
3. Pressure sensing.

In addition, some experiments were conducted using an impact detection scheme. The theoretical aspects of the first three methods will now be treated in some detail.

PARTICLE SENSING METHODS

Optical Sensing

The volume concentration of an aerosol may be measured by optical means provided a certain degree of optical characterization has been performed upon the specific aerosol. Two methods commonly have been used. In the first, the extinction of a beam of light is measured as it passes through a known aerosol path length from source to detector. In the second method, light scattered by aerosols is collected and measured. Optical methods of aerosol measurement suffer from a number of disadvantages. The scattering cross-section is not a simple function of size but varies in a complex way which yields ambiguities in size versus intensity of scattered light. Departures from sphericity and differing refractive indices further complicate the method. However, where the size separation is performed inertially as in the current situation, and large ensembles of particles are involved whose diameters span a factor of two or so, a substantial amount of smoothing occurs and a single calibration constant is required for each stage for each type of dust mainly due to differing refractive index.

A method using scattering must eliminate the primary beam from the measurement and, since particles whose diameter exceeds the wavelength of light scatter mainly in or near the direction of incident light, either a rather sophisticated optical system is required or rather inefficient light collection is achieved. The nature of the "in-stack" environment under consideration strongly suggested the use of extinction as a measurement method. A schematic of the sensing configuration explored within this program is shown in Figure 6. All particles with diameters larger than d enter the optical scattering volume, attenuating the light entering I_o to the level I according to:

$$I/I_o = e^{-\bar{k}\, n\, \bar{A}\, L}$$

where L is the optical path through the aerosol

$\bar{A}$ is the mean particle cross section area

n is the number concentration

$\bar{k}$ is the average extinction efficiency.

The values of I and I_o are obtained from detectors which respectively measure the light exiting the optical chamber and a sample of the incoming beam at the light source itself. $\bar{A}$ and $\bar{k}$ may be determined from the aerosol size cutoffs employed in the particular stage and the nature of the aerosol, and L is, of course, characteristic of the instrument. Adjustment of the amplifier gain associated with the detectors is set to $I = I_o$ when no aerosol is present. The ratio is obtained directly with an electronic divider circuit. Thus, a value of n may be obtained and by operating for a known time at a specific flow volume comparisons may be made with a gravimetric sample collected on the filter.

In practice, within the stagnation volumes of a virtual impactor, the concentration of particles undergoes a substantial enhancement that must be incorporated in the calculations of n. To calculate the response time of such a system; i.e., the concentration of particulates in the particulate size interval of a given virtual impaction stagnation volume, the following equation applies:

$$c(t) = c_o e^{-qt/v} + \left(E \frac{Ac}{Aj} \frac{Q}{q} + 1 \right) c_s \left(1 - e^{-qt/v} \right)$$

where c(t) is stagnation volume concentration

c_o is initial concentration in the stagnation volume

c_s is unenhanced or inlet concentration for the size fraction retained by the stage under consideration

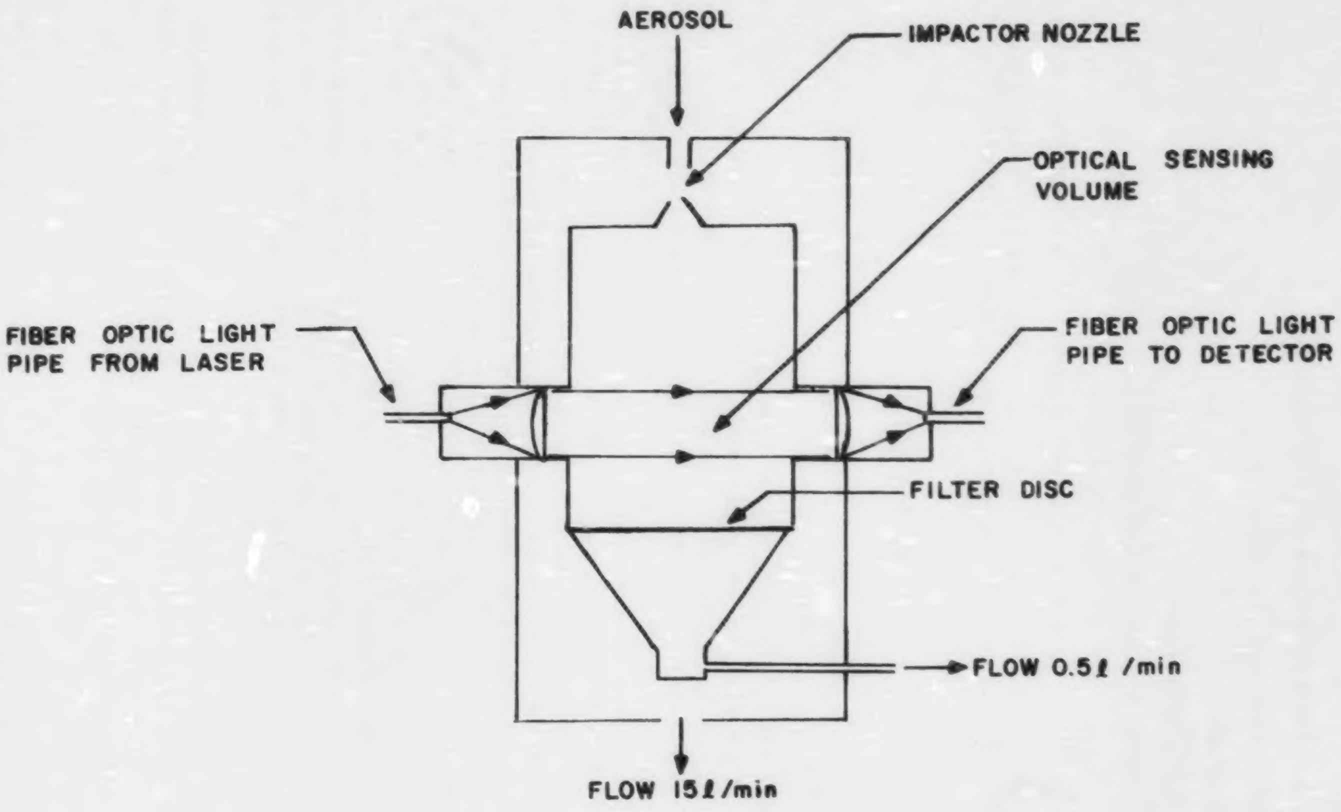
AEROSOL
IMPACTOR NOZZLE
OPTICAL SENSING VOLUME
FIBER OPTIC LIGHT PIPE FROM LASER
FIBER OPTIC LIGHT PIPE TO DETECTOR
FILTER DISC
FLOW 0.5ℓ /min
FLOW 15ℓ/min

Figure 6. Optical sensing configuration.

v is stagnation volume

t is time

E is collection efficiency of the stage

Ac is centripeter opening area

Aj is jet area

Q is primary flow rate

q is secondary or extraction flow rate.

The factor $E\frac{Ac}{Aj}\frac{Q}{q} + 1$ is the enrichment factor or concentration enhancement factor, which in many cases where E = 1 and Ac = Aj, can be approximated by Q/q. Thus the free stream number concentration n_o can be calculated as follows:

$$n_o = n\ q/Q$$

Electrical Detection

Two electrical sensing approaches of the particulate fraction captured by each centripeter stage will now be considered. The first of these consists of an electric charging section preceding the cascade centripeter. This charging section can be either a corona discharge stage or a radioactive source with unipolar charge removal (by means of an electric field). All entering particulates (larger than 0.1 μm approximately) would receive a charge (by a combination of field and diffusion charging for the corona case, and diffusion for the radioactive source) commensurate with particle size (the actual size-charge relationship would be unimportant as long as it remains constant), these charged particles would then be sensed by impaction on a receiving electrode[36] such as a thin wire placed at, or immediately after each centripeter inlet. Upon impaction on the insulated wire the particles transfer their charge to the wire and are then re-entrained and enter the stagnation volume from which they are continuously removed by the previously mentioned secondary extraction flow. The signal from each of these sensing wires consists of a current which can be transmitted to the outside of the stack. An empirical calibration constant for each stage would relate total charge per unit time (signal current) to the number of particles in each size interval. The accuracy of this method obviously depends on how narrow the segregated size fractions are.

Table 2 shows typical parameters relevant to this detection scheme. Although only three size fractions are shown (for simplicity), as mentioned above a larger number of size subdivisions would be desirable. This table is based on a 20 percent detection efficiency; i.e., approximately 20 percent of the available charges are sensed.

As Table 2 shows the range of current to be detected exceeds 5 decades and while it is simple to detect a current of 2×10^{-8} amperes at the high end, it is by no means trivial to do so for 10^{-13} amperes, especially within the

TABLE 2. APPROXIMATE SIGNAL CURRENTS RESULTING FROM AN ELECTRIC CHARGE-WIRE SENSOR, 30 LIT/MIN TOTAL FLOW RATE

Size range	Signal current	
	Control inlet	Control outlet
>3 μm	8×10^{-11} ampere	10^{-13} ampere
1 - 3 μm	5×10^{-10} ampere	10^{-13} ampere
0.3 - 1 μm	2×10^{-8} ampere	3×10^{-12} ampere

far-from-ideal environment under which this device must operate. An alternative to current sensing is the use of a charge integration approach wherein a small capacitance is charged up by the sensing current. This accumulated charge can then be processed electronically by a high input impedance charge detector and displayed with typical integration times of the order of 100 seconds corresponding to an accumulated charge of 10^{-11} coulombs (e.g., 0.1 volt across a 100 pf capacitor). This capacitance could be obtained directly from a coaxial conductor feeding the signal to the outside of the stack. Range switching would be accomplished by external paralleling of additional capacitance.

The disadvantage of this method resides in the relative complexity of the electric charging stage which would require a high voltage feed or possibly a radioisotope.

An alternative electrical detection technique is based on contact electrification or turbulent charge transfer, a method which does not require particle charging. This phenomenon is the basis for two commercial particulate monitors (Konitest and Ikor). Although their strict correlation with particulate mass concentration; i.e., mass flow, is questionable for a large variety of particle compositions, this technique nevertheless, can be applied to the performance of such relative measurements as those intended for the present application. The signal from the sensing electrode is a current I_s which has been reported to be proportional to the mass flow $\dot{m}$ and the flow velocity v squared[26]

$$I_s \propto \dot{m}\, v^2$$

The frictional charge removal is performed by a high velocity flow, impinging either rectilinearly or centrifugally on a sensing electrode, which for the Konitest consists of a semiconductor surface (magnesium hydrosilicate).[27] Velocities of the order of 100 m/s or more are required at the sensing surface, both for collection and for the continuous removal of particles by turbulent reentrainment. Concentration ranges of more than 10^5 have been reported.[26] This sensing technique can be combined with the cascade centripeter sizing system by using the secondary flow and scaling down the usual Konitest geometry to a flow rate of the order of a few liters/min (the secondary or token flow rate), thus measuring the particles as they are extracted from the stagnation volume (see Figure 7). The resulting electrical signal is then carried to the exterior of the stack. If the flow velocity at the sensor is maintained sufficiently high, no significant particle deposition is to be expected and a minimum of maintenance would be required.

Pressure Drop Method

A prime candidate method for the determination of mass accmulation for each stage of the virtual impactor is to measure the pressure drop across each stage filter as a function of time (see Figure 8). To do this, the dependence of pressure drop on time, filter loading, particle size, particle characteristics, filter face velocity, and filter efficiency, must be understood.

Mechanisms for aerosol collection by fibrous filters are described in Fuchs[6] as impaction, diffusion, interception, and sedimentation. Table 3 may be constructed which shows whether the efficiency of each mechanisms increases or decreases as filter velocity, V_o, and particle size, D_p, are increased:

TABLE 3. EFFECTS OF VELOCITY AND PARTICLE SIZE ON FILTRATION MECHANISMS

Mechanism	$V_o\uparrow$	$D_p\uparrow$
Impaction	↑	↑
Diffusion	↓	↓
Interception	No effect	↑
Sedimentation	↓	↑

Note: ↑ designates increase;
↓ designates decrease.

Many investigators have predicted an aerosol size which has maximum penetration through fibrous filters, based on theoretical single fiber filtration mechanisms as listed above, but usually ignoring electrostatic charge effects which generally act to increase filter efficiency. This maximum penetration has been verified experimentally in some studies,[28] whereas other studies report a continuously increasing penetration as particle size decreases.[29] The work of Thomas and Yoder[30] as reported in Fuchs is shown in Figure 9. This work is included here rather than some others available,[29,31] because the filter face velocities are on the order of those used within the virtual impactor stages. Calculation shows that for a 5 percent token flow of a 1/2 cfm (14.15 ℓpm) virtual impactor with 50 mm diameter filters the resulting face velocity is approximately 0.62 cm/sec.

Inspection of Figure 9 indicates that penetration increases with filter face velocity and that the size at minimum collection efficiency (maximum penetration) decreases with filter face velocity.

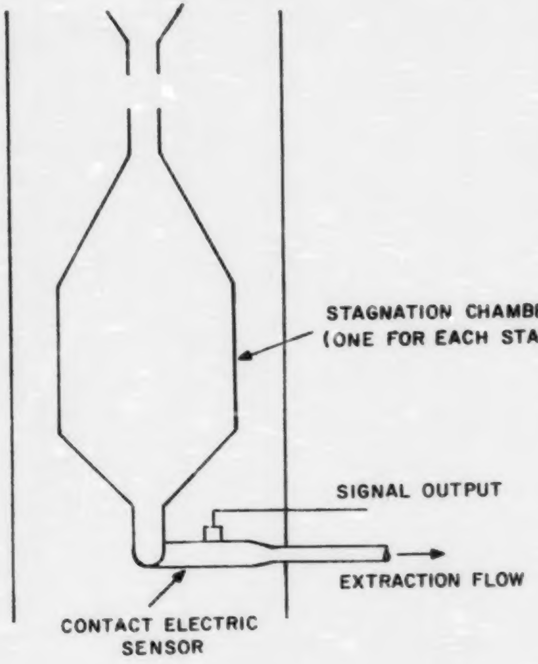
STAGNATION CHAMBER
(ONE FOR EACH STAGE)
SIGNAL OUTPUT
EXTRACTION FLOW
CONTACT ELECTRIC
SENSOR

Figure 7. A contact electric sensor technique.

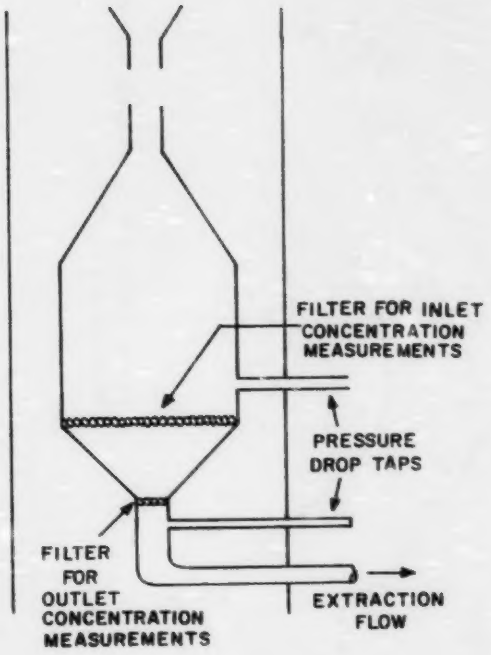
FILTER FOR INLET
CONCENTRATION
MEASUREMENTS
PRESSURE
DROP TAPS
FILTER
FOR
OUTLET
CONCENTRATION
MEASUREMENTS
EXTRACTION
FLOW

Figure 8. Filter pressure drop technique.

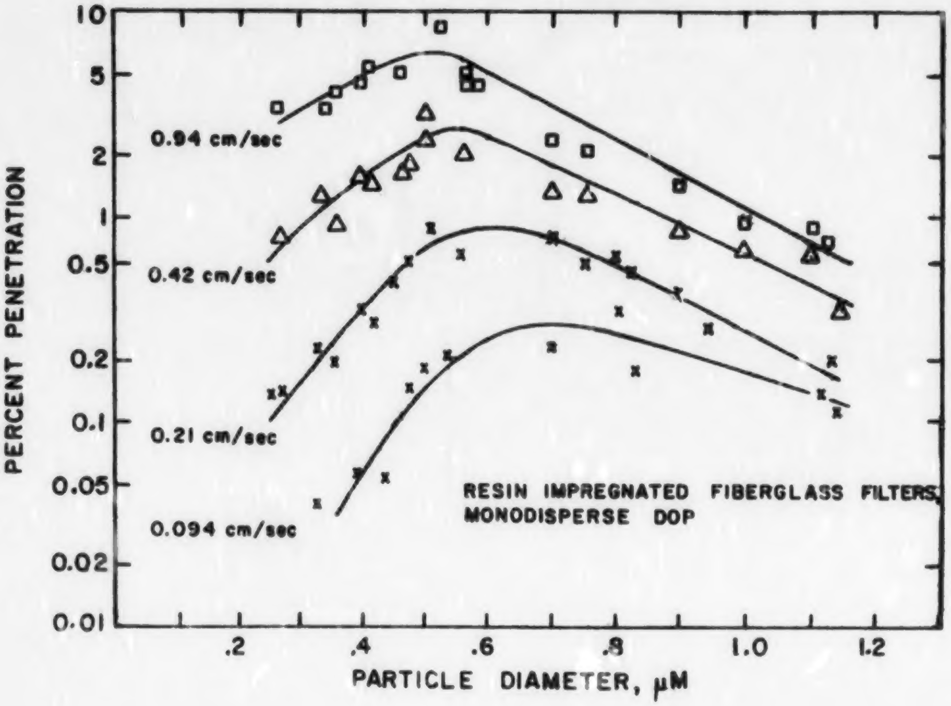

Figure 9. Efficiency of glass-fiber filters as a function of particle size and flow rate.

Very little work has been found in the literature describing filtration during cake buildup, and none at the low face velocities (<2 cm/sec) of interest to this project. One of the investigators, Anderson,[32] studied filtration efficiencies of various filter media collecting cotton picker machine effluent (mostly lint free) at face velocities of approximately 50 cm/sec and 100 cm/sec. Penetration decreased as the filter cake and pressure drop grew, and the resultant dependence of pressure drop on time was exponential. In fact, after a cake had formed, pressure drop was an excellent indication of collection efficiency.

Figure 10 shows pressure drop versus time, and therefore loading, for monodisperse latex particles (D_p = 0.088 μm), collected on nuclepore filters, at a face velocity of 5 cm/sec.[36] Figure 11 shows pressure drop and collection efficiency versus cake thickness for polydisperse ammonium chloride fume (D_p = 0.1 to 3.0 μm) collected by gravel bed filters and fiber filters at a face velocity of 2.0 cm/sec.[33] Figure 12 shows pressure drop versus cake thickness for various face velocities and various fiber filters.[34] The work of LaMer as reported by Billings[34] is presented in Figure 13. Experiments performed at GCA/Technology Division with polydisperse General Motors AC fine air cleaner test dust (Arizona Road Dust) are presented in Figures 14 and 15.

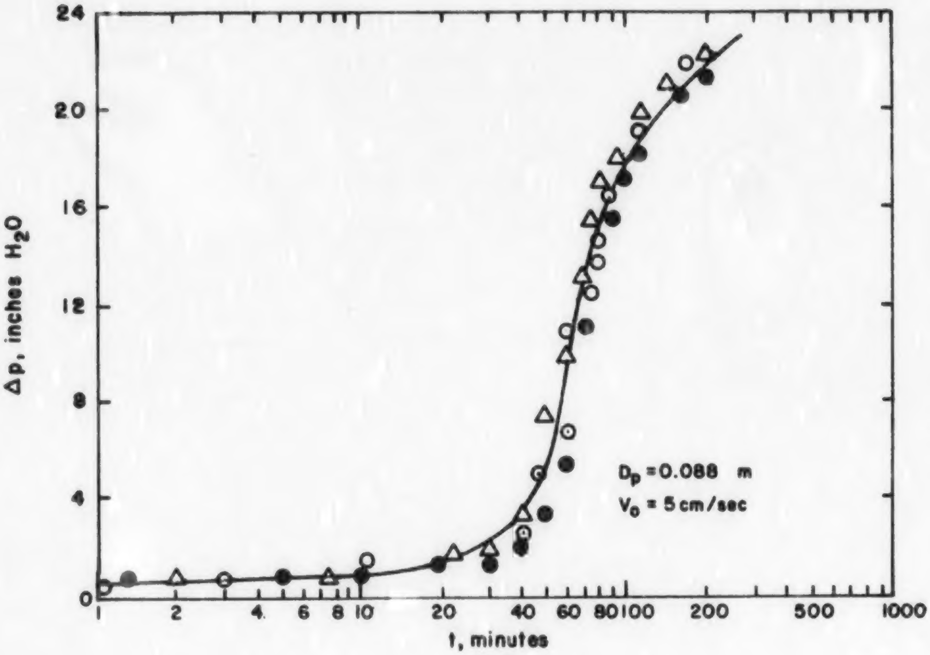

Figure 10. Measured dependency of Δρ on time (three successive experiments).[36]

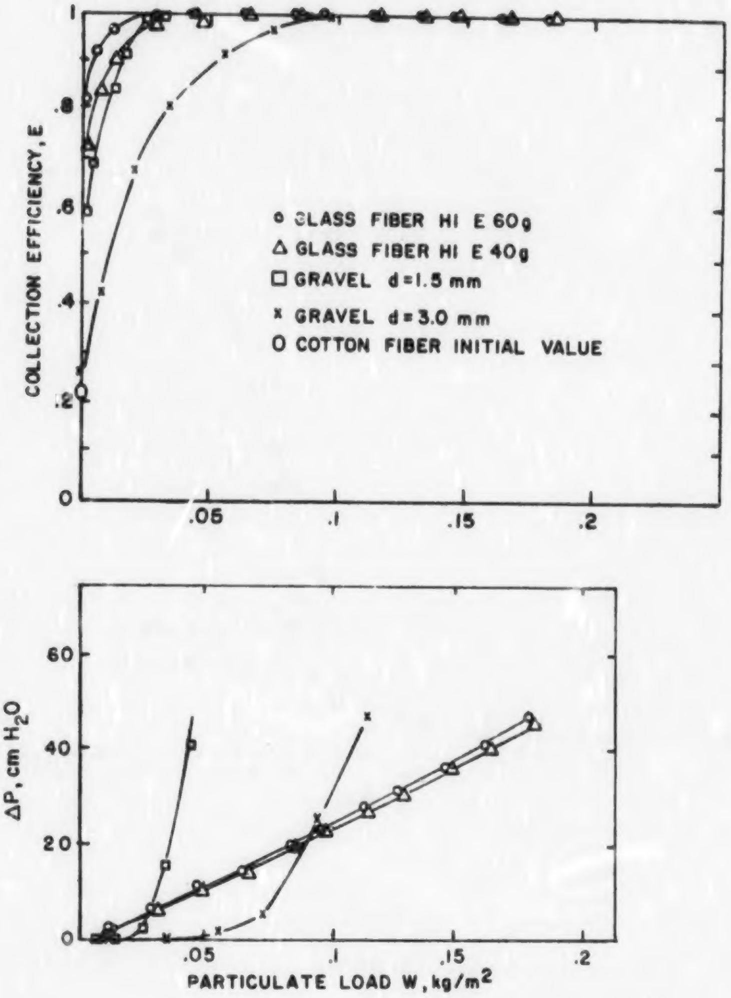

Figure 11. Comparison of collection efficiency E and pressure drop ΔP in gravel and fiber filters at Darcy air flow velocity v_D = 2.0 cm/sec and gravel layer thickness L = 30 cm.[33]

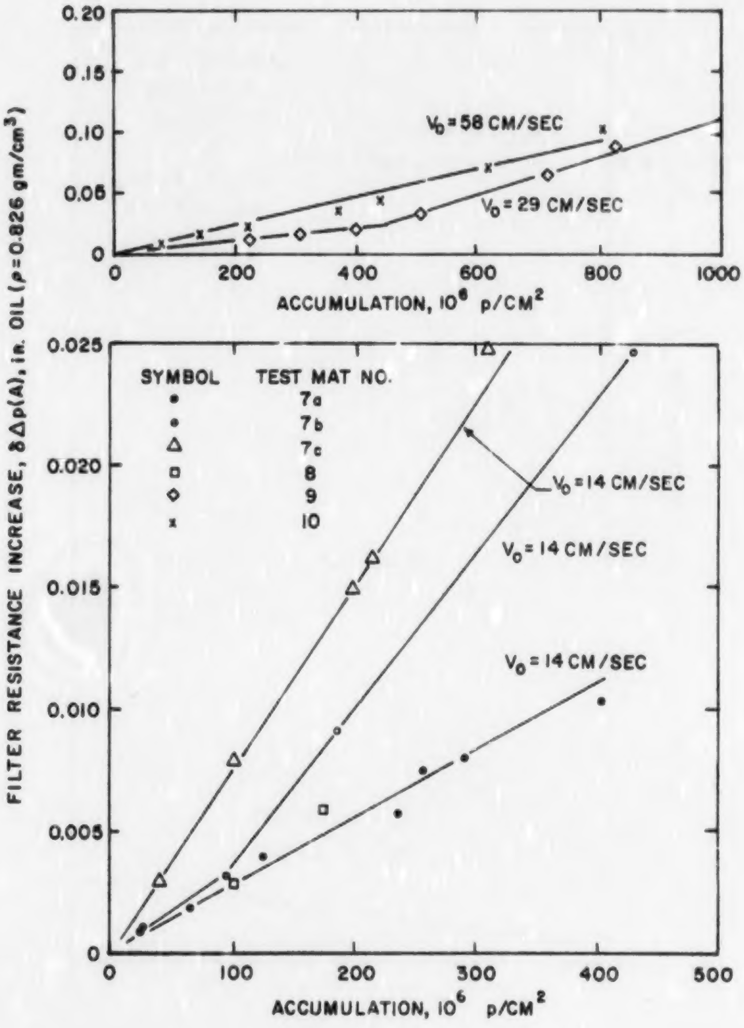

Figure 12. Resistance increase as a result of solid particle accumulation in tests 7 through 10. Test mat numbers refer to various glass fiber filter mats (see reference 34).

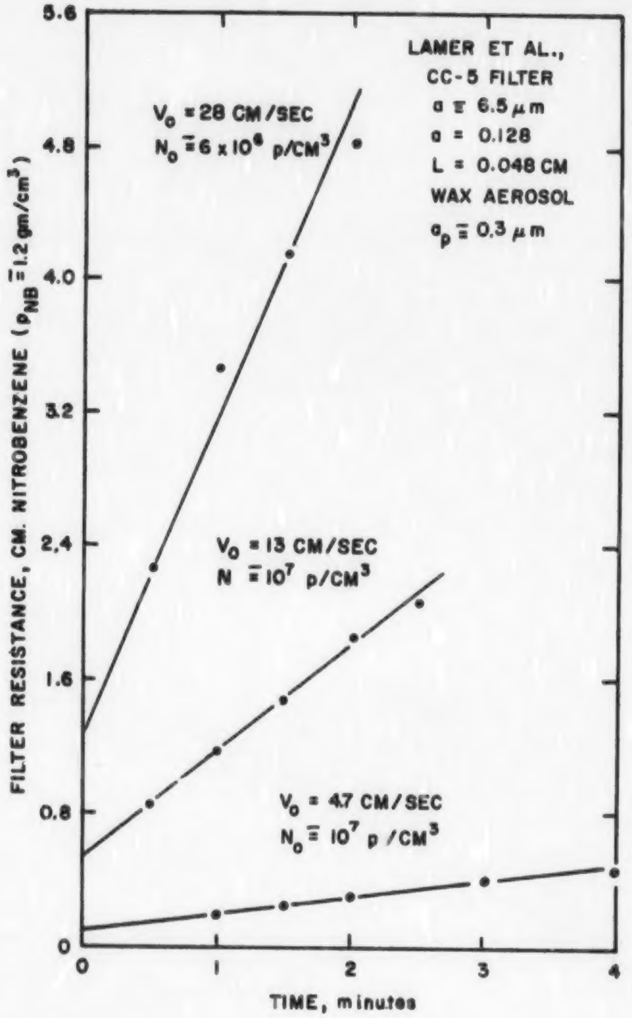

Figure 13. Filter resistance during operation.[34]

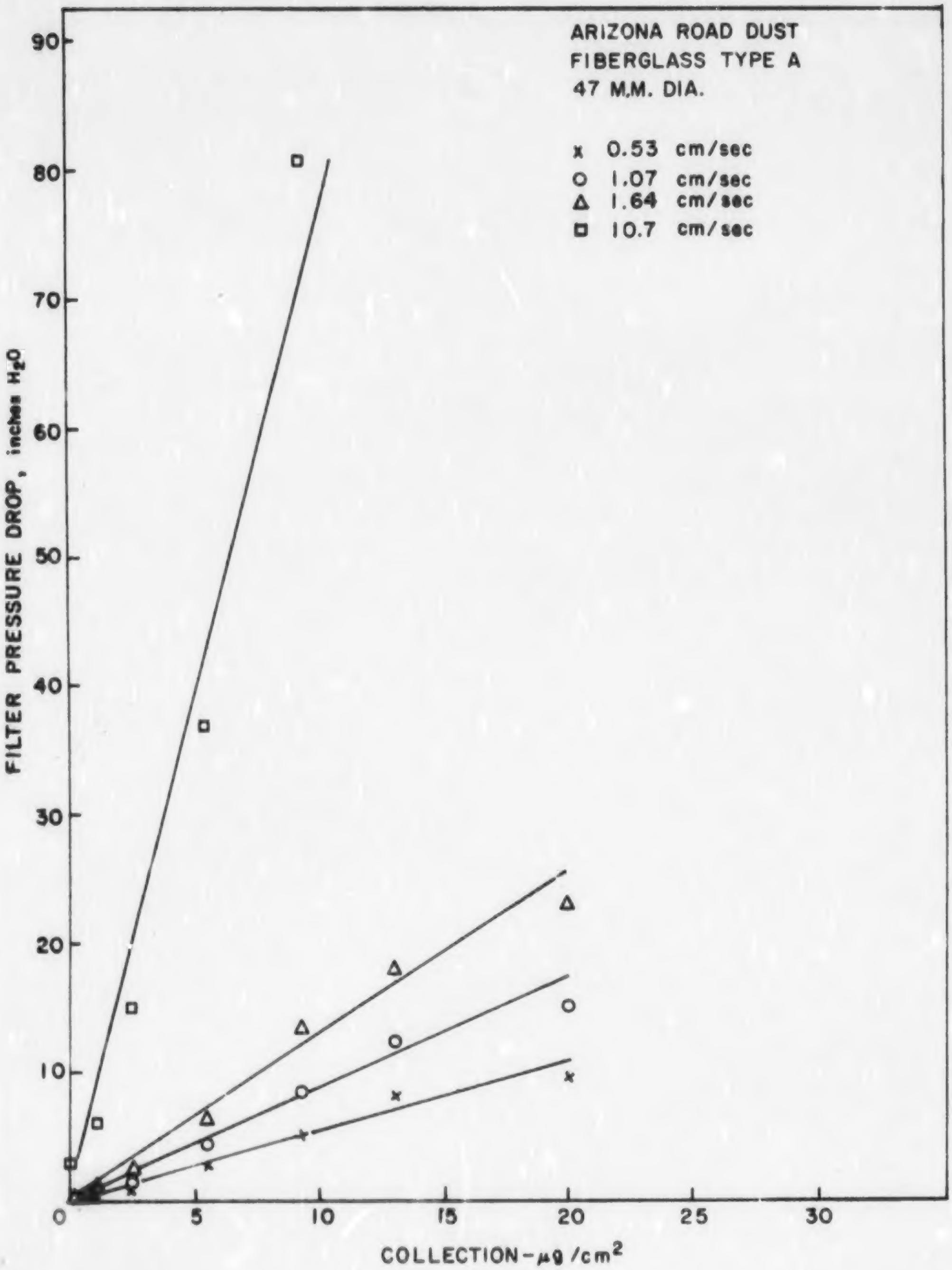

Figure 14. Pressure drop versus collection density at various filter face velocities (GCA data).

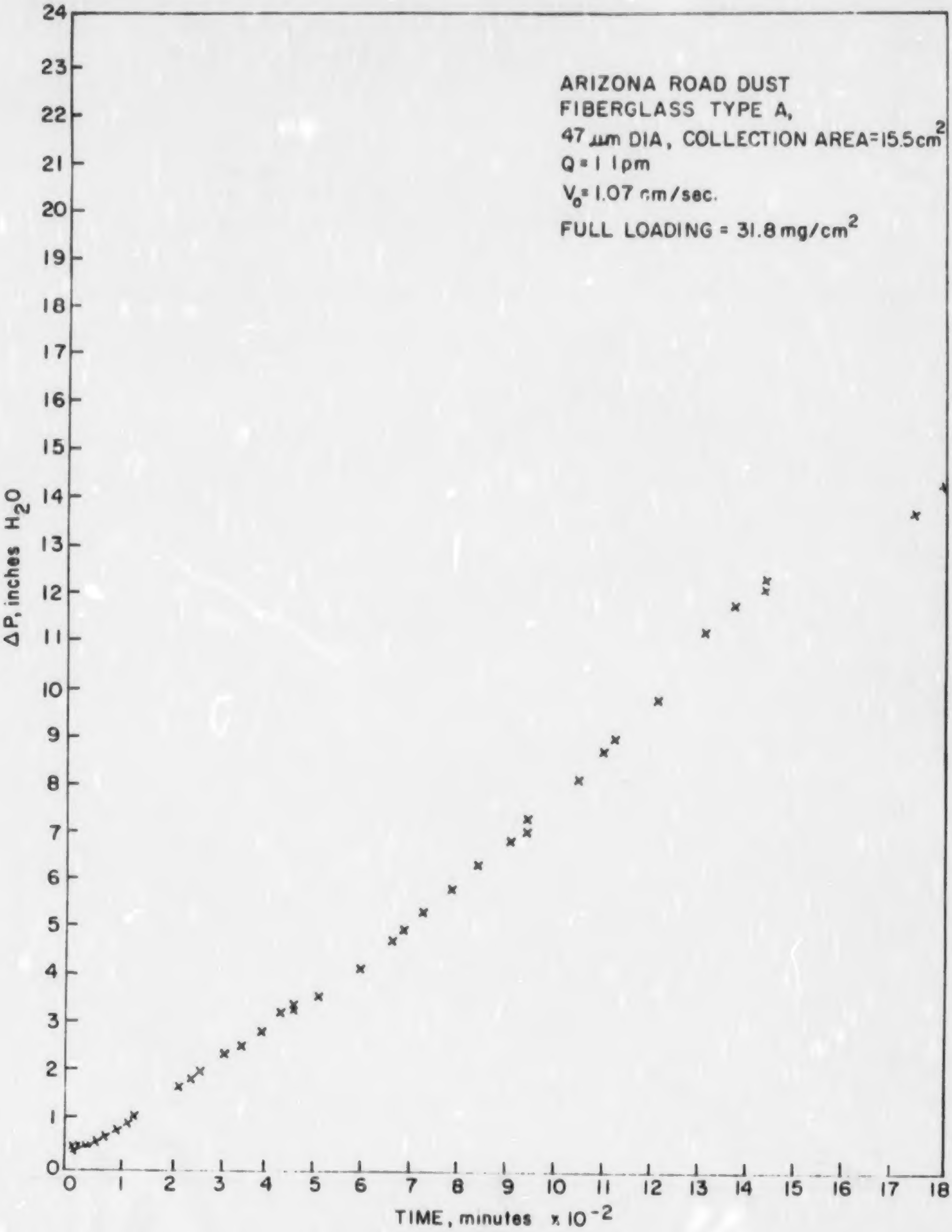

Figure 15. Pressure drop as a function of time for extended operation at nearly constant concentration (GCA data).

The foregoing curves shows that fiber filters behave quite differently from nuclepore filters or gravel bed filters, in that fiber filters display a rather steady increase in pressure drop as accumulation proceeds. Although it appears at first glance that pressure drop versus loading is linear for a time for nuclepore filters as shown in Figure 10, closer examination reveals that nuclepore filters clog at a very low pressure drop, in this case at about 2 in. H_2O. Comparing Figures 14 and 15 with Figure 10 it is obvious that nearly linear pressure drop increase proceeds to much higher values in the case of fiber filters. The shape of a pressure drop versus time curve for a fibrous filter under constant loading can be expected to be somewhat concave upward because the penetration will decrease as the filter cake builds up, if it is assumed that pressure drop is proportional to accumulation. From Billings,[34]

$$\frac{dA}{dt} = V_o \, N_o \left(1-P(A)\right)$$

where A = accumulation

V_o = filter face velocity

N_o = aerosol concentration

$P(A)$ = aerosol penetration.

and

$$\delta \, \Delta p = S_p \, \mu \, V_o \, D_p \, \delta A$$

where Δp = pressure drop

μ = gas viscosity

D_p = particle diameter

S_p = particle resistance coefficient

and assuming that $S_p \neq f(A)$.

From this it can be understood why the pressure drop versus time curves of Anderson's high face velocity tests showed an exponential form. Initial penetration was quite high (as much as 30 percent), and decreased as the cake formed. The curve in Figure 15 from data gathered at GCA/Technology Division as well as the curves in Figure 12 only hint at upward concavity. From the earlier discussion of filter penetration as a function of particle size and face velocity,[6] it is anticipated that the filters behind the final virtual impactor stages (those collecting the smallest particles) are the most likely to display upward concavity.

This effect may be minimized by reducing filter face velocity (increasing filter area), or by choosing a filter of higher initial efficiency. From the foregoing data it can be expected that pressure drop versus time curves are nearly linear for the low filter face velocities to be used in the virtual impactor. Another aspect of importance to this method of measuring accumulation, is the slope of the pressure versus time (or cake thickness, A) for varying particle size.

The Kozeny equation is presented in Happel and Brenner[35]

$$\Delta p = V_o \mu L \left(\frac{36 \ (1 - \varepsilon)^2 \ K}{\varepsilon^3 \ D_p^{\ 2}} \right)$$

describes pressure drop across a porous bed

where ε = porosity, fraction of void volume; and,

K = Kozeny factor (5.0 approx.)

L = length of bed.

The other parameters being the same as defined for the previous equation. For close packing of spheres, ε = constant, and it is expected that pressure drop increases as particle size decreases for the same mass loading as shown in Figure 16. Experimental data in the literature has not been found to support the conclusions from Kozeny's equation. For real aerosols ε is probably a complicated function of particle size, shape, compressibility, hygroscopicity, etc.

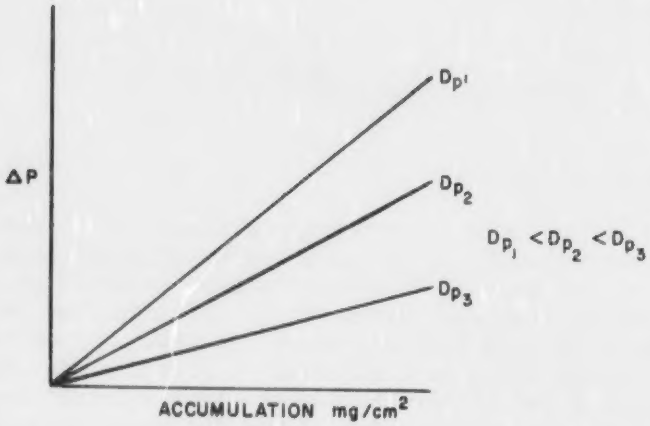

Figure 16. Expected variation of pressure drop as a function of accumulation and particle size.

SECTION 7

VIRTUAL IMPACTOR DEVELOPMENT

METHODOLOGY— DESIGN TOOLS

The main three laboratory tools used for the experimental development of the virtual impactor were a Research Engineers, Ltd. air driven spinning disc generator for monodisperse aerosol production, a G. K. Turner fluorometer for quantitative analysis of uranine tagged aerosol, and an American Optical Series 10 microscope for particle sizing.

With this equipment a monodisperse, fluorometrically active aerosol was introduced into the virtual impactor prototype. Aerosol deposition on the virtual impactor filters as well as undesired aerosol deposition within the virtual impactor was quantitatively measured with the fluorometer. The measurement range of the fluorometer from 1 μg/liter of solution (deionized water for these experiments) to 250 μg/liter, allowed quantitative analysis of extremely small amounts of material.

The experimental procedure was as follows: (1) All impactor parts were thoroughly washed with deionized water and the wash from each part was fluorometrically analyzed to insure that the fluorescence level was not much different from that of the deionized water, (2) the impactor parts were assembled with the aid of a Jones and Lamson Machine Company optical comparator to accurately measure jet orifice diameter, collection nozzle diameter, and orifice to nozzle distance, (3) 51 mm diameter, RAWP, Millipore filter media were weighed and mounted in the stage filter holder, backup filter holder, and second (independent) probe filter holder, (4) the completely assembled impactor stage with the backup filter holder and the second probe filter holder were connected to identical probes in the wind tunnel, (5) critical orifices were used to control flow through the impactor, the token flow through the impactor stage filter, and the second probe, (6) a solution of deionized water, ethyl alcohol, and methylene-blue and fluorescein was prepared and placed in a syringe to supply the spinning disc, (7) appropriate spinning disc speed and liquid feed rate were chosen and the test was run taking care to exchange wind tunnel probes between the impactor and second probe filter assembly to minimize any possible bias between probe location in the wind tunnel, (8) after a suitable collection period the impactor was disassembled and the filters were sectioned to provide wedges for microscopy and for fluorometry, (9) the second or reference probe filter was photomicrographed in several fields to record enough aerosol particles (usually around 50) to determine aerosol size, (10) wedges from the stage filter, backup filter, and second probe filter were weighed and then washed in a known amount of deionized water and the wash analyzed with the fluorometer to determine aerosol concentration, and (11) the impactor parts were washed with a known amount of deionized water and the wash analyzed with the fluorometer to determine aerosol losses.

Aerosol size was determined by particle diameter measurements from the photomicrographs. The average diameter determined by measurement was converted to aerodynamic diameter by

$$D_{aero} = \frac{D_{meas.} \, (\rho_p)^{\frac{1}{2}}}{\text{magnification power}}$$

where ρ_p is assumed to be 1.3 for uranine.

TESTS WITH FIRST VIRTUAL IMPACTOR BREADBOARD

Figure 17 is a cross-sectional view of the first stage of the initial version of the virtual impactor breadboard, which was designed so that orifices and collection nozzles could be changed and the spacing between the orifice and nozzle could be varied.

The design also allowed for stages to be cascaded. Figure 17 is labeled to indicate the manner in which internal surfaces were washed to measure aerosol deposition.

Seven tests were performed with this breadboard using monodisperse uranine (fluorescein) aerosol. Six tests were done using only one impactor stage, but one test used two stages in a cascade arrangement. These tests resulted in the redesign of the virtual impactor to further minimize aerosol collection by parts other than the filters.

The size of the aerosol was kept in the 4 to 6 μm aerodynamic diameter range, although great effort was not expended toward accurate size analysis for each test because attention was primarily focused on minimizing losses within the impactor. Further, there was a nonneglible satellite population produced by the spinning disc generator whose size appeared to be near the limit of resolution of the optical microscope used for size analysis, probably in the sub to 1 micrometer size range. The mass contribution of this satellite population was estimated to be about 10 percent of the total aerosol concentration.

Table 4 summarizes data collected during these tests. For each test, concentrations are reported in $\mu g/m^3$ (of uranine), and as a percentage of the concentration measured by the second probe for the purpose of comparison between tests that may contain incomplete data. For the column labeled "Can" the concentrations are from the surfaces labeled "Can, outer surface" and "Can, inner surface" as labeled in Figure 17. For the column labeled "All other," concentrations are summed for those surfaces such as "Outer can," "Outlet plate," etc., that do not contribute significantly to the total impactor losses. Figure 18 shows the various orifice and nozzle configurations that were tested. Table 5 indicates which nozzle and orifice designs were used for each test, as well as orifice diameter, nozzle diameter, and spacing between orifice and

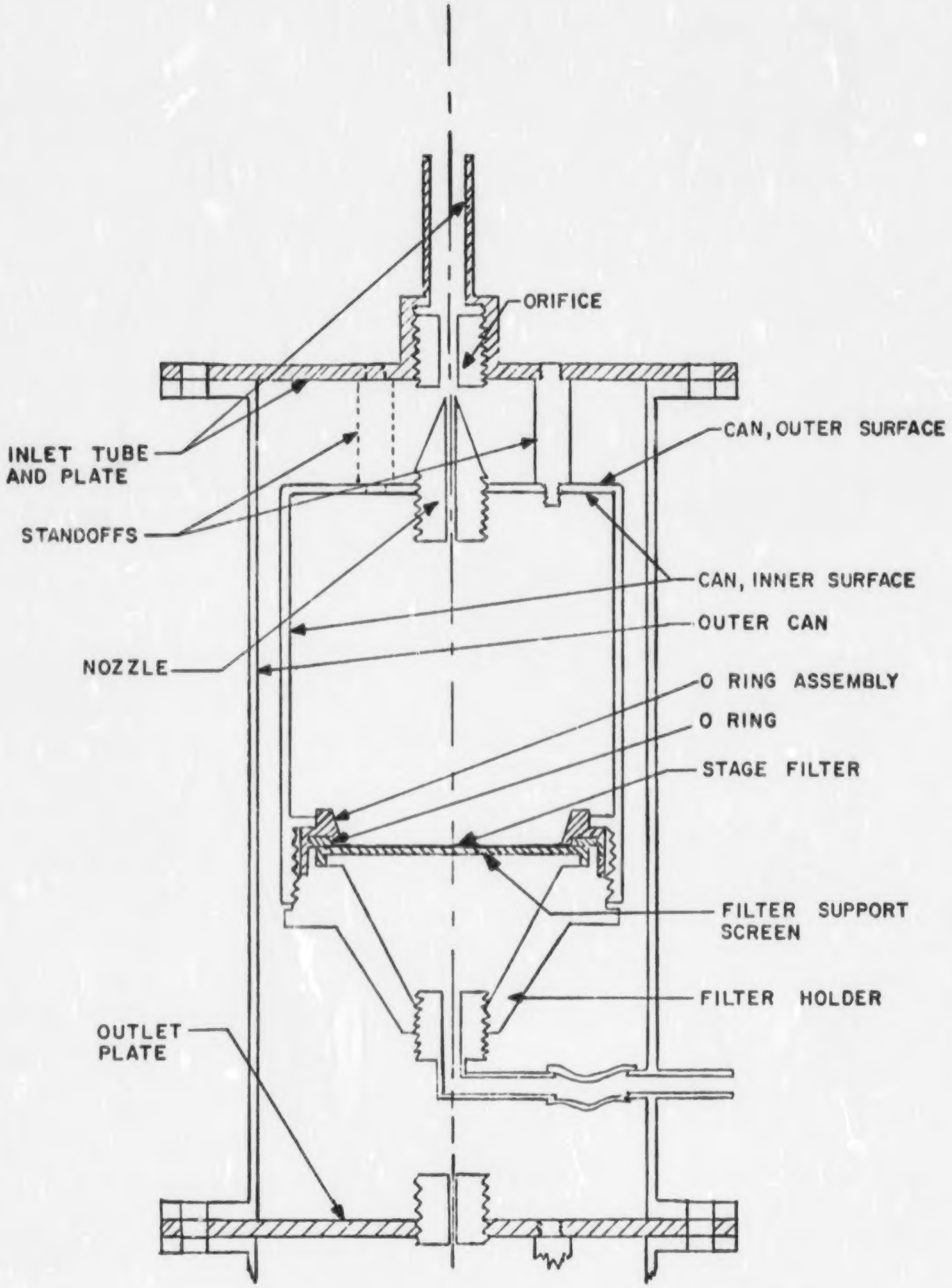
ORIFICE
CAN, OUTER SURFACE
INLET TUBE AND PLATE
STANDOFFS
CAN, INNER SURFACE
OUTER CAN
NOZZLE
O RING ASSEMBLY
O RING
STAGE FILTER
FILTER SUPPORT SCREEN
FILTER HOLDER
OUTLET PLATE

Figure 17. Cross-section of initial version of virtual impactor breadboard.

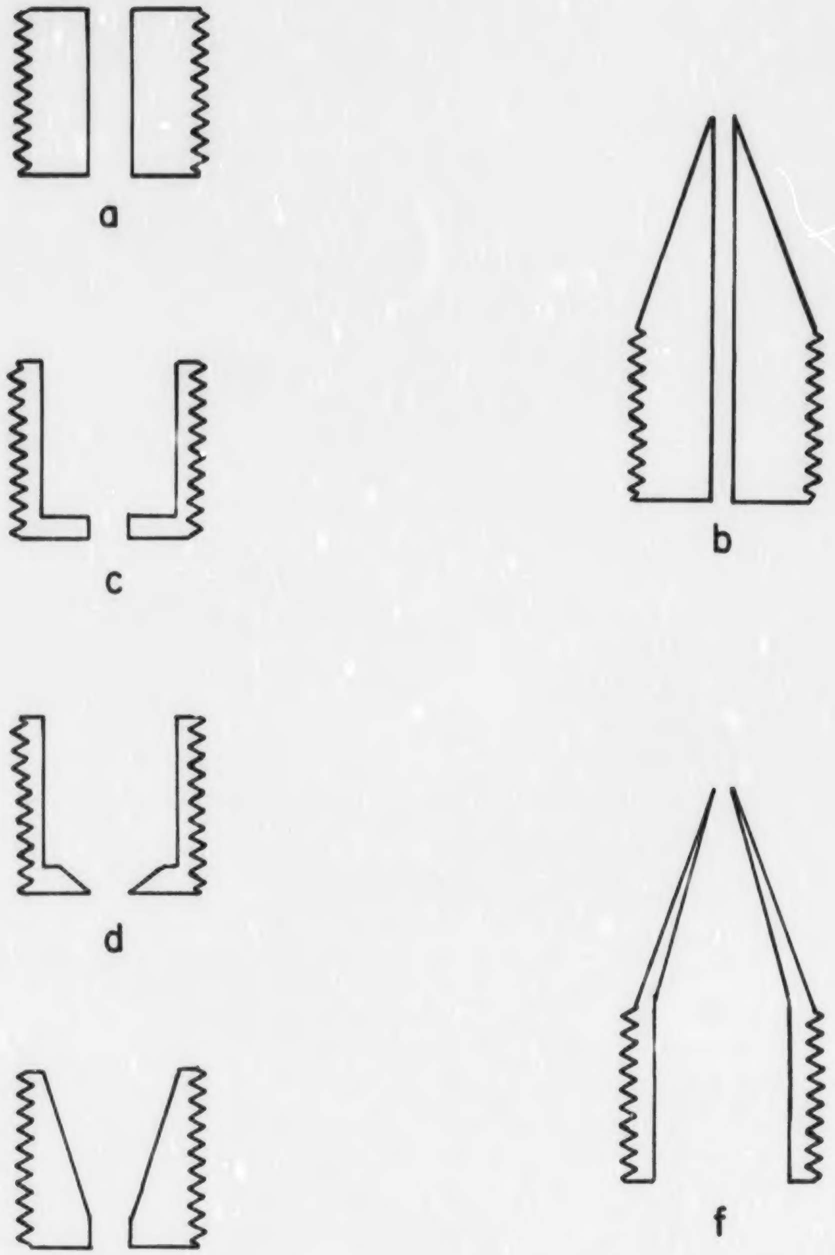

Figure 18. Various orifice and nozzle designs.

TABLE 4. VIRTUAL IMPACTOR TEST DATA (FIRST VERSION)

Date	Stage filter	Backup filter	Can	Nozzle	Orifice	O-ring assembly	All other	Σ impactor	Second probe
8/4/75	31.5 $\mu g/m^3$	—	4.0	60.0	8.4	—	2.6	106.5	233
No. 1	13.5%	—	1.7	25.8	3.6	—	1.1	45.7	100
8/6/75	7.8 $\mu g/m^3$	20.4	—	132	25.9	—	1.1	187.2	239
No. 2	3.3%	8.5	—	55.2	10.8	—	0.5	78.3	100
8/20/75	71.9 $\mu g/m^3$	19.3	20.0	9.3	17.8	—	4.3	142.6	240
No. 3	30.0%	8.0	8.3	3.9	7.4	—	1.8	59.4	100
8/21/75	62.1 $\mu g/m^3$	45.3	35.4	18.4	7.0	19.1	15.4	202.7	212.7
No. 4	29.2%	21.3	16.6	8.7	3.3	9.0	7.2	95.3	100
8/26/75	24.3 $\mu g/m^3$	24.0	2.2	35.3	—	15.8	—	101.6	176.6
No. 5	13.8%	13.6	1.2	20.0	—	8.9	—	57.5	100
8/29/75	23.6 $\mu g/m^3$	14.5	18.5[a]	15.7[a]	4.6[a]	2.4[a]	1.5	80.8	103.4
No. 6	22.8%	14.0	17.9[a]	15.2[a]	4.4[a]	2.3[a]	1.5	78.1	100
Stage 1	11.7%		17.3	12.2	4.1	0.8	—	—	—
Stage 2	11.1%		0.6	3.0	0.4	1.5	—	—	—
9/4/75	33.6 $\mu g/m^3$	55.8	3.9	41.3	13.2	9.4	—	157.2	161
No. 7	20.9%	34.7	2.4	25.7	8.2	5.8	—	97.6	100

[a] Stages 1 and 2.

TABLE 5. VIRTUAL IMPACTOR DIMENSIONAL DATA

Test	Orifice diam, in.	Nozzle diam, in.	Orifice-nozzle distance, in.	Design		Designed aerodynamic D_{50}, μm
				Orifice	Nozzle	
No. 1	0.1195	0.1187	0.1204	a	b	3.5
No. 2	0.1195	0.1862	0.1196	a	b	3.5
No. 3	0.1195	0.0660	0.0615	c	f	3.5
No. 4	0.1207	0.0660	0.0657	d	f	3.5
No. 5	0.1235	0.0660	0.0635	e	f	3.5
No. 6	0.1861	0.0902	0.0902	c	f	7.0
	0.1193	0.0661	0.0652	c	f	3.5
No. 7	0.1848	0.1838	0.0915	c	f	7.0

nozzle. The aerodynamic cut diameter is also included, as predicted from the impaction equation, when a value of $\psi^{\frac{1}{2}} = 0.66$ is chosen as a compromise between the data from Conner,[15] $\psi^{\frac{1}{2}} = 0.6$, and the data from Hounam and Sherwood,[14] $\psi^{\frac{1}{2}} = 0.73$, when the impactor was operated at 1/2 cfm (14.15 ℓpm) as was the case of these tests.

For the first three tests, the "O-ring assembly" which holds the stage filter in place, was not washed for its contribution to impactor concentration measurements because the O-ring was glued to the metal assembly with rubber cement and probably for this reason the fluorescent background levels were never able to be brought down to an acceptable level. At that time it was reasoned that the O-ring assembly was small and its aerosol collection potential could be ignored. After Test No. 3, however, the O-ring was separated from the assembly, both parts were carefully scrubbed with steel wool and solvent removing the rubber cement, and these parts were analyzed for aerosol collection in subsequent tests. Another procedure instituted after Test No. 3 was to repeatedly wash each impactor part until the background fluorescence level was reached, record the wash volume and concentration for each repetition, and sum all these contributions to determine the concentration for that part. With these procedural modifications, good agreement was achieved in Test No. 4 between concentrations determined by the second probe and concentrations determined by summing all impactor part concentrations. Test No. 5 was an abbreviated test because the orifice design used drastically increased aerosol deposition on the nozzle.

Evaluating impactor design in regard to losses within the impactor, tests No. 1 and No. 2 demonstrated that orifice type a and nozzle type b were unequal to the assigned task. In both tests, aerosol deposits were observed inside and on the outside tip of the collection nozzle. Nozzle deposition measurements confirmed what was observed visually. Test No. 3 resulted in much reduced nozzle deposition, although orifice losses seemed unaffected. Test No. 4 attempted to reduce deposition within the orifice by making the gas flow channeling less abrupt, but this resulted in increased deposition on the can and nozzle. Microscopic examination of the backup filter showed quite a few primary particles, unlike other tests, indicating that this geometry reeuced the sharpness of size cut. Orifice type e was tried in Test No. 5, again toward the purpose of reducing deposition within the orifice, but this resulted in heavy aerosol deposits forming on the outside tip of the nozzle. The type e orifice made for this test had galled in the inlet plate and had to be machined out, thus the missing data point for Test No. 5.

From these tests, orifice type c and nozzle type f gave the best results. It seems that an abrupt change in flow contour is needed within the orifice to properly focus aerosol particles into the collection nozzle. Test No. 6 was designed to give information about impactor losses and size cut characteristics when the aerosol was somewhat smaller than the designed aerodynamic cut diameter of the stage. An orifice of design c and a nozzle of design f were made with larger diameters to provide a calculated cut diameter of 7.0 μm. For this test two stages were cascaded, with the calculated cut diameters of 7.0 and 3.5 μm bracketing the test aerosol particle size. The result indicated that the aerosol was unable to negotiate the sharp deflection of the airstream around the nozzle and can, evidenced by deposition on the outside of the nozzle and by annular deposition on the can at the nozzle base. Test No. 7 generally reinforced this conclusion, although deposition was less on the can and more on the nozzle.

Further information regarding impactor loss sites was obtained from a test conducted with high concentrations of polydisperse Arizona road dust (AC Fine Air Cleaner Test Dust). During this test 550 mg of dust was collected on the stage plus backup filter, whereas 714 mg of dust was washed from the various impactor parts. Deposition was heaviest on the inside and outside of the nozzle, on the can top (outer surface), within the can near the O-ring assembly, and on the inlet side of the orifice. Deposition to a lesser degree was also observed on the standoffs and on the outer can (not to be confused with the "can, outer surface") where the airstream turns to follow the passage between the outer can, and the "can, outer surface" on its way toward the next stage.

To resolve some of these difficulties, the breadboard was redesigned as presented in Figure 19. A taper of 20 degrees within the can was expected to reduce losses within the nozzle. The flange that connects the can to the inlet plate by means of the standoffs was lowered by almost 1/2 inch and reduced in diameter compared to the former can to reduce obstruction to the gas flow.

The O-ring assembly which holds the stage filter in place within the can had also been a site of aerosol deposition, collecting from 2.3 to 9.0 percent of the total aerosol concentration. The redesigned breadboard eliminated the O-ring assembly from the internal volume of the can which allowed this previously lost fraction of aerosol to be collected on the stage filter.

As mentioned above, the satellite population of small aerosol produced along with the primary particles by the spinning disc generator is estimated to be 10 percent of the total population. This is based on microscope examination of the backup filters, where primary particles were observed to a significant degree only in Test No. 4 and Test No. 7. In Test No. 4, the presence of primary particles on the backup filter was ascribed to poor separation characteristics of orifice type d, and in Test No. 7, by experimental design, as the calculated aerodynamic cut of the stage was greater than the test aerosol size. It was further assumed that the secondary aerosol population should not be inertially deposited on impactor surfaces because of their much smaller size. In fact, satellite aerosols were rarely observed on stage filters.

Microscope examination was encouraging in the sense that primary particles are found on the stage filter, and satellite particles on the backup filter, indicating good size segregation.

TESTS WITH SECOND VIRTUAL IMPACTOR BREADBOARD

Seven tests were performed with the redesigned virtual impactor, whose results are presented in Table 6.

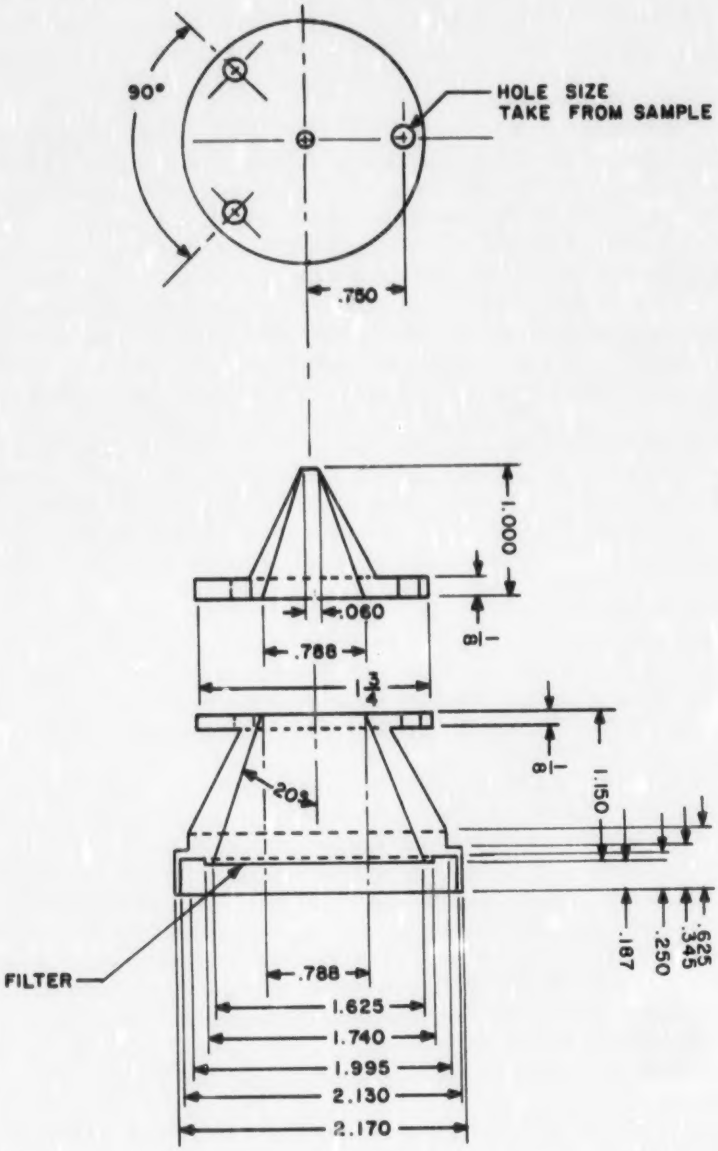
90°
HOLE SIZE
TAKE FROM SAMPLE
.750
1.000
.060
1/8
.788
1 3/4
1/8
1.150
20°
.187
.250
.345
.625
FILTER
.788
1.625
1.740
1.995
2.130
2.170

Figure 19. Redesigned collection nozzle.

TABLE 6. VIRTUAL IMPACTOR TEST DATA (SECOND VERSION) WITH MONODISPERSE AEROSOL

1	2	3	4	5	6	7	8	9	10	11	12	13
Date	Test no.	Stage, %	Backup, %	Inner nozzle, %	Outer nozzle, %	Submerged nozzle, %	Orifice, %	Σ impactor, %	Second probe, $\mu g/m^3$	D aero, μm	D_{50} μm	Nozzle and spacing
9/22	8	25.8	34.5	07.7	—	28.9[a]	5.1	105.4	102.6	6.54	7	1/2 wj
9/25	9	34.4	39.4	18.0	3.9	1.3	6.2	103.2	120.2	7.69	7	wj
9/29	10	27.4	35.2	17.8	6.1	3.2	1.9	91.6	118.6	5.18	7	3/4 wj
9/30	11	33.8	38.0	12.5	~0	0.2	6.9	91.4	169.1	6.33	7	5/4 wj
10/6	12	13.3	93.3	~0	—	5.6[a]	2.8	115.0	2.85	<1[b]	7	5/4 wj
10/7	13	66.4	0.8	14.7	—	2.9[a]	1.1	85.9	45.3	3.66	2.0	wj
10/10	14	5.9	84.9	~0	—	2.0[a]	2.6	95.4	3.05	<1[b]	7	5/4 wj

[a] Includes outer nozzle measurements.

[b] Aerosol was polydisperse, most particles were submicron.

A pure uranine aerosol was used for tests 8, 9, 10, and 11, the aerosol particles being less than spherical, although regular enough in shape to permit size analysis. Geometric standard deviation was typically 1.2. For tests 12, 13, and 14, the aerosol was composed of 90 percent uranine with 10 percent methylene blue added to enhance sphericity. The aerosol produced for tests 12 and 14 was largely submicron. The 3.66 μm aerosol generated for test 13 was very good, the particles being spherical with a geometric standard deviation of 1.14, although a satellite population about 1/3 as numerous as the primary population was sized at 1.38 μm, aerodynamic diameter. The satellite population was calculated to contribute less than 2 percent of the aerosol mass and is therefore considered insignificant.

Tests 8, 9, 10, and 11 were conducted for the purpose of determining collection nozzle diameter and orifice to collection nozzle distance that minimized losses. Column 12 of Table 6 indicates orifice diameter, W_j (width of jet), in terms of the calculated aerodynamic cut diameter at the test flow rate of 1/2 cfm (14.15 ℓpm). Column 13 indicates both the collection nozzle diameter and the orifice-nozzle spacing in terms of the orifice diameter. It can be observed that test 11, using the largest nozzle diameter and spacing resulted in the lowest loss within the impactor. Table 7 is presented to elucidate data presented in Table 4. In Table 7 percentages are calculated in terms of the total concentration measured within the impactor, whereas percentages in Table 6 are calculated in terms of concentration reported by the second, independent probe.

Test 8, in addition to providing information concerning nozzle diameter and orifice-nozzle spacing, was performed with great care to evaluate the impactor redesign. All parts were carefully washed to eliminate spurious fluorescence prior to testing, and all parts were analyzed for aerosol collection. Results were encouraging; only 3.3 percent of the aerosol was collected on parts other than the filters, nozzle, and orifice. In subsequent tests, only the filters, nozzle, and orifice were analyzed for aerosol collection, therefore the sum of aerosol concentrations for the impactor (column 9) is generally less than concentration reported by the independent probe (column 10).

Work by Langmead and O'Connor[37] in the U.K. in the late sixties on the development of a personal centripeter indicated that losses were maximum for aerosols slightly smaller than the cut diameter of the impactor stage. With this observation in mind, tests 12, 13, and 14 were conducted for the purpose of evaluating losses when aerosol size was much different from the cut diameter of the impactor stage. For the case in which the aerosol has much smaller particle size than the size which the stage was designed to collect, losses are much reduced (tests 12 and 14). This is fortunate, because as an aerosol passes through several impactor stages, that fraction destined for the last stages will not be significantly depleted by losses in the preceding stages. On the other hand, test 13 indicated that substantial losses could be anticipated when the aerosol was composed of particles greater in size than the cut diameter.

TABLE 7. IMPACTOR LOSSES

Test no.	Stage and backup %	Loss in impactor %
8	57.2	42.8
9	71.5	28.5
10	68.4	31.6
11	78.6	21.4
12	92.7	7.3
13	78.2	21.8
14	95.2	4.8

It may be noticed that token flow has not been mentioned in the preceding description of the impactor design. Token flow for the design phase was held constant at 0.5 ℓpm because it was felt that introduction of this variable would serve to obscure effects of design changes. Token flow was varied in subsequent tests with polydisperse aerosols (while keeping impactor geometry the same) with the important result that increased token flow decreased losses, but probably at the cost of reduced sharpness of cut.

The development phase reported above resulted in the decision that the optimum impactor geometry would be as it was in tests 11, 12, and 14; that is with the orifice to collection nozzle distance equal to 5/4 of the orifice diameter and the collection nozzle diameter also equal to 5/4 the orifice diameter.

COLLECTION EFFICIENCY VERSUS PARTICLE SIZE

An important determination for an impactor is the curve of collection efficiency versus particle aerodynamic diameter for a given stage, from which the particle size which has a 50 percent collection efficiency may be found. This is called the stage cut size or D_{50}. The slope of this curve at the D_{50} point, or the D_{84} minus the D_{16} points of this curve divided by the D_{50} point (geometric standard derivation) are measures of the stage sharpness of cut. Figure 20 illustrates this concept.

It was intended, at the onset of this program, to completely define this curve for at least one stage of the final recommended design. The GCA aerosol laboratory has the necessary equipment to perform this calibration given that a fairly accurate measure of particle density may be assumed.

However, as the program continued, other laboratory and field tests were deemed more important toward developing an instrument capable of providing on-site size distribution information and a calibration curve was not obtained. As noted in an earlier section, values of $\psi^{\frac{1}{2}}$ for the impaction equation from the work by Conner[15] and from Hounam and Sherwood[14] were considered in reasonable

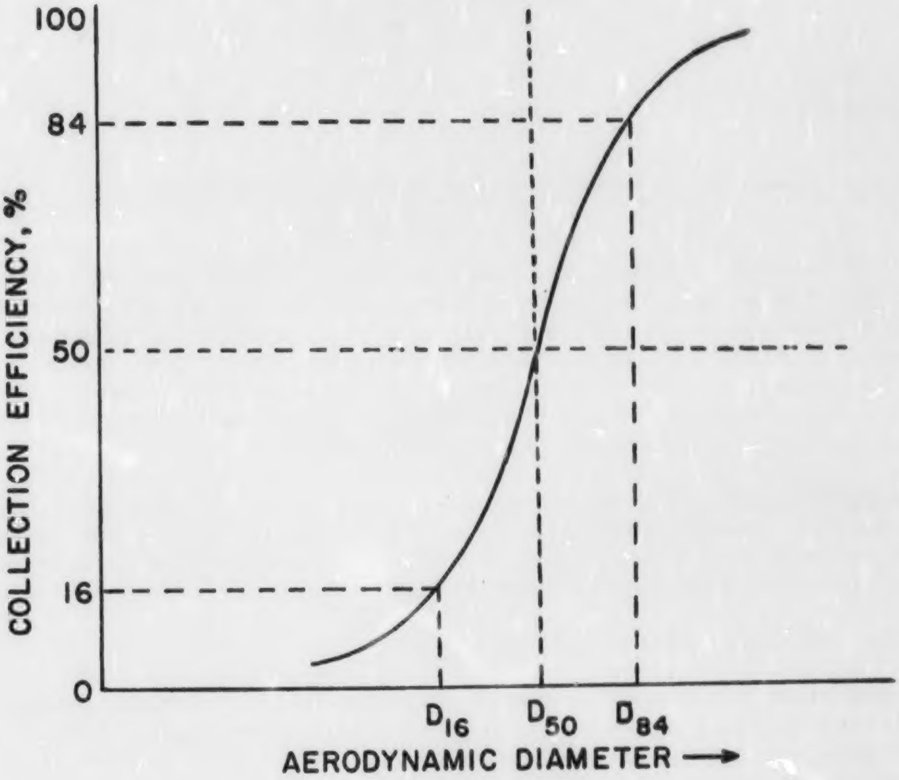

Figure 20. Collection efficiency versus particle size.

agreement with each other. The calculated cut size of the virtual impactor, obtained by taking an average of these values to obtain $\psi^{1/2} = 0.66$, was confirmed for those tests performed with monodisperse aerosol. Data in Table 6 supports the proposition that the calculated cut sizes are quite correct when one compares percentages caught on the stage and backup filters with the measured size of the aerosol and the calculated cut size.

Table 8 presents data taken near the end of the program toward establishing the cut size for the virtual impactor. The aerosol was 90 percent uranine and 10 percent methylene blue, displayed good sphericity, and was assumed to have a density of 1.3 g/cm^3 for the purpose of determining aerodynamic diameter. The aerosol was tainted, however, by the presence of the usual secondary or satellite population. Concentrations obtained by fluorometry therefore misrepresent the true segregating ability of the virtual impactor. In an effort to more accurately measure the capture efficiency, equal areas of the stage, backup, and second probe filters were examined under the microscope for test no. 37. Particle counts of the primary aerosol, also presented in Table 8, indicate better segregation than was indicated by the fluorometric analysis. Again, data in Table 8 supports the calculated cut size.

TABLE 8. CUT SIZE DATA

Test no.	Stage 1, 7.0 μm	Stage 2, 2.0 μm	Backup <2.0 μm	Second probe, total	D_{aero} aerosol	Comment
37	136 μg/m^3	56	4.3	235	7.4 μm	1.5 μm secondary aerosol present
	69.3%	28.5%	2.2%	120%		
38	156 μm/m^3	283	4.9	Not obtained	5.3 μm	Secondary present
	35.1%	63.8%	1.1%			
37	275	46	0	483		By count of primary 7.4 μm aerosol in equal areas
By particle count	85.7%	14.3%	0	150		

SECTION 8

PARTICLE SENSING METHODS

PRESSURE SENSITIVE TRANSISTOR

In addition to the three particle sensing techniques described in the original proposal; i.e., optical, electrical and pressure drop, a fourth method was investigated experimentally: impact momentum (or energy) detection. This technique is based on the detection of particles impacting on a diaphragm which in turn is part of a capacitor or other component whose electrical properties are altered by the deflection of the diaphragm. The device used in this particular set of tests was a pressure sensitive transistor (trade name PITRAN) whose collector current is a function of a force (or pressure) transmitted by the integral diaphragm onto the base-emitter junction. A full scale output of 2 volts is obtained with a pressure of 1/4 psid applied to the transistor top which forms the diaphragm.

The PITRAN was installed in an impactor configuration such that the diaphragm was used as the impaction surface. By recessing the transistor within a stagnation volume behind an orifice facing the impactor nozzle, the system was made into a centripeter-sensor combination. The output of the pressure-sensitive transistor was a.c.-amplified and displayed on an oscilloscope. The main problem encountered was the noise level expectedly associated with the turbulence of the air jet. This noise level was found to be a strong function of flowrate; i.e., of air velocity of the jet. At about 30 m/s the noise component of the signal was about 2 mV, whereas at 240 m/s it reached 50 mV. When large particles of Arizona road dust (estimated size >20 μm) where injected into the impactor inlet distinct signal pulses were discerned on the oscilloscope display, with a signal/noise ratio of the order of 2 to 4. Smaller particles could thus not be detected as their signal was buried in the noise. An attempt was made to perform a frequency analysis of the noise-signal combination in order to distinguish the signal by a possible frequency discrimination but this attempt was not successful.

The turbulence-generated noise appeared to be an intrinsic limitation of this technique, which was therefore not pursued.

OPTICAL SENSING OF PARTICLE CONCENTRATIONS WITHIN THE VIRTUAL IMPACTOR STAGE

The optical extinction method of measurement was pursued to perform aerosol concentration sensing within the centipeter stage. The electronic circuitry designed for this purpose is depicted in Figure 21. The optical path is shown in Figure 22. A reference source is derived from the laser and transferred to

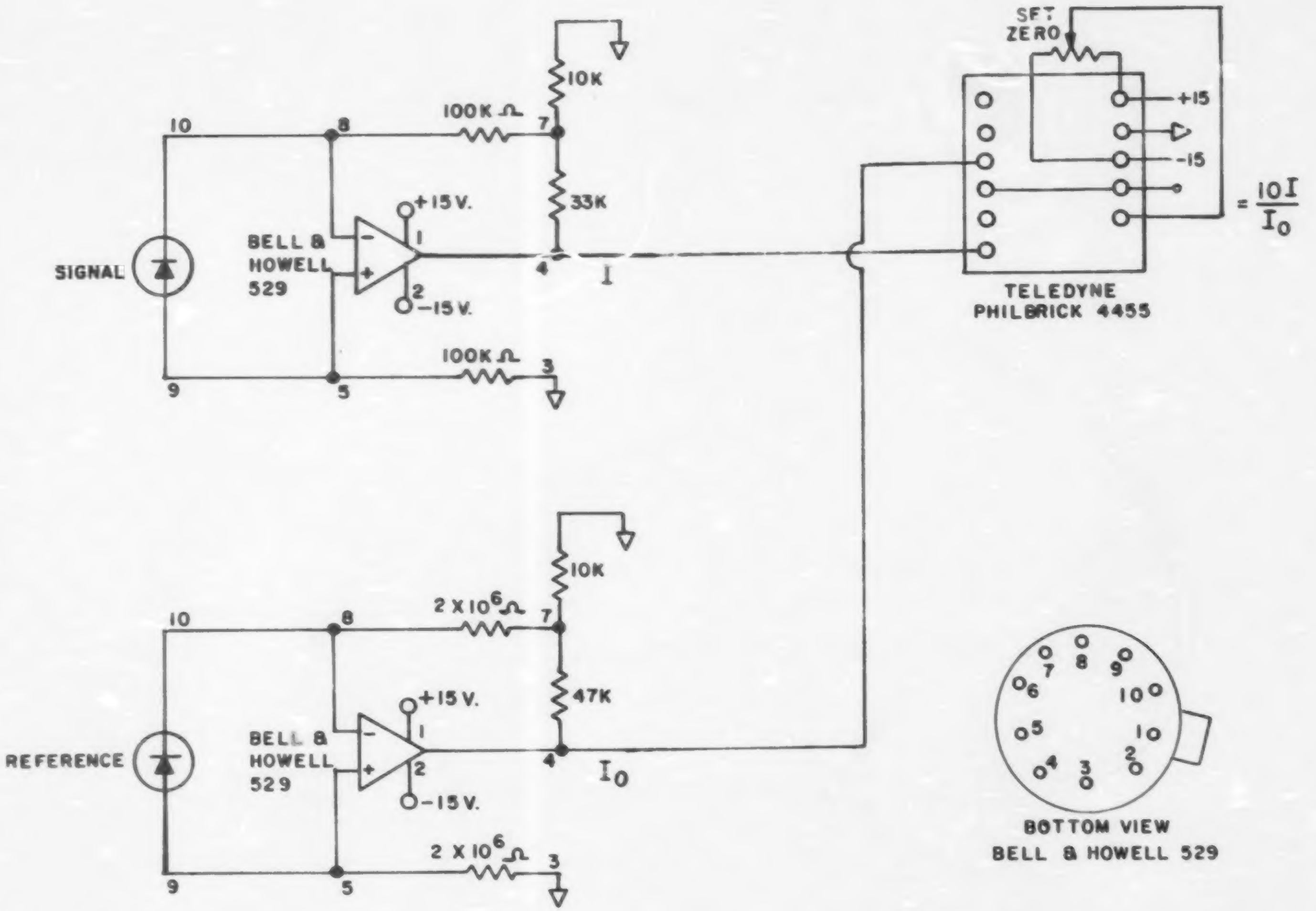
SET ZERO
10K
100K Ω
10
8
7
+15 V.
33K
BELL & HOWELL 529
SIGNAL
1
2
−15 V.
4
I
100K Ω
9
5
3
+15
−15
$= \frac{10I}{I_0}$
TELEDYNE PHILBRICK 4455
10K
2 X 10^6 Ω
47K
REFERENCE
BELL & HOWELL 529
I_0
2 X 10^6 Ω
BOTTOM VIEW
BELL & HOWELL 529

Figure 21. Electronic schematic.

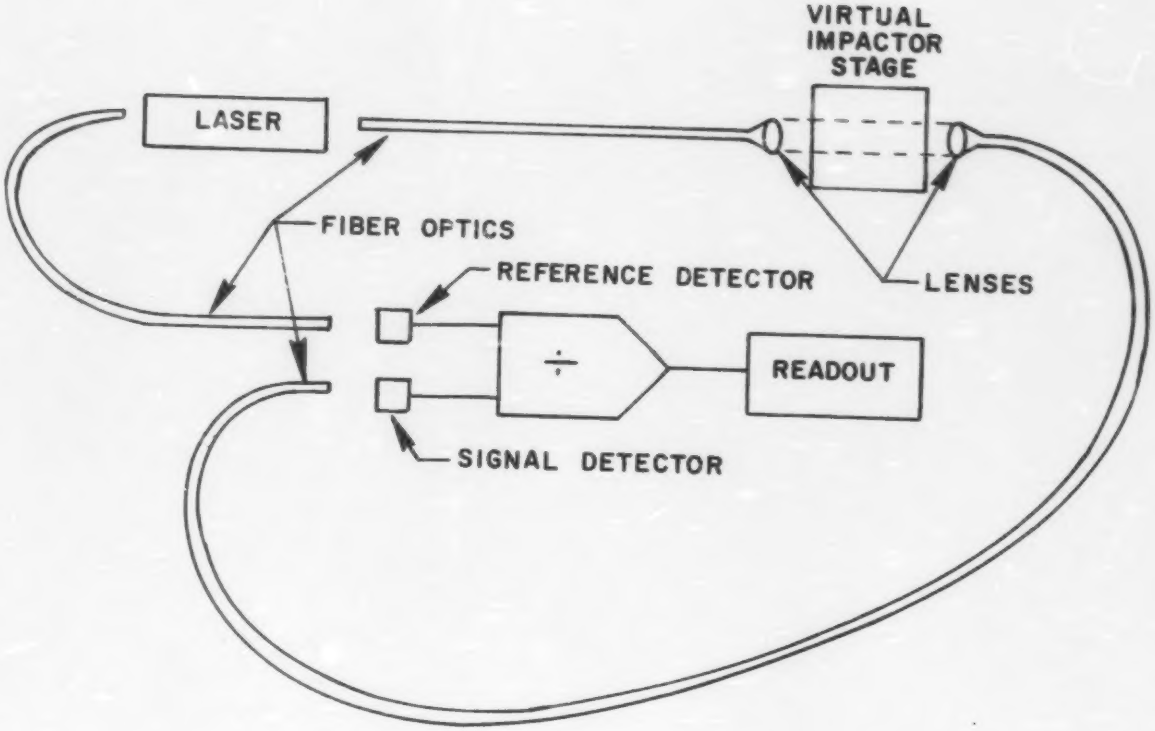
VIRTUAL
IMPACTOR
STAGE
LASER
FIBER OPTICS
REFERENCE DETECTOR
LENSES
÷
READOUT
SIGNAL DETECTOR

Figure 22. Optical sensing system.

the reference diode by fiber optics directly. It may be noted that where several optical stages were employed, only one reference channel is required. The signal is taken from the output of the centripeter stage (Figure 6). Suitable gain was provided by the feedback shown and the two outputs connected to the divider circuit (Teledyne Philbrick 4455) which yields 10 I/I_0 volts output.

Two successful experimental runs were made. In the first, a Wright dust feeder was connected to the inlet of the virtual impactor stage with a calculated cutoff of 3.5 μm. All larger particles therefore entered into the optical detector volume. From the size fraction data provided with the AC fine air cleaner test (Arizona road dust), a mass median diameter of 14.5 μm was derived. The procedure adopted after some experimentation was as follows. With the entire apparatus clean a fairly low dust feed rate was provided to the impactor inlet for a measured 5 minutes. A reading on a digital voltmeter of the output of the divider was taken prior to the initiation of dust feed and again after the dust had been drawn completely out of the optical path. During the run, measurements of I/I_0 were taken every 15 seconds and subsequently averaged. The filter was weighed to obtain a gravimetric measurement. Knowing the flow rate, and assuming a value for particle density $\rho = 2.5$, optical extinction coefficient $\bar{k} = 2$ and $\bar{A} = 1.65 \times 10^{-6}$ cm^2, two values of number concentration may be derived, the gravimetric and the optical value. The results are plotted for several increasing dust feed rates in Figure 23. Some scatter is observed in the data and it was noted that I_0 had declined to 70 percent of its initial value after five runs at fairly high overall concentration, due to dust deposition on the optics.

A second run was made with another impactor stage ahead of the optical measurement stage. This first stage had a nominal cutoff of 3.5 μm and the impactor at the optical stage had a nominal cutoff of 1.5 μm so that the optical volume received particles between 1.5 and 3.5 μm. The measurements were made as before except that the readings of I/I_0 were only used after an equilibrium had been reached, usually after about 1 minute. The results of this run are shown in Figure 24. As can be seen there is less scatter in this data, but the slope is lower.

In both cases (Figures 23 and 24), the optical readings gave higher number concentrations than the gravimetric measurements which is most probably due to simplifications in the optical model. However, losses to the gravimetric method were not trivial and may reasonably have contributed to this slope.

Improvements may be made to the optical system by inhibiting the contamination of the optics. In the system tested the surfaces were recessed about 0.5 cm into the chamber wall and this undoubtedly reduced the problem. Further recessing as well as simple baffles would result in additional improvement. Purge air around the lenses would improve the situation considerably at the cost of much greater complexity. In any redesign of the instrument for optical sensing, a reduction in the volume without a reduction in optical path length would decrease the time required to obtain a steady reading of I/I_0.

ELECTRICAL SENSING

Two methods have been considered for measuring the output of a virtual impactor stage using electrical sensing. One of these is to use corona charging

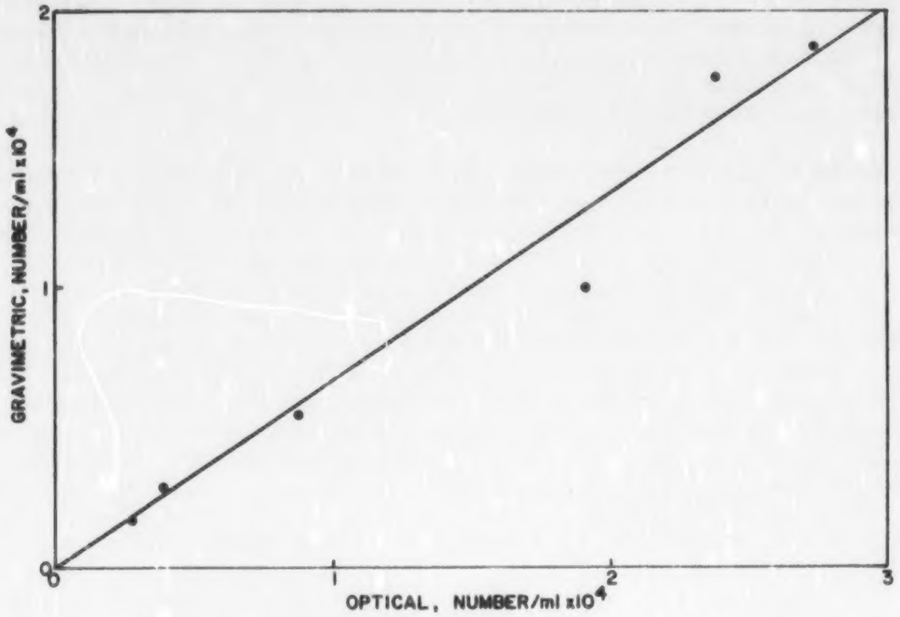

Figure 23. Aerosol number concentration by gravimetric versus optical detection for Arizona road dust, aerosol particles greater than 3.5 μm.

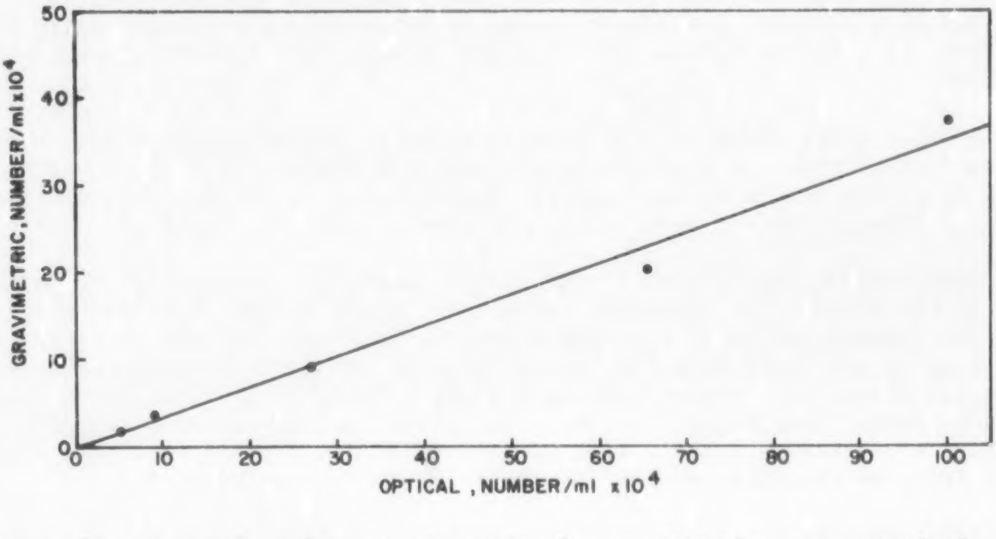

Figure 24. Aerosol number concentration by gravimetric versus optical detection for Arizona road dust, aerosol particles less than 3.5 μm but greater than 1.5 μm.

of the dust as in an electrostatic precipitator, and to collect the dust on an appropriate electrode. While this method would undoubtedly yield usable signals, the disadvantages are several. Highly charged dust precipitates everywhere, thus much of it may not be collected on the desired surface. The electrical noise of the corona discharge will tend to interfere with the small electrical signal currents and implementation is inherently complicated.

The alternative was to use contact charging, a relatively little understood phenomenon whereby dust contacting an electrode at high velocity (100 m s^{-1}) yields a charge to the electrode. The response of such a system is not quite linear and exhibits some temperature dependence.

Figure 25 shows the design of the contact charging device. The dust laden gas is forced through a constriction which (1) forms a critical orifice to ensure constant gas flow and (2) impacts the dust particles onto an electrode. This electrode is coupled to a sensitive electrometer for current measurement.

Initial tests were performed with clean filtered air to determine background current signal levels. These were determined to be about 10^{-12} A using the first test fixture which was fabricated entirely out of teflon with the exception of the sensing needle (steel). Subsequently a series of tests was performed with Arizona road dust at concentrations ranging from about 1 mg/m^3 to 300 mg/m^3, and a monotonic increase of signal current with dust concentration was observed. During these tests an unusual phenomenon was observed: after one or two hours of operation the polarity of the signal suddenly reversed from an initial positive current to a negative one. This phenomenon was consistently observed each time the test was performed. It was suspected that a gradual charging up of the teflon body of the test fixture resulted in a sudden breakdown transferring this charge to the sensing needle when the potential reached a critical value. In order to preclude this problem a similar test fixture was then fabricated out of aluminum with a small insulating ring separating the body of the fixture from the sensing needle. The metallic body was then electrically grounded to provide a leakage path for any charge buildup. This new device was tested in a similar manner as the teflon fixture and no evidence of polarity reversal was observed. Background signal current dropped to about 10^{-13} A at the same time as signal currents 10^{-10} to 10^{-9} A were detected for dust concentrations between about 30 and 300 mg/m^3, respectively. These readings were obtained with a flowrate of 0.55 liters/min typical of the token flows required for a virtual impactor stage.

This test fixture was further tested to determine repeatability and reliability of the method. Arizona road dust concentrations were varied between about 3 mg/m^3 to 300 mg/m^3 as measured by a GCA model RDM 101 dust monitor which had previously been calibrated against gravimetric samples over the subject concentration range. For concentration levels up to about 120 mg/m^3 the current from the sensing needle remained steady for test periods of about 20 to 30 minutes, but for concentration levels greater than about 120 mg/m^3 to about 300 mg/m^3 the current was observed to decay from a higher value down to values associated with the 120 mg/m^3 concentration level. Data for the tests up to about 120 mg/m^3 (X's) and the data collected earlier (circles) are presented in Figure 26 which indicates a measure of repeatability for this method.

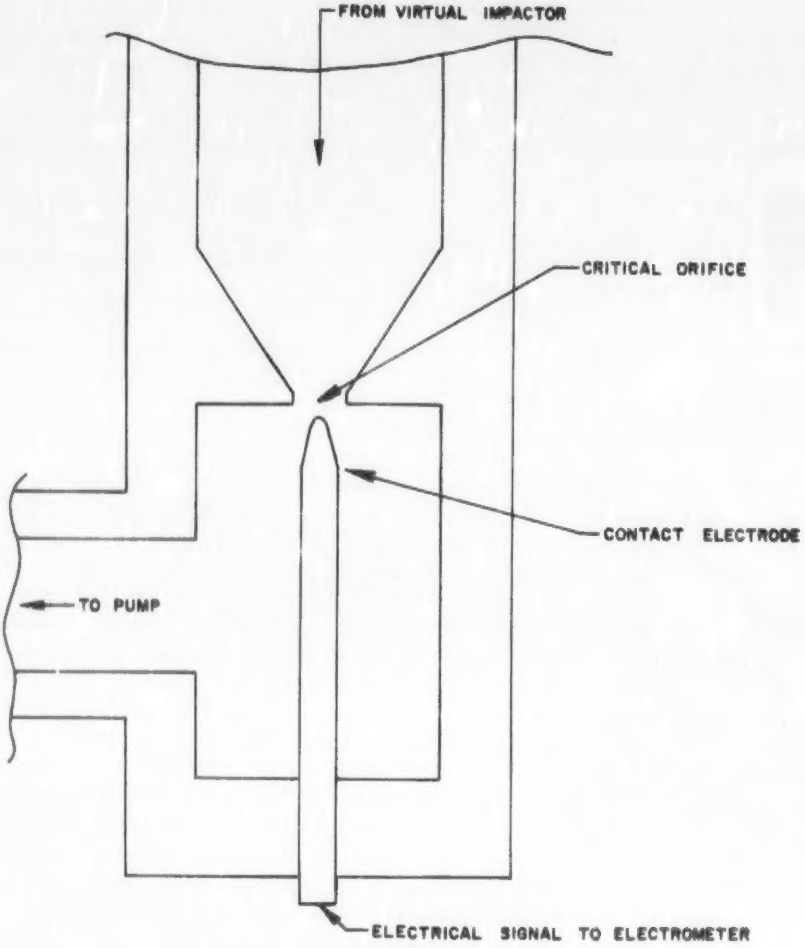
FROM VIRTUAL IMPACTOR
CRITICAL ORIFICE
CONTACT ELECTRODE
TO PUMP
ELECTRICAL SIGNAL TO ELECTROMETER

Figure 25. Electrical sensing design.

The test fixture was run at temperatures elevated above ambient. After some experimentation to find a heating method which did not disturb the normal operation of the device, the following was adopted. A few turns of resistance wire was bifilar-wound around the device and connected to the secondary winding of a filament transformer. The center tap of this winding was grounded to the body of the test device. The input power to the primary of the filament transformer was connected to a Variac transformer. The whole assembly was insulated thermally with asbestos cloth, and a thermocouple probe attached to the body of the device, thermally insulated from direct contact with the heater element.

Trial runs were made with the heater energized at very low power to check that no disturbance to the normal operation was occurring on account of the

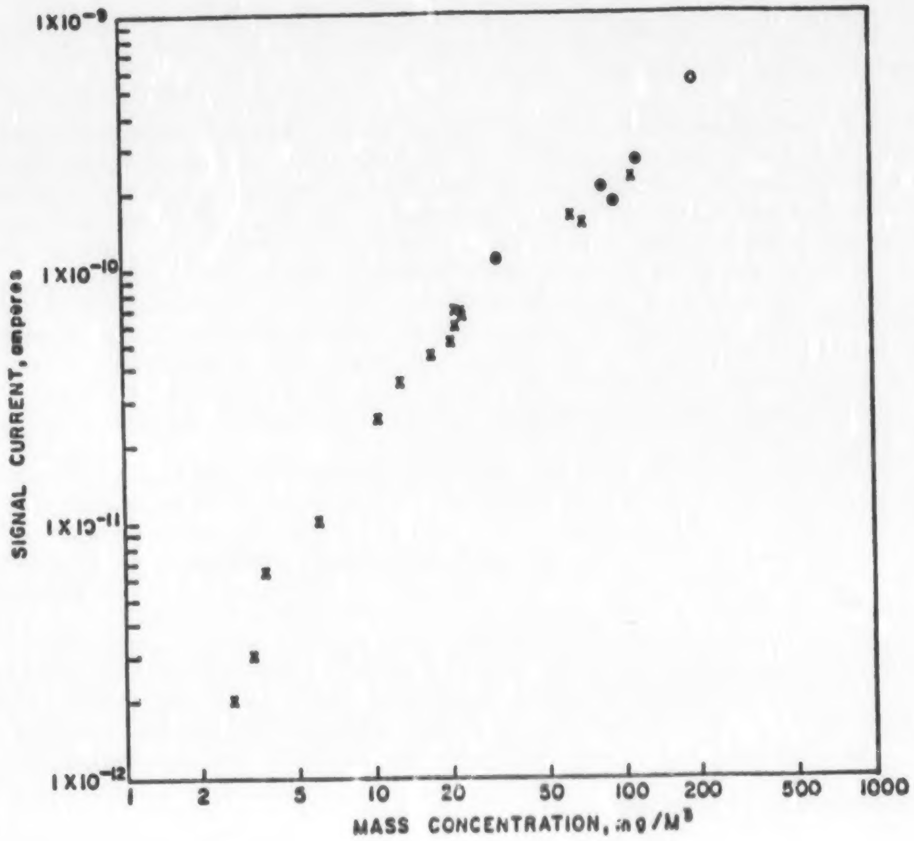

Figure 26. Electronic sensing data.

modification. No detectable temperature rise occurred and normal operation was verified. As before, at high dust concentrations (200 mg/m^3) the current fell after 30 minutes or so, to a value typically half of the initial value. Since the dust feed could not be assumed constant, electrical measurements were compared with values obtained by a GCA RDM 101 Dust Monitor, as noted previously.

Several runs were performed at elevated temperatures. As the temperature is steadily elevated, various forms of erratic behavior manifested themselves. At temperatures up to 70°C slight changes in sensitivity (either increasing or decreasing) were observed but operation could be described as stable. Above this temperature the current generally became negative instead of positive. The precise temperature at which this happened depended on several variables which have been incompletely unfolded. Among these are the thermoelectric effect (due to different temperatures at the junctions of different conductors), the rate of change of temperature as well as the temperature itself, and the dust loading at the inlet. A particular feature that was noted was that the device frequently responded more as a voltage source than as a current source. This could be determined by the indicated electrometer current being strongly dependent on input impedance.

In some instances this voltage source characteristic (whether positive or negative), and the polarity reversal disappeared if the device was permitted to cool slightly, and in other cases it required a return to room temperature. The rate of heating and cooling was a significant factor, giving more erratic responses for higher rates. This latter effect is presumably due to thermoelectric effects which have their most dramatic impact with greatest temperature differences. Efforts were made to make all the device components of aluminum. The collector electrode was originally stainless steel and a new aluminum one was fabricated, but with no improvement in stability. Since the electrode lead attachment could not be made at the same point as the ground return an intrinsic difficulty is seen, owing to inevitable temperature differences.

It is believed, however, that most of these problems could be substantially mitigated. The change in sensitivity after a period with high concentrations is most probably due to the aggregation of dust in the vicinity of the impaction site and would surely yield to improved aerodynamic design that would enhance scouring. Careful attention to intermetallic connections would also help to make the unit operable at sufficiently elevated temperatures. However, it is judged that in the scope of the current program that other approaches are more viable, especially when one considers the small magnitude of the current (down to 10^{-12} A) that has to be measured accurately at a location several meters from the device itself. Thus, work was discontinued on the contact electriciation method of particulate detection and measurement within this program.

PRESSURE DROP SENSING METHOD

The pressure drop sensing method was the selected method within the present program because of its simplicity, reliability, repeatability, and self-calibrating ability. Data, which are more conveniently presented in the next section on lab and field tests, support this selection.

SECTION 9

VIRTUAL IMPACTOR-PRESSURE DROP LAB AND FIELD TESTS

LAB TESTS

After the impactor design had been reasonably well optimized using monodisperse aerosol, the impactor was modified by fitting it with pressure taps to permit the sensing of the pressure drop across the stage filters. Figure 27 is a schematic of the modified three-stage virtual impactor prototype. Figures 28 and 29 are photographs of this final version of the device as used during the subsequently reported laboratory and field tests.

Tables 9 and 10 contain data collected during the first trials of the pressure drop sensing method. During Tests 15, 16 and 17, some further modification was performed by varying the second stage collection nozzle diameter. Arizona road dust was used for all tests in Tables 9 and 10 in concentrations high enough that deposition on the various internal impactor surfaces could be readily observed, thus facilitating those changes in the second stage collection nozzle required to minimize losses. It was encouraging that the ratio of collection nozzle diameter to orifice diameter determined to result in minimum losses using Arizona road dust was 5/4 as had been determined from the monodisperse aerosol tests. However, the orifice to collection nozzle distance was closed down to one orifice diameter, rather than 5/4 orifice diameter, without any apparent detrimental effect. This, it was felt, would result in a sharper cut size.

In regard to the pressure drop sensing method, difficulties were encountered in Tests 15 through 22 in that a linear pressure drop versus time curve was not obtained for Stage 1. Careful inspection of the first stage filter holder, revealed a leak between the downstream side of the filter and the surrounding volume which carries the main impactor flow. Sealing of this leak resulted in linear pressure drop versus time curves in Test 23, which are presented in Figure 30. Curves for Stage 2 were all linear for these tests.

For the following tests, data for which are presented in Table 11, the impactor was set up and operated in the same manner as it had been for Test No. 23 (Table 9). Exceptions included two tests during which the token flow was increased, and one test in which a novel geometry was tried in the second stage. Aerosols sampled during these tests included Arizona road dust (AC Fine Air Cleaner Test Dust), coal dust, fly ash, and iron oxide. The calculated aerodynamic diameter cut size was 7.0 μm for the first stage and 2.0 μm for the second stage for those tests conducted with a nominal token flow of 0.5 ℓpm; i.e., for those tests conducted as in Test No. 23. For the two tests in which token flow was increased, total inlet flow also increased due to the fact that

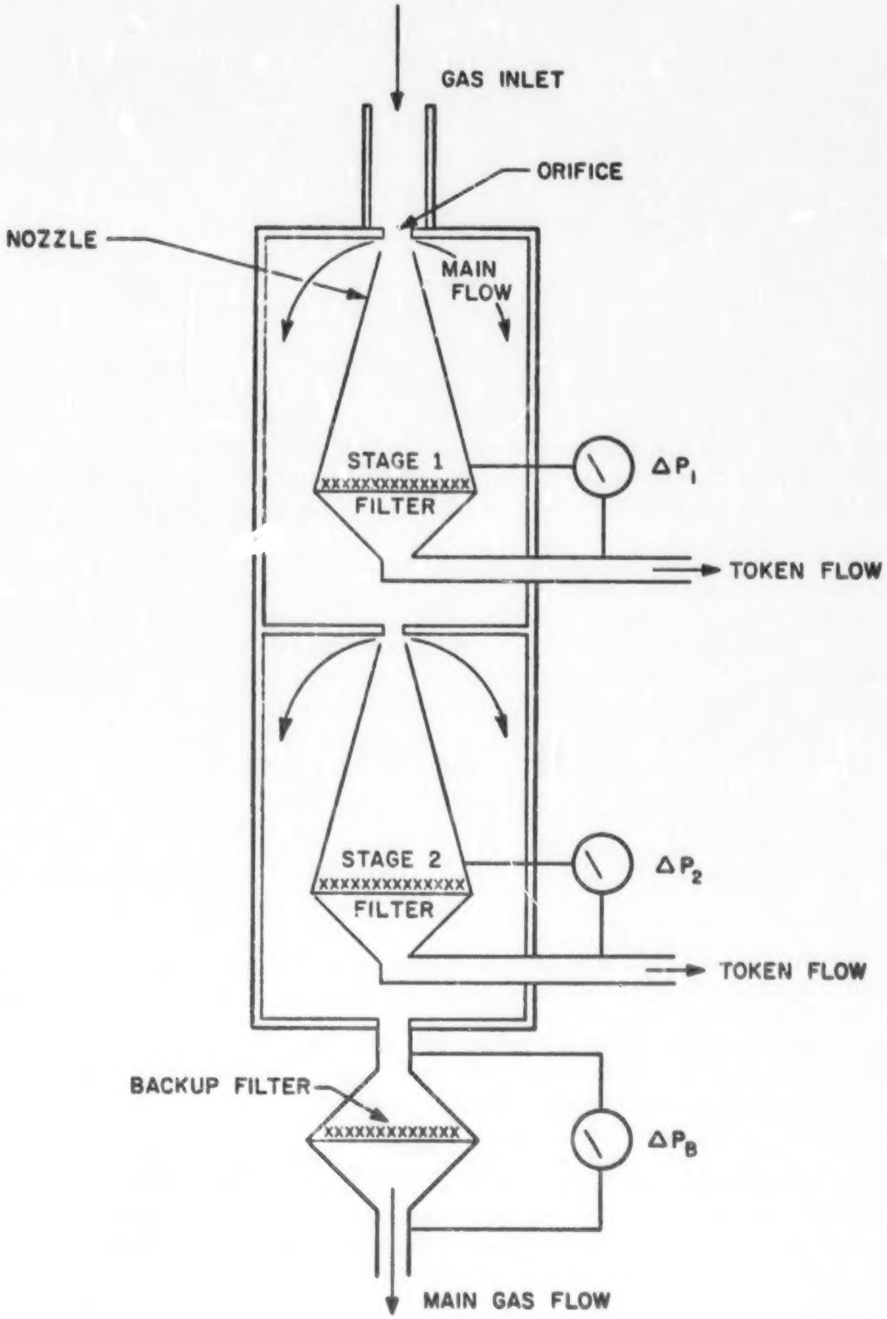
GAS INLET
ORIFICE
NOZZLE
MAIN FLOW
STAGE 1
FILTER
ΔP1
TOKEN FLOW
STAGE 2
FILTER
ΔP2
TOKEN FLOW
BACKUP FILTER
ΔPB
MAIN GAS FLOW

Figure 27. Virtual impactor schematic.

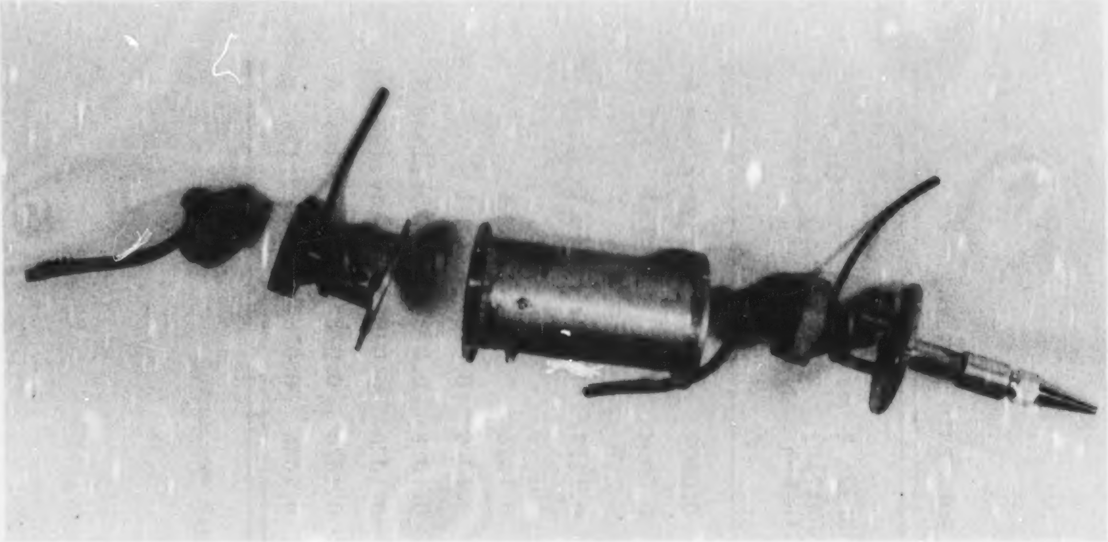

Figure 28. Final version of prototype virtual cascade impactor, disassembled.

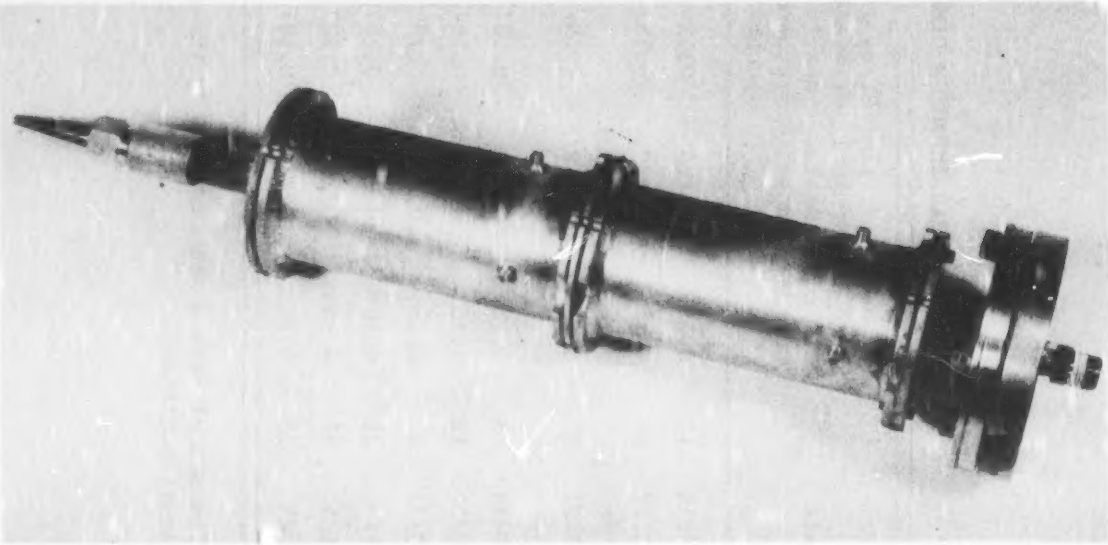

Figure 29. Final version of prototype virtual cascade impactor, assembled with backup filter.

TABLE 9. VIRTUAL IMPACTOR DIMENSIONAL DATA FOR TESTS 15 THROUGH 23

Date	Test no.	Stage 1 orifice, inches*	Stage 1 nozzle, inches	Stage 1 orifice-nozzle distance, inches	Stage 2 orifice, inches	Stage 2 nozzle, inches	Stage 2 orifice-nozzle distance, inches	Filter media used
10/19	15	0.185	0.229	0.184	0.0835	0.0802	0.0817	Fiberglass A
10/27 a.m.	16	0.185	0.229	0.187	0.0835	0.0802	0.0803	VM-1
10/27 p.m.	17	0.185	0.229	0.187	0.0835	0.1417	0.0887	VM-1
10/28	18	0.185	0.229	0.187	0.0835	0.1026	0.0787	VM-1
10/29	19	0.185	0.229	0.187	0.0835	0.1026	0.0787	VM-1
10/31	20	0.185	0.229	0.187	0.0835	0.1026	0.0787	Fiberglass A
11/3	21	0.185	0.229	0.187	0.0835	0.1026	0.0787	Fiberglass A
11/4	22	0.185	0.229	0.187	0.0835	0.1026	0.0787	Fiberglass A
11/5	23	0.185	0.229	0.187	0.0835	0.1026	0.0787	Fiberglass A

*The use of inches was dictated by the available length measuring instrumentation.

TABLE 10. VIRTUAL IMPACTOR TEST DATA (WITH ARIZONA ROAD DUST)

Test no.	Stage 1 conc., mg/m^3	Stage 2 conc., mg/m^3	Backup conc., mg/m^3	Total[a] impactor conc., mg/m^3	Second[b] probe conc., mg/m^3	Stage 1, %	Stage 2, %	Backup, %	Impactor as % of 2nd probe, %	Impactor loss, %	Test duration, minutes
15	0.98	1.17	0.56	2.71	3.97	36.2	43.1	20.7	68.3	31.7	173
16	torn	131.4	46.9	—	250.9	—	—	—	—	—	35
17	66.1	27.1	134.8	228.0	263.1	29.0[d]	11.9	59.1	86.7	13.3	36
18	65.5	116.2	43.8	225.5	234.6	29.0[d]	51.6	19.4	96.1	3.9	36
19	72.4	113.3	56.6	242.3	261.3	29.9[d]	46.7	23.4	92.7	7.3	36
20	30.8	76.8	44.4	152.0	162.8[c]	20.3	50.6	29.2	93.4[e]	6.6	43
21	48.1	130.7	61.1	239.9	244.2	20.1	54.4	25.5	98.2[e]	1.8	60
22	44.4	124.4	67.3	236.1	243.1	18.8	52.7	28.5	97.1[e]	2.9	43
23	34.1	123.0	96.7	253.8	269.4	13.4	48.5	38.1	94.2	5.8	60

[a] Impactor flowrate = 14.25 (main flow) + 0.6 + 0.5 (token flows) = 15.35 ℓpm.

[b] Second probe flowrate = 15.0 ℓpm.

[c] The Wright Dust Feeder failed; therefore concentration is reduced in this test.

[d] Replica tests for first stage; note repeatability for 7.0 μm size cut.

[e] Replica tests (all conditions similar).

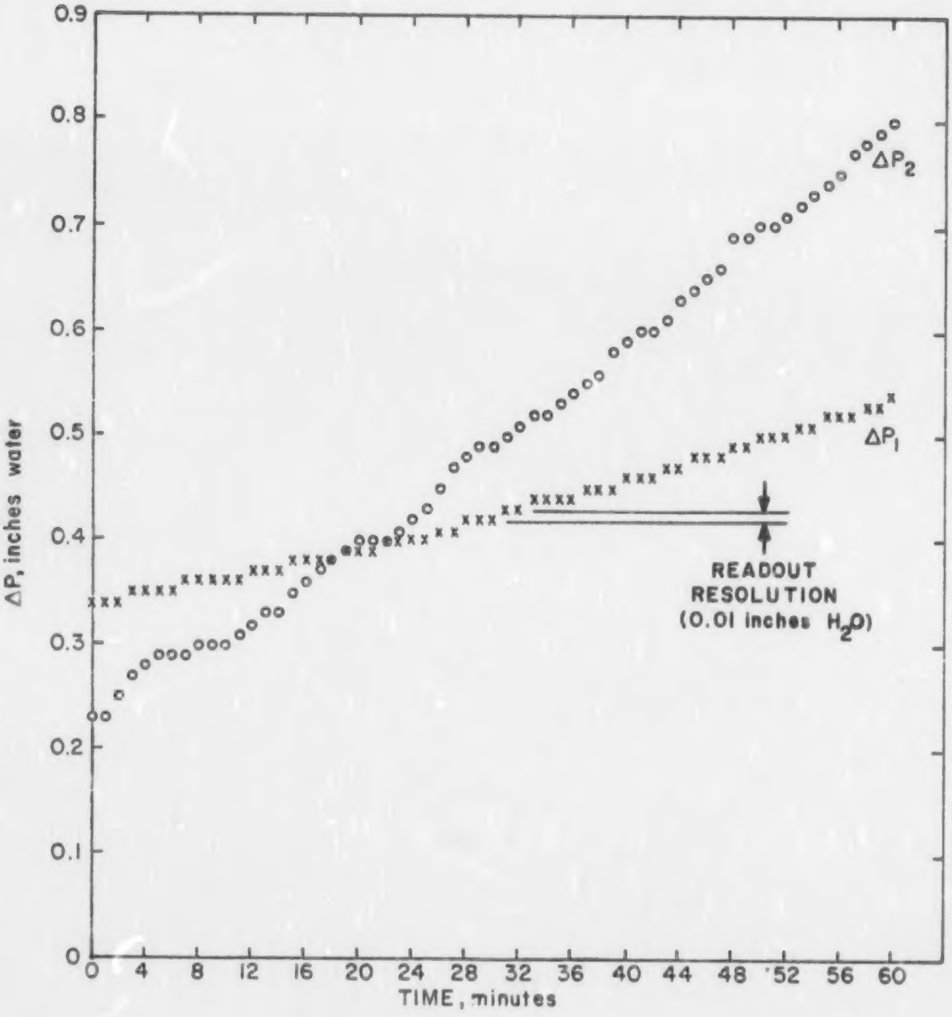

Figure 30. Data for Test 23.

TABLE 11. VIRTUAL IMPACTOR DATA (POLYDISPERSE DUSTS)

Test no.	Stage 1 conc., mg/m³	Stage 2 conc., mg/m³	Backup conc., mg/m³	Impactor total conc., mg/m³	Second probe conc., mg/m³	Test duration, min.	Token flow, lpm	Dust	Test no.	Impactor distribution			Impactor as % of 2nd probe %	Impactor loss, %	Stage 1 Cp, 10⁵ sec⁻¹	Stage 2 Cp, 10⁵ sec⁻¹	Backup Cp, 10⁵ sec⁻¹	Total filter		
										Stage 1, %	Stage 2, %	Backup, %						1st half of test Cp, 10⁵ sec⁻¹	2nd half of test Cp, 10⁵ sec⁻¹	
23	34.1	123.0	96.7	253.8	269.4	60	0.5	Arizona road dust	23	13.4	48.5	38.1	94.2	5.8	3.67	3.48	–	–	–	Fiberglass A
24	31.1	113.4	79.8	224.3	274.1	36	0.5	Arizona road dust	24	13.9	50.5	35.6	81.8	18.2	1.96	3.09	–	–	–	Gelman VM-1 media
25	34.3	108.7	84.6	227.6	266.4	36	0.5	Arizona road dust	25	15.1	47.7	37.2	85.4	14.6	3.01	4.43	–	–	–	Millipore AAWP media
34	34.5	132.2	105.0	271.7	321.6	36	0.5	Arizona road dust	34	12.7	48.7	38.6	84.5	15.5	2.88	2.90	16.6	8.37	9.98	Fiberglass A
35	35.4	130.3	80.1	245.8	267.0	25	1.0	Arizona road dust	35	14.4	53.0	32.6	92.1	7.9	2.93	3.71	13.8	8.87	9.30	Fiberglass A
36	64.4	142.5	57.1	264.0	276.9	30	1.7	Arizona road dust	36	24.4	54.0	21.6	95.4	4.6	3.35	5.20	15.3	8.88	9.02	Fiberglass A
26	9.4	13.2	2.7	25.3	24.5	60	0.5	Coal dust	26	37.1	52.2	10.7	103.4	-3.4	0.69	1.17	–	–	–	Fiberglass A
27	30.6	62.4	9.8	102.8	143.2	72	0.5	Coal dust	27	29.8	60.7	9.5	71.8	28.2	0.90	1.57	7.44	–	–	Fiberglass A
28	–[a]	126.1	12.2	–	349.1	60	0.5	Fly ash	28	–	–	–	–	–	0.42[b]	1.10	8.99	–	–	Fiberglass A
29	126.9	98.9	8.2	234.0	288.0	84	0.5	Fly ash	29	54.3	42.2	3.5	81.2	18.8	0.32	1.08	6.96	–	–	Fiberglass A
30	42.6	38.8	34.8	116.2	138.6	40	0.5	Iron oxide	30	36.7	33.4	29.9	83.8	16.2	0.43[c]	1.85	72.0[d]	–	–	Whatman backup
31	34.8	105.7	128.7	269.2	357.1	60	0.5	Iron oxide	31	12.9	39.3	47.8	75.4	24.6	1.97	2.20	7.81	–	–	Fiberglass A
32	41.3	94.0	112.0	247.3	316.4	60	0.5	Iron oxide	32	16.7	38.0	45.3	78.2	21.8	1.46	2.11	6.70	–	–	Fiberglass A
33	29.2	86.6	64.3	180.1	294.7	60	0.5	Iron oxide	33	16.2	48.0	35.8	61.1	38.9[e]	1.81	2.20	6.88	5.19	5.19	Fiberglass A

[a] Filter fumbled, data lost.

[b] Based on estimate of Stage 1 Δm, by subtracting Stage 2 & backup Δm from 82 percent of 2nd probe Δm.

[c] Unreliable because pressure change here was only 0.02 in. H_2O.

[d] A Whatman type filter paper was used here, which apparently is unsuitable for air sampling.

[e] High loss due to trial of novel Stage 2 geometry.

the same critical orifice was used downstream of the backup filter for flow control. Accordingly, the calculated aerodynamic cut diameter decreases. Since the dependence is inversely proportional to the square root of the total flow, the actual particle cut size was barely affected.

The total flow and token flows as well as the flow through the independent filter were measured before and after each test with calibrated rotometers. The total flow and independent filter flow decreased during the tests, always by a small amount, because of the method of flow control employed; that is, the use of critical orifices between the filter and the air pumps. As pressure builds across the filter, the gas density between the filter and the critical orifice decreases and the volume flow upstream of the filter, where pressure is near ambient, decreases. The flow change for the token flows was always undetectable because the pressure drop was very slight, usually less than 1 in. H_2O^* = 0.003 atm, but the flow change for the independent filter was often significant, with pressure drops across that filter sometimes as great as 2 psi = 0.14 atm. After a certain number of tests, the area of the impactor backup filter was increased, by a factor of about 4, to decrease the pressure drop across it, thus improving impactor flow control. The test data as presented in Table 11 have been corrected for flow variation. Concentrations, as reported, have been calculated using average flow, as determined by flowmeter measurements. The nominal impactor flow for these tests was 1/2 cfm = 14.15 ℓpm.

Discussion of the test data in Table 11 will begin with the assessment of the pressure drop particle sensing method in mind. Pressure drop across the filters was recorded as a function of time. For the tests performed with Arizona road dust and coal dust a Wright dust feeder was employed, which can be relied upon to generate dust at a fairly constant rate. For the tests performed with fly ash and iron oxide an improvised auger type feeder with an aspirator for dust pickup and dispersion was employed, the feed rate for which was probably not as constant. Figures 31, 32, 33 and 34 show the pressure drop versus time relationship for coal dust, fly ash, iron oxide, and Arizona road dust, respectively. It may be observed that the plots are rather straight, after some initial transient. The reasons for the initial transient, or nonlinear response, are unclear, although initial cake formation and initial buildup of aerosol concentration in the dust chamber are easily cited. In these figures, Δp_1 denotes the pressure drop across the first impactor stage, and Δp_2 denotes the pressure drop across the second stage. It will be observed that the initial pressure drop across the first and second stage filters are different in Figures 31, 32, and 33. This is because the critical orifices for the token flow are exceedingly small and slightly different. The Stage 1 token flow was measured as 0.6 ℓpm, and the Stage 2 token flow as 0.5 ℓpm. The token flows in Figure 34 were more nearly equal, at slightly less than 1.0 ℓpm, resulting in equal initial pressure drop across both stage filters. It will be observed that the initial pressure drop across the backup filter is higher for Figures 30 and 31, compared with Figures 32 and 33 because a larger area backup filter was used in the latter two tests. It may also be observed that some of the Δp versus t curves for the

---

*The use of English units of pressure; e.g., inches H_2O and inches Hg was indicated by the scale calibrations of available pressure drop sensors.

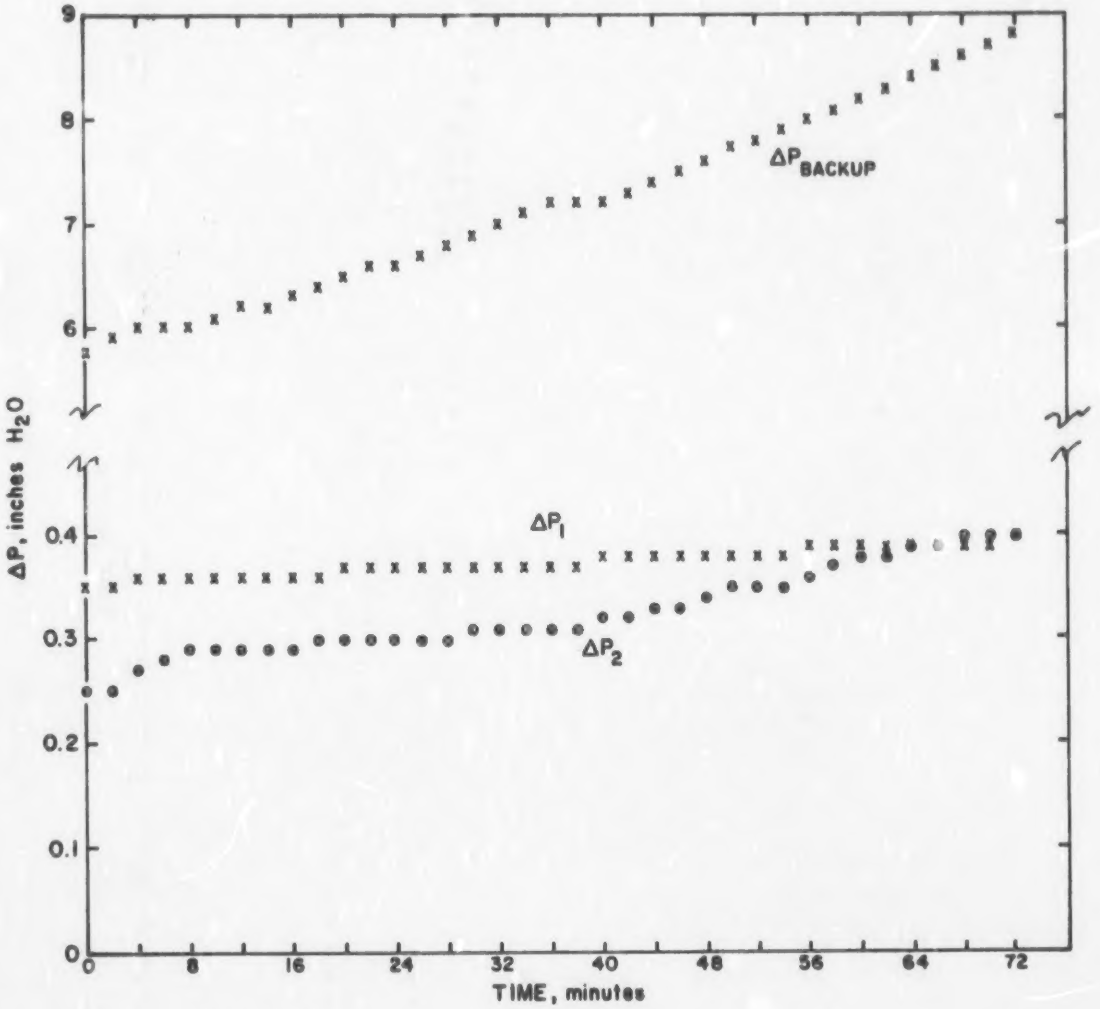

Figure 31. Test number 27, coal dust.

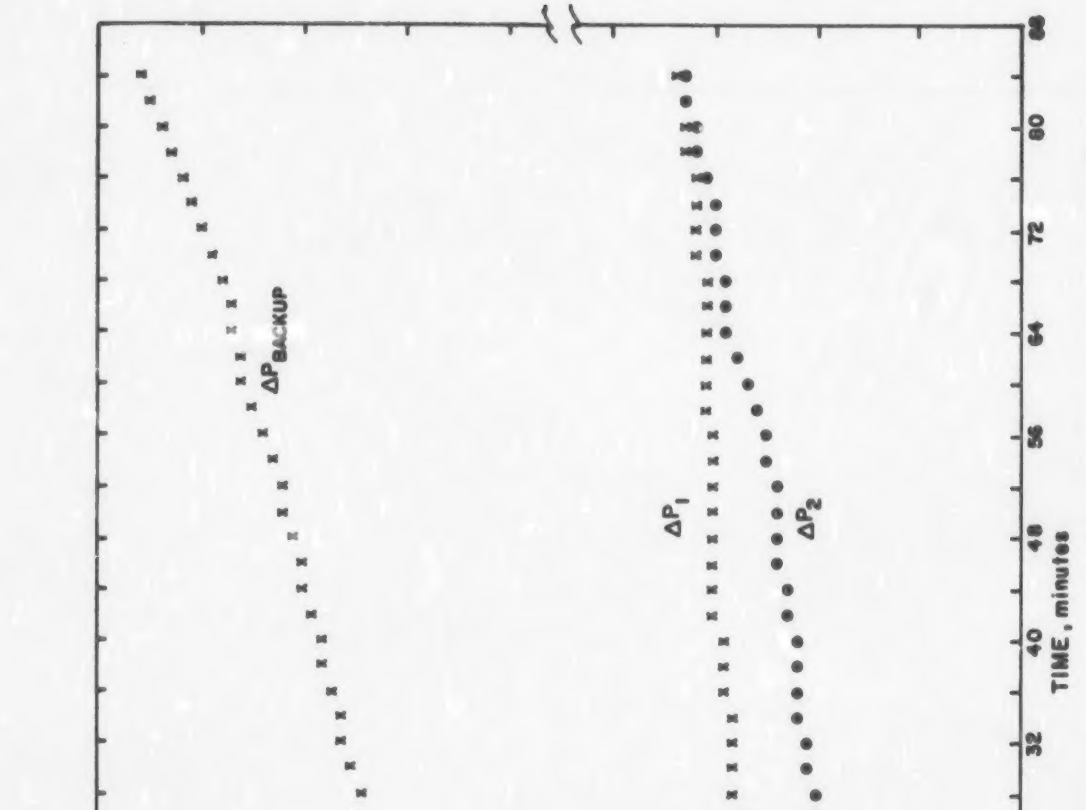

Figure 32. Test number 29, fly ash.

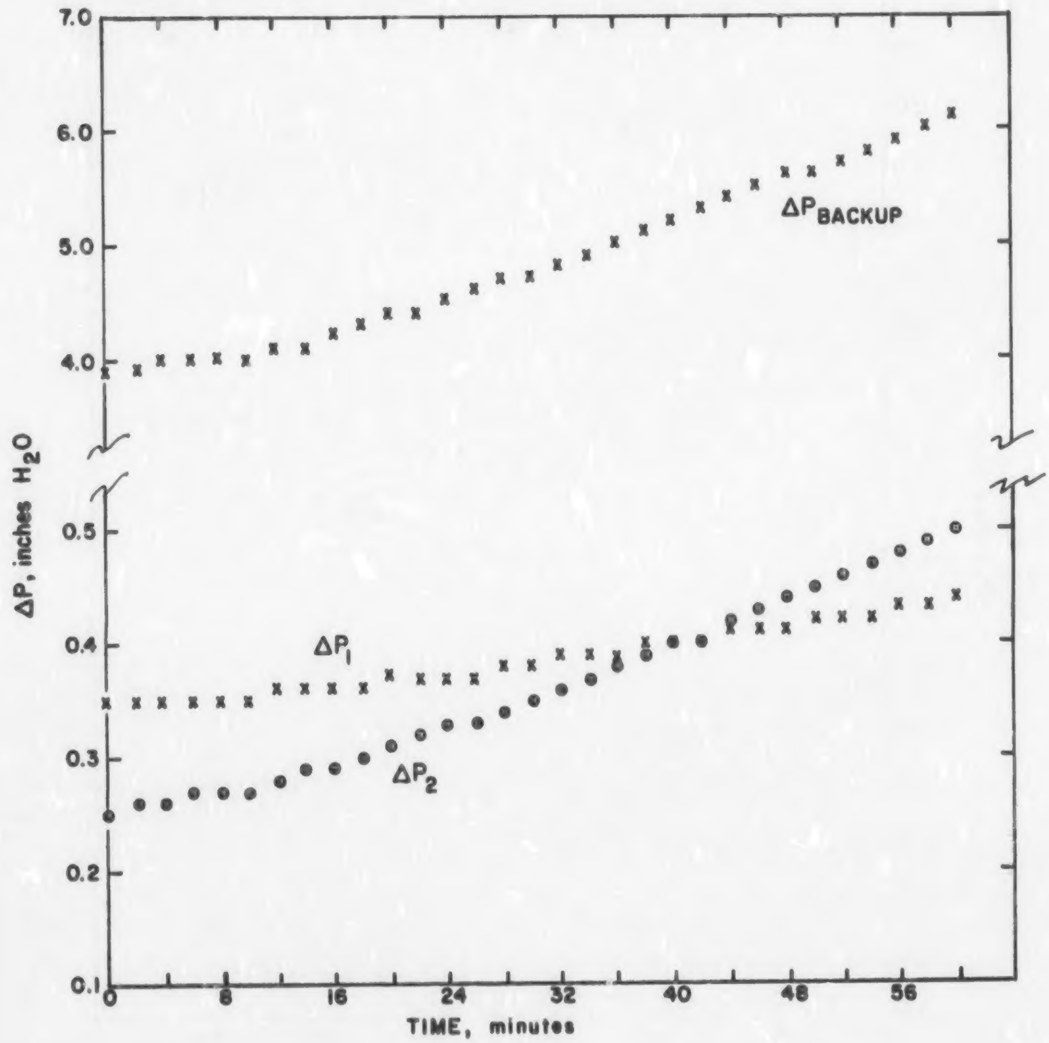

Figure 33. Test number 32, iron oxide.

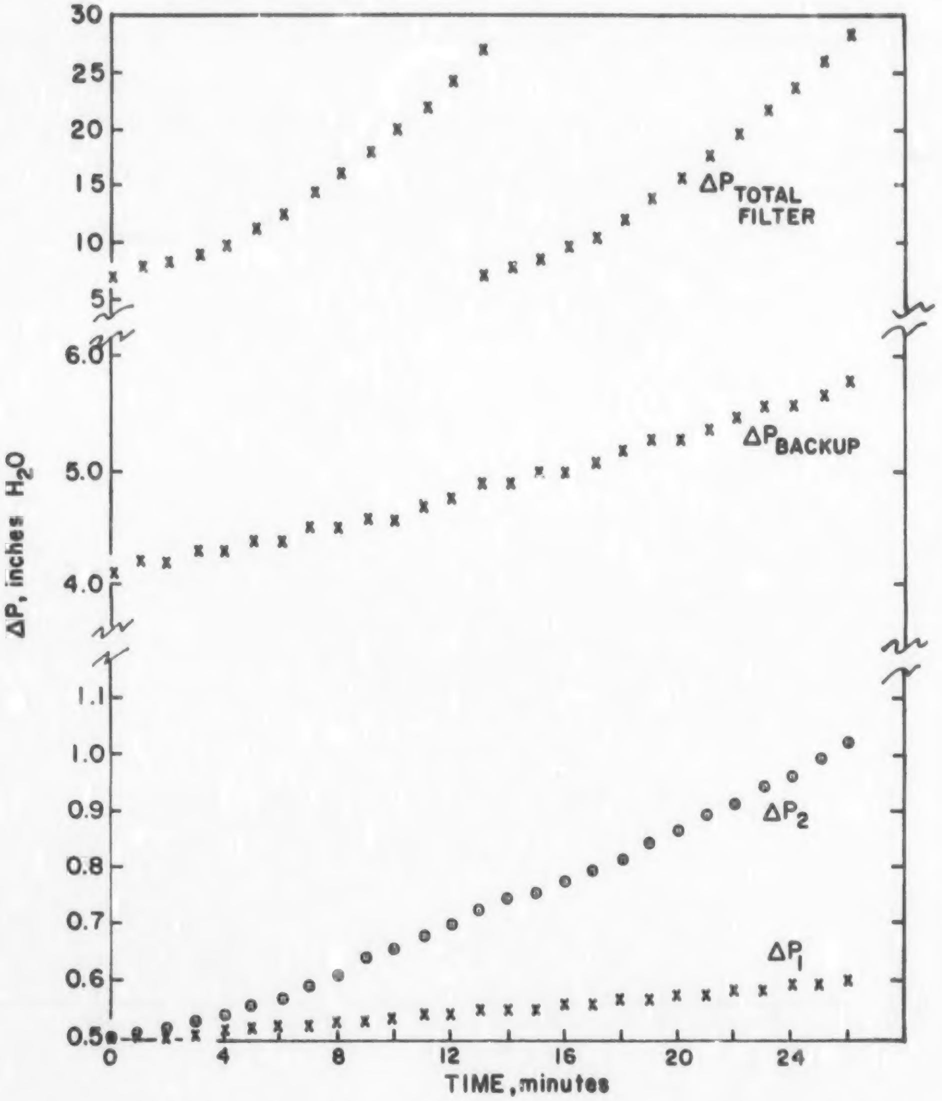

Figure 34. Test number 35, Arizona road dust.

backup filters display some slight upward concavity, probably due to the combined effects of higher face velocity and small particle size, as discussed in Section 5.

From the pressure drop information and the mass collected on the filters a drag coefficient, C_D, representative of the slope of a pressure drop versus cake weight curve (different from pressure drop versus time as presented in Figures 31 through 34), may be calculated as follows:

$$C_D = \frac{\frac{\Delta p}{v}}{\frac{\Delta wt}{A}} = \frac{\frac{\Delta p}{\frac{Q}{A}}}{\frac{\Delta wt}{A}} = \frac{\Delta p\ (A^2)}{Q\ (\Delta wt)}$$

where C_D = drag coefficient

Δp = final pressure drop across filter minus initial pressure drop across filter

v = filter face velocity

Δwt = weight of material collected by filter

A = filter area

Q = flowrate through filter = vA.

Examination of the drag coefficient data in Table 11 impactor loss data indicates that increased token flow reduces impactor losses judging from Test No. 35 and Test No. 36. Test No. 23 appears to be spurious and Test No. 26 was done at a much lower dust concentration than usual.

NEW BEDFORD FIELD TESTS

Virtual Impactor Stack Tests

Two trips were made to New England Power and Light which graciously allowed GCA to test their No. 3 oil-fired boiler downstream of an electrostatic precipitator, within a horizontal duct with an approximate square cross section of 2m × 2m. The stream temperature was 155°C (310°F).

Tests conducted on January 21, 1976 were of preliminary nature. Problems were encountered in control of gas flows due to vapor condensation and icing in the flow lines. Initial filter pressure drop data were worthless because of poor flow regulation. These shortcomings were corrected for the second visit by installing critical orifices for token flow control within the stack environment and by controlling main impactor flow using a calibrated orifice and dry gas meter downstream of a condenser and dessicant column. This same method was used for flow control of the Andersen In-Stack impactor, which was run in parallel with the virtual impactor in these tests.

Flowrate through the Andersen reference impactor was maintained near 14.15 ℓpm (1/2 cfm) at stack gas conditions. Manipulation of the impaction equation yields:

$$\frac{D_{p_1}}{D_{p_o}} = \left\{ \frac{\mu_1}{\mu_o} \frac{C_o}{C_1} \right\}^{1/2}$$

where the subscript 1 refers to stack conditions and the subscript o to ambient conditions. Application of this relationship to Andersen 2000, Inc. calibration data results in the 50 percent aerodynamic cut diameters of Table 12.

Flowrate entering the virtual impactor was maintained at 18.3 ℓpm, that flow being determined by the sum of the 14.15 ℓpm (1/2 cfm) through the backup filter and the 2.1 ℓpm token flow (see Appendix for token flow calculation) through each of the two stage filters.

However, for the conditions under which these tests were conducted the predicted aerodynamic size cut is altered less than 5 percent from the cut sizes of 7.0 μm for the first stage and 2.0 μm for the second stage, which had been tentatively assigned to the virtual impactor at a flowrate of 14.15 ℓpm (1/2 cfm) in the lab.

Virtual impactor data obtained during the New Bedford in-stack tests were corrected for token flow effect as discussed in a preceding section of this report. The Appendix, at the end of the report, is included to show how this correction procedure is implemented.

The test run on 29 January was a parallel test between the virutal impactor and the Andersen impactor. Results for these tests are presented in Tables 12 and 13. Salient features of the 29 January test are that total average concentration agreed well, 13.3 mg/m^3 for the Andersen impactor and 15.4 mg/m^3 for the virtual impactor, and that size distribution is almost identical for the two devices. Figure 35 shows the cumulative size distribution as measured by the two impactors.

Unfortunately, this test was marred by a failure in the pressure sensing line of the first stage of the virtual impactor, which necessitated its removal from the stack for repairs. The 4-inch port available for these tests just barely allowed the insertion of the virtual impactor prototype into the stack, and the attendant shaking and jarring of the impactor most likely shook loose some of the cake formed on the stage filters; thus pressure drop across the stages was not wholly regained after restarting. It is interesting to note that the pressure drop across the backup filter was regained, probably due to the much tighter cake formed by the fine particles at the much higher face velocity and the much higher pressure drop resulting therefrom.

TABLE 12. ANDERSEN IN-STACK IMPACTOR DATA OBTAINED DURING IN-STACK TESTS AT NEW BEDFORD

		January 29				January 30											
						Number 1				Number 2				Number 3			
Stage	Aero dia, μm	Δwt, mg	Conc., mg/m³	%	Cum. %	Δwt, mg	Conc., mg/m³	%	Cum. %	Δwt, mg	Conc., mg/m³	%	Cum. %	Δwt, mg	Conc., mg/m³	%	Cum. %
Probe		5.2	3.69	28		2.5	2.94	15		1.1	1.30	6		5.7	6.71	25	
1	>15.5	3.8	2.70	20	48	2.0	2.36	12	27	5.4	6.36	27	33	5.3	3.89	14	39
2	> 9.8	2.4	1.70	13	61	1.9	2.24	11	38	2.3	2.71	12	45	3.2	3.77	14	53
3	> 6.3	0.9	0.64	5	66	0.9	1.06	5	43	1.5	1.77	8	53	1.1	1.30	5	58
4	> 4.5	0.8	0.57	4	70	0.5	0.59	3	46	0.8	0.94	4	57	1.8	2.12	8	66
5	> 2.8	0.7	0.50	4	74	0.7	0.82	4	50	0.9	1.06	4	61	2.1	2.47	9	75
6	> 1.4	1.0	0.71	5	79	0.5	0.59	3	53	0.8	0.94	4	65	1.8	2.12	8	83
7	> 0.9	0.4	0.28	2	81	0.3	0.35	2	55	0.6	0.71	3	68	0.9	1.06	4	87
8	> 0.6	0	0	0	81	0.1	0.12	1	56	0.1	0.12	1	69	0.1	0.12	1	88
Backup	< 0.6	3.6	2.55	19	100	(7.6)[a]	(8.95)	(44)	100	6.1	7.18	31	100	2.7	3.18	12	100
Total		18.8	13.3			(17.0)	(20.0)			19.6	23.1			22.7	26.7		

[a] Filter weight gain considered unreliable; filter appeared stiff as though some condensation and subsequent evaporation took place, leaving some condensate.

TABLE 13. IN-STACK VIRTUAL IMPACTOR DATA TAKEN AT NEW BEDFORD (CORRECTED FOR TOKEN FLOW EFFECT) (SEE APPENDIX)

	Δwt, mg	Corrected Δwt, mg	Conc., mg/m^3	Percent	Cumulative %
January 29					
Probe	11.1	11.1	4.85	32	
Stage 1 (7.0 μm)	12.4	10.9	4.76	31	63
Stage 2 (2.0 μm)	3.5	2.6	1.14	7	70
Backup	8.1	10.5	4.59	30	
Total	35.1	35.1	15.3		
January 30					
Probe	20.2	20.2	6.0	22	
Stage 1 (7.0 μm)	37.6	33.4	9.91	37	59
Stage 2 (2.0 μm)	11.3	9.3	2.76	10	69
Backup	(21.0)[a]	27.2	8.07	30	
Total	(90.1)[a]	90.1	26.7		

[a] Calculated from pressure drop data as follows:

$$\Delta wt_F = \frac{\Delta p_F \left(\Delta wt_T\right)}{\Delta p_T}$$

where Δwt_F = weight gain, Friday, January 30

Δp_F = pressure gain, Friday, January 30 = 5.7 in. Hg

Δwt_T = weight gain, Thursday, January 29 = 8.1 mg

Δp_T = pressure gain, Thursday, January 29 = 2.2 in. Hg.

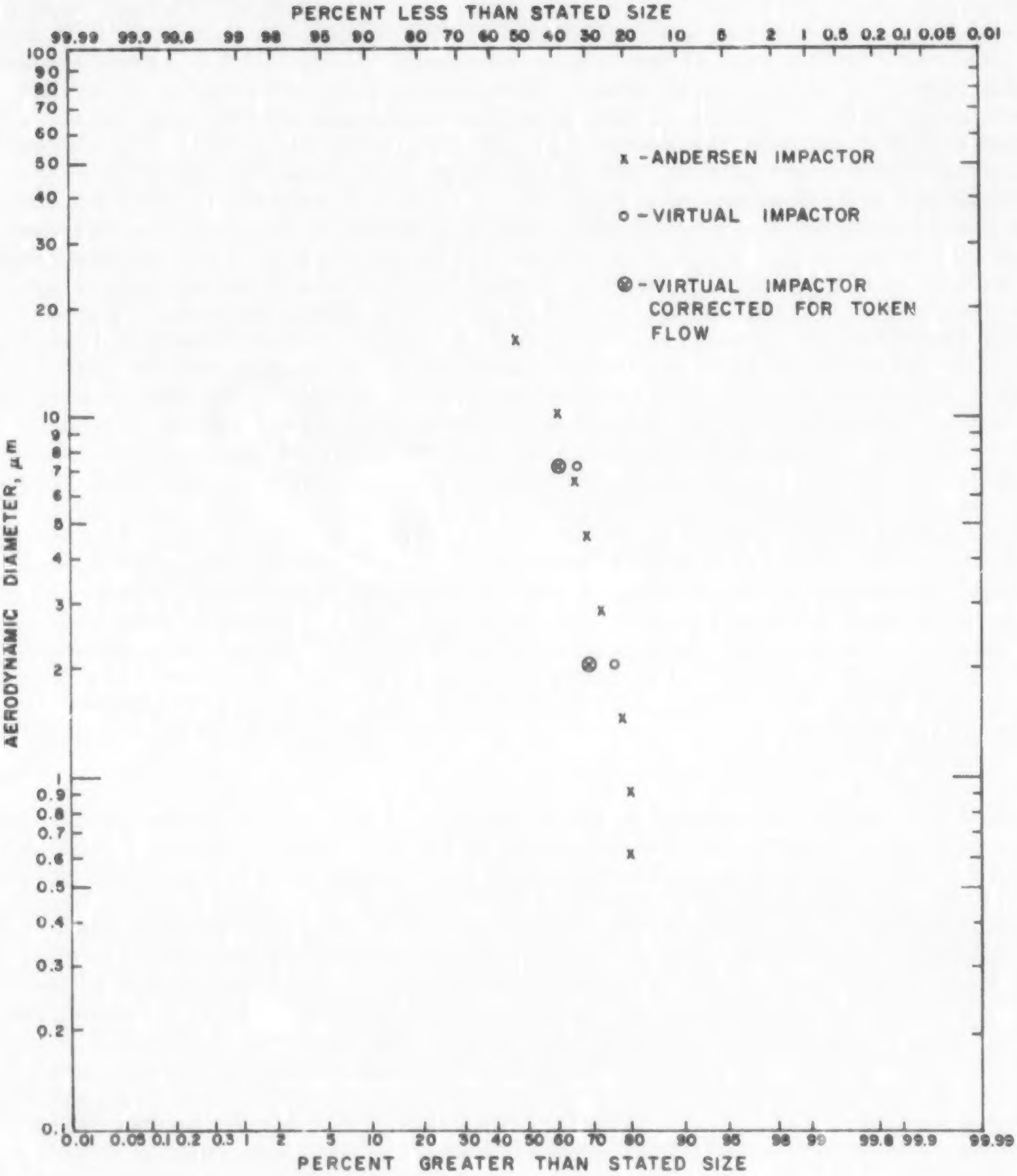

Figure 35. Cumulative size distribution for January 29, 1976.

The test run on 30 January was designed to demonstrate that the virtual impactor flow could be shut off, leaving the impactor in the stack (with the probe turned 180° to the duct velocity) and restarted some time later to regain the pressure drops recorded before shut-down. Figure 36 shows virtual impactor pressure drop data for the second 2 hours of the 30 January test. The 30 January test was divided into three 1-hour sections, during which a freshly loaded Andersen impactor was run each hour. Once again, pressure sensing lines had failed in the 4200 ft/min stack gas velocity, requiring removal and repair after the first hour. Between the second and third hours of this test, the virtual impactor prototype was left off for 45 minutes, and identical pressure drops were regained when flow was again started. Total concentration agreement between the virtual impactor (26.7 mg/m^3 for the 3-hour test), and the Andersen impactors (20.0, 23.1, and 26.7 mg/m^3 for each hour) was good. Size distribution information from the virtual impactor indicated 69 percent above 2.0 μm, and 59 percent above 7.0 μm, whereas the average of the three Andersen impactor samples indicated 66 percent was above 2.0 μm, and 49 percent above 7.0 μm, as shown in Figure 37. These results are based on an assumed value for the material collected by the virtual impactor backup filter, which was in poor condition from rust stains when the virtual impactor was disassembled in the lab after returning. Presumably, this filter was wetted by vapor that had condensed in the 3/4-inch iron pipe that carried the main virtual impactor flow and supported the whole assembly inside the stack. This could have happened if the impactor was held at a lower level than the connecting pipe upon extraction from the stack; a not unlikely event as movements of that day are mentally reconstructed. A similar type of event seems to have occurred to the backup filter of the first hour Andersen sample, but to a much lesser degree. That value, it will be noted, is enclosed in parenthesis in Table 12. It may also be noted that had the weight gain of that first hour Andersen backup filter been less, the cumulative size distribution curve for that run, in Figure 37, would have agreed better with the other Andersen samples and the virtual impactor data as well.

Table 14 compares virtual impactor pressure drop data with the weight gained in the same size fraction by the Andersen impactor. These data were obtained from the cumulative size distribution curves of Figure 37 and the total weight gain of the Andersen impactors reported in Table 12. For example, for the No. 2 Andersen sample of 30 January, the 7 μm line and the cumulative size distribution curve of that run intersect at 52 percent greater than stated size. It will be noted that 52 percent of 19.6 mg, the total weight gain of the Andersen impactor, is 10.2 mg as reported in Table 14. During that same time period the first stage filter pressure gain of the virtual impactor was 0.06 in. H_2O. Examination of Table 14 shows that pressure drop roughly followed weight gain as reported by the Andersen impactor samples. It will be noted that the only discrepant data point is reported for the case where the Andersen backup filter weight was questionable. It will also be seen from the data that if drag coefficients, representative of the slopes of the pressure drop versus cake weight gain curves, are computed, that the finer size fractions resulted in a greater pressure gain; a conclusion reported for tests with various laboratory generated aerosols.

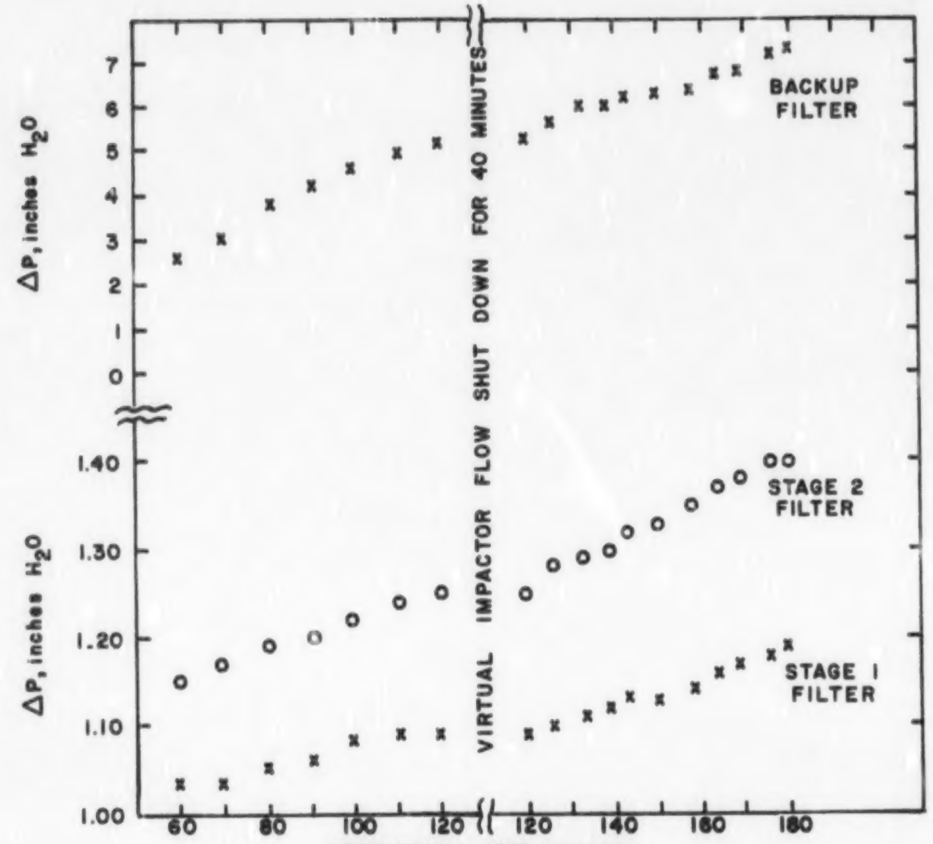

Figure 36. Virtual impactor pressure drop data for January 30, 1976.

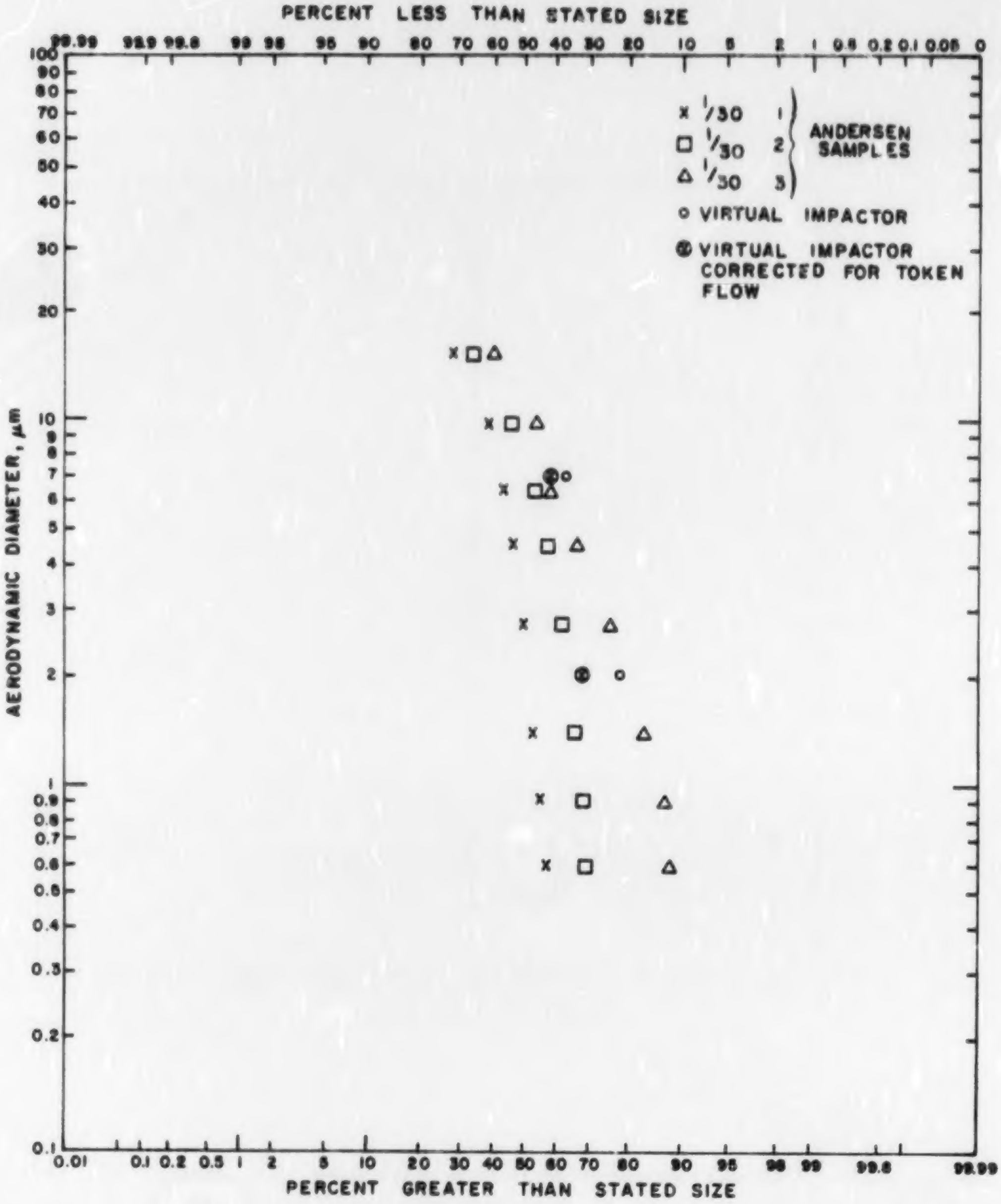

Figure 37. Cumulative size distribution data for January 30, 1976.

TABLE 14. VIRTUAL IMPACTOR FILTER PRESSURE GAIN COMPARED WITH LOADING AS REPORTED BY THE ANDERSEN IMPACTOR

Andersen test	> 7.0 µm			< 7.0 µm, > 2.0 µm			< 2.0 µm		
	Andersen, %	Δwt, mg	V.I. Δ p "H_2O	Andersen, %	Δwt, mg	V.I. Δ p "H_2O	Andersen, %	Δwt, mg	V.I. Δ p "H_2O
1/29	64	12.0	—	12	2.3	—	24	4.5	2.2
1/30, No. 1	40	6.8	—	11	1.9	—	49[a]	8.3[a]	1.0
1/30, No. 2	52	10.2	0.06	12	2.4	0.10	36	7.1	2.6
1/30, No. 3	58	13.2	0.10	22	5.0	0.12	20	4.5	2.0

[a] This Andersen Impactor test contains a backup filter weight gain considered unreliable.

TABLE 15. VIRTUAL IMPACTOR DATA FROM PRELIMINARY FIELD TEST

Collection stage	January 21, concentration, mg/m^3	
	No. 1	No. 2
Stage 1	7.9	5.6
Stage 2	1.6	2.5
Backup	5.6	5.4
Total	15.1	13.5

Table 15, which reports concentrations determined during the preliminary field trip, is included to show that the virtual impactor, even though operated with poor flow regulation, gave results consistent with the later measurement; i.e., that particles within this stack are mostly large and small with few in the 1 micrometer range. Concentrations determined during these earlier tests are seen to agree well with later data.

The main conclusions of the stack tests are here summarized:

1. The virtual impactor reports concentrations and size distribution in good agreement with Andersen impactor data.
2. The virtual impactor may be left with zero flow in the stack for some time after a collection period, and upon restarting the flow the pressure drops at each stage will return to the values recorded just before the flow was interrupted.
3. Stage filter pressure drops indicate well the size fractionated concentrations.

RESEARCH TRIANGLE PARK TESTS

Tests were conducted with the virtual impactor at two different EPA wind tunnels to demonstrate the viability of this instrument.

On 24 March 1976 a test was run at the Environmental Sciences Research Laboratory (ESRL) wind tunnel in the Beaunit building with the objective of seeing how large a load the virtual impactor could handle before the pressure drop output data became useless. An Andersen sampler was run for 20 minutes during the 2-hour run, data for which may be found in Table 16, which is labeled Andersen Run No. 1. Virtual impactor data is presented in Table 17. Pressure drop versus time data for the virtual impactor are shown in Figure 38. The curve for the first stage displays some upward concavity, the cause for which is debatable, although it must be admitted that upon disassembly of the virtual impactor a large amount of loose fly ash was contained on the first stage, some of which was spilled and some of which was weighed as probe catch. Change of weight for Stage 1 in Table 16 is unreliable. It will be noted that pressure drop versus time for Stage 2, as shown in Figure 38, is well-behaved.

Virtual impactor run No. 2, also performed in the ESRL wind tunnel, was a test to check the responsiveness of the instrument to a change of concentration. After 30 minutes of this 60-minute test had elapsed, the setting of the Acrison dust feeder rate control was reduced from 70 to 18. Andersen run No. 2 was a 5-minute sample during the first 30 minutes of this test and Andersen run No. 3 was a 20-minute sample taken during the last 30 minutes of this test. Pressure drop versus time are plotted in Figure 39 for this test, from which it is evident that the lower concentration for the second half of the test resulted in reduced slopes. Further, the magnitude of the pressure gain for the first stage, which was 0.33 in. H_2O for the high concentration segment and 0.09 in. H_2O for the low concentration segment indicates the high concentration was

TABLE 16. ANDERSEN IN-STACK DATA[a]

Stage	Aero. size cut, μm	Andersen run no. 1			Andersen run no. 2			Andersen run no. 3			Andersen run no. 4		
		Δwt	%	Cum. %	Δwt	%	Cum. %	Δwt	%	Cum. %	Δwt	%	Cum. %
Probe		48.1	15.9		11.4	22.6		14.7	36.3		36.5	68.4	
1	13.6	113.3	37.4	84.1	12.5	24.8	87.4	8.4	20.7	63.7	4.2	7.9	31.6
2	8.6	67.8	22.3	46.7	10.5	20.8	52.6	6.5	16.1	43.0	3.8	7.1	23.7
3	5.6	43.2	14.2	24.4	7.5	14.9	31.8	4.3	10.6	26.9	4.3	8.1	16.6
4	4.0	16.4	5.4	10.2	4.4	8.7	16.9	2.9	7.2	16.3	2.2	4.1	8.5
5	2.5	8.4	2.8	4.8	2.1	4.2	8.2	1.7	4.2	9.1	1.6	3.0	4.4
6	1.3	5.0	1.6	2.0	1.2	2.4	4.0	0.9	2.2	4.9	0.3	0.6	1.4
7	0.8	0.8	0.3	0.4	0.3	0.6	1.6	0.8	2.0	2.7	0.2	0.4	0.8
8	0.54	0.4	0.1	0.1	0.1	0.2	1.0	0	0	0.7	0.1	0.2	0.4
Final		0.1	0	0	0.4	0.8	0.8	0.3	0.7	0.7	0.1	0.2	0.2
Total		303.5	100		50.4	100		40.5	100		53.3	100	
Q = 14 ℓpm		Δt = 20 min			Δt = 5 min			Δt = 20 min			Δt = 2 min		
		Conc. = 1084 mg/m³			Conc. = 720 mg/m³			Conc. = 145 mg/m³			Conc. = 1904 mg/m³		
		= 0.47 gr/ft³			= 0.31 gr/ft³			= 0.063 gr/ft³			= 0.83 mg/m³		

---

[a] Nozzle = 1/4 in. for isokinetic sampling at 1800 fpm.

TABLE 17. VIRTUAL IMPACTOR DATA

		V.I. run no. 1	V.I. run no. 2	V.I. run no. 3	V.I. run no. 4
Probe, Δwt		819.9 mg	52.9	345.2	2,068.0
Stage 1	Δwt	313.8 mg[a]	406.2	81.1	3,215.5
	$\Delta\rho$	1.82 "H_2O	0.42	0.10	1.28[b]
Stage 2	Δwt	60.8 mg	15.6	4.0	153.0
	$\Delta\rho$	0.68 "H_2O	0.15	0.05	1.63
Backup, Δwt		4.0 mg	3.4	3.2	8.2
Total Δwt		1,198.5 mg	478.1	433.5	5,444.7
Δt		118 min	60	5	186
Concentration		584 mg/m^3	458	4,983	1,900.8

[a] Unreliable.

[b] $\Delta\rho$ for first 55 minutes of run, after which pressure drop became erratic due to overloading; see Figure 37.

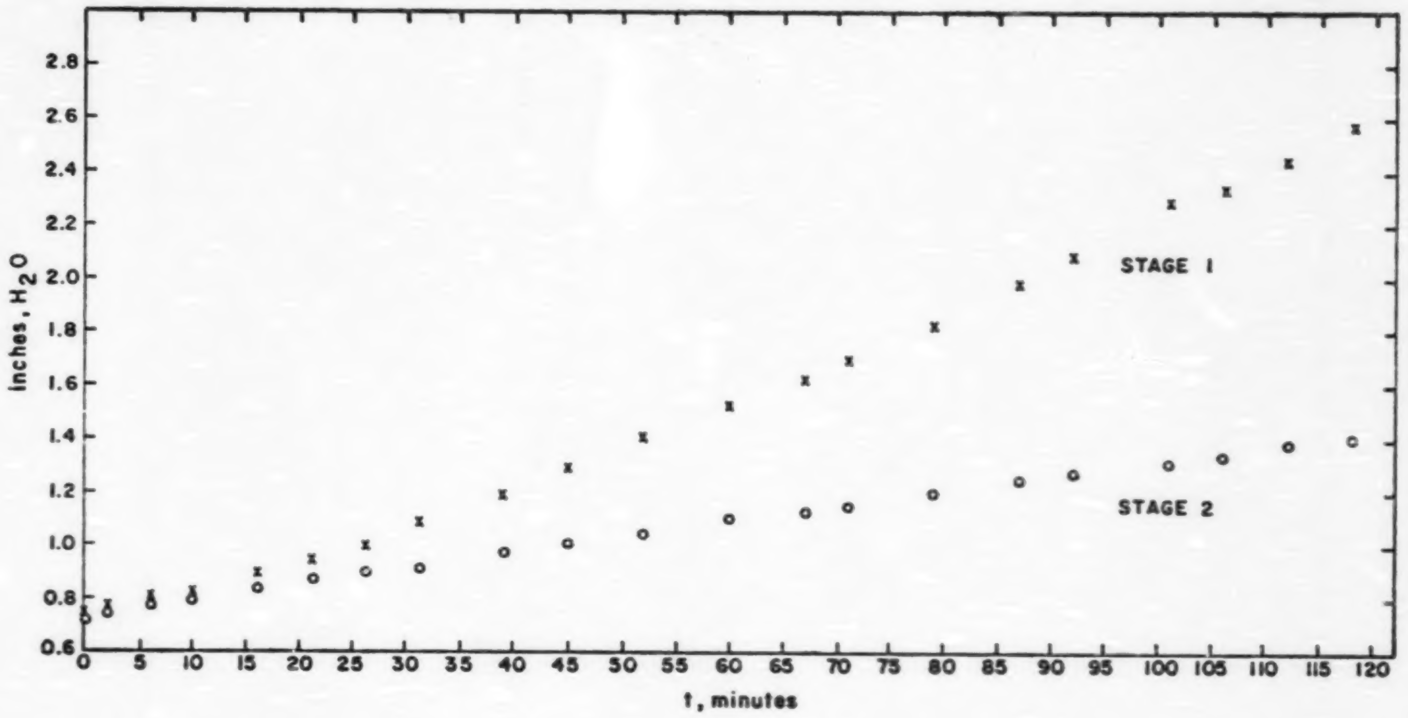

Figure 38. Pressure drop versus time for run no. 1, 24 March 1976.

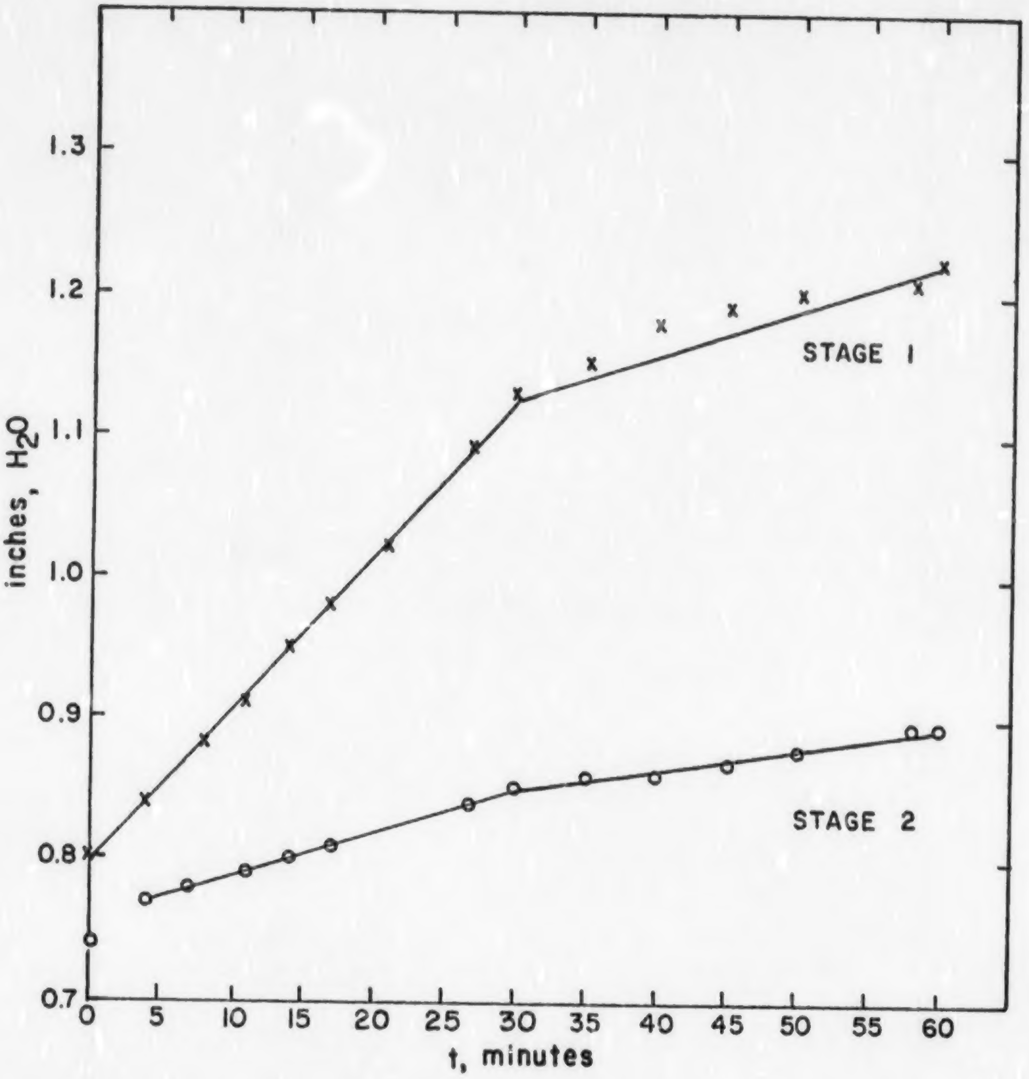

Figure 39. Pressure drop versus time for test in which concentration was varied.

0.33/0.09 = 3.67 times greater than the low concentration. Data from the Andersen samples indicate a ratio of 720/145 = 5. Average concentration from the two Andersen samples is 433 mg/m^3 whereas the virtual impactor reports 458 mg/m^3. The ratio of the Stage 1 gain to the Stage 2 gain is lower for the low concentration portion of the test indicating a shift in particle size distribution toward smaller particles for the lower concentration; a result consistent with that one expects from agglomeration at higher concentrations, and a result borne out to some degree by the Andersen data.

A switch was made to the Industrial Environmental Research Laboratory (IERL) wind tunnel and virtual impactor run No. 3 was taken simultaneously with a Brink sampler. The probe wash dominates this sample and results in total concentration twice as great as expected. The virtual impactor was in the stack for approximately 1-1/2 hours while the Brink was readied and the probe may have been contaminated somehow during this time.

The fourth Andersen run was taken at the IERL wind tunnel. It may be seen that total concentration agrees with virtual impactor concentration for virtual impactor run No. 4, which was a test to better define the ultimate overload point. Pressure drop versus time data are plotted in Figures 40 and 41. The pressure drop versus collected mass overload point was apparently never reached on Stage 1 even after 3 hours of operation at the end of which more than 3000 mg had been collected on that stage. Stage 2 pressure drop remained linear for the same period of time with a possible overload condition beyond 180 minutes at a collection of about 150 mg. The loadings on Stages 1 and 2 are indicative of the notable collection capabilities of this device, which exceed typical collection limits of commonly used in-stack jet-to-plate impactors by factors between 10 and 100. The pressure drop of both stages tracked concentration as measured by an Ikor monitor. Three different slopes may be seen in Figures 40 and 41, corresponding to three different concentration levels as measured by the Ikor.

The above discussed performance also demonstrates the relatively long unattended measurement duration capability of this collection system, which would be extended even more if a larger number of sizing stages is used.

Table 18 presents dust load drag coefficients derived from the virtual impactor data, for the two virtual impaction stages. It is apparent that the characteristic drag coefficient for these tests all fall within about ±20 percent for each of the two stages.

In addition to the significant performance characteristics demonstrated by the device investigated within this program, the cascade virtual impactor-pressure drop sensor was found to be intrinsically self calibrating because the collection on the individual stage filters can be assessed gravimetrically at the completion of a run. This method can be applied either routinely or as a means for sporadic spot checking the pressure drop-loading relationship at a particular source under surveillance.

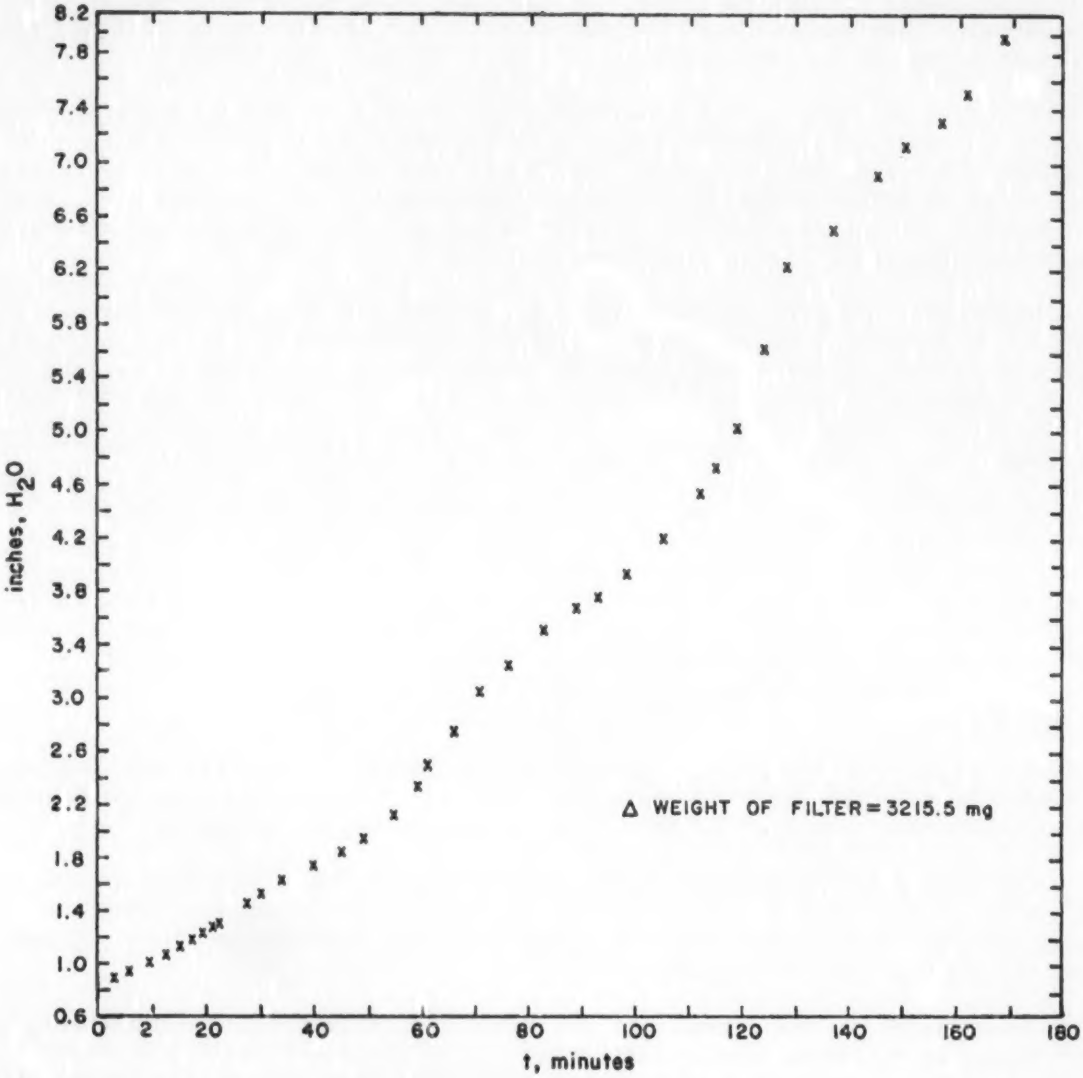

Figure 40. Pressure drop versus time for Stage 1, 26 March 1976.

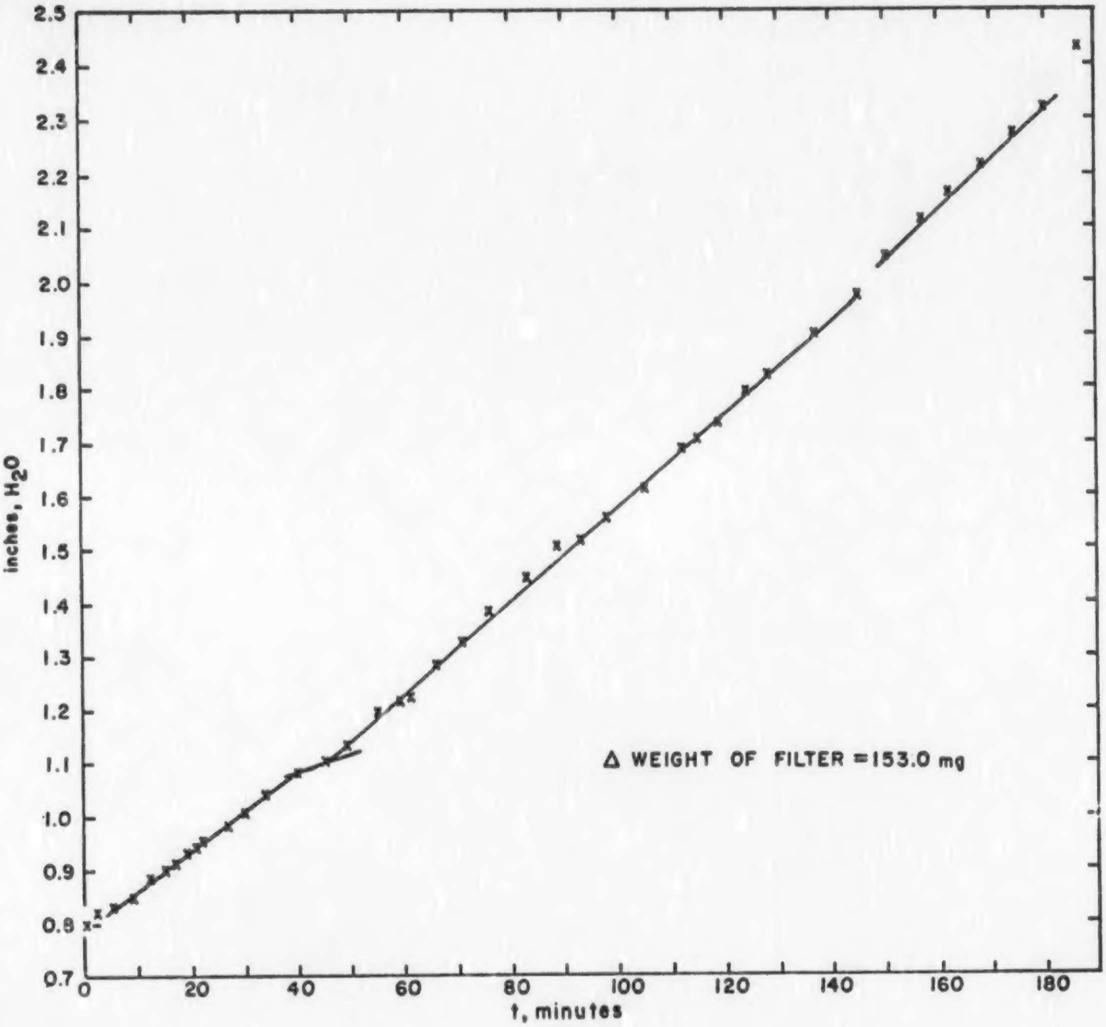

Figure 41. Pressure drop versus time for Stage 2, 26 March 1976.

TABLE 18. VIRTUAL IMPACTOR PRESSURE-DROP DRAG COEFFICIENTS[a]

	V.I. run no. 1	V.I. run no. 2	V.I. run no. 3	V.I. run no. 4
C_D, Stage 1	—	0.21×10^5 sec^{-1}	0.25×10^5	0.27×10^5 [b]
C_D, Stage 2	2.27×10^5 sec^{-1}	1.95×10^5	2.54×10^5	2.16×10^5

[a] $C_D = 1.49 \times 10^5 \dfrac{\Delta\rho(A)^2}{Q(\Delta wt)}$ sec^{-1}, when A is in cm^2,
Q is in ℓpm,
Δwt is in mg,
Δρ is in in. H_2O.

$$A = \frac{\pi(4.4)^2}{4} \text{ cm}^2.$$

Q = 1.7 ℓpm (token flow).

[b] Calculated by assuming Δwt for first 55 min = 3215.5 mg × $\frac{55}{186}$.

REFERENCES

1. Lippmann, M. and R. E. Albert. The Effect of Particle Size on the Regional Deposition of Inhaled Aeros-ls in the Human Respiratory Tract. Am Ind Hyg Assoc J. Vol. 30, p. 257, 1969.

2. Guide for Respirable Mass Sampling. Aerosol Technology Committee, American Industrial Hygiene Association. Am Ind Hyg Assoc J. Vol. 31, p. 133, 1970.

3. Lippmann, M. Respirable Dust Sampling. Am Ind Hyg Assoc J. Vol. 31, p. 138, 1970.

4. Lilienfeld, P. and D. W. Cooper. Literature Review and Selection of Design Principle for the Development of a Fine Particulate Source Testing Instrument. Prepared for U.S. Environmental Protection Agency, Contract No. 68-02-1314. GCA Technical Report Number 73-22-G. October 1973.

5. Bird, A. N., Jr., J. D. McCain, and D. B. Harris. Particulate Sizing Techniques for Control Device Evaluation. APCA Meeting. Paper Number 73-282. Chicago, Illinois. 1973.

6. Fuchs, N. A. The Mechanics of Aerosols. Pergamon Press, 1964.

7. Green, H. L. and W. R. Lane. Particulate Clouds: Dusts, Smokes, and Mists. Princeton, New Jersey, D. Van Nostrand Co., 1964.

8. Lundgren, D. A. An Aerosol Sampler for Determination of Particle Concentration as a Function of Size and Time. J Air Pollut Control Assoc. Vol. 17, p. 225, 1967.

9. Mitchell, R. I. and J. M. Pilcher. Measuring Aerosol Particle Sizes. Ind Eng Chem. Vol. 51, p. 1039, 1959.

10. Ranz, W. E. and J. B. Wong. Jet Impactors for Determining the Particle Size Distribution of Aerosols. Arch Ind Hyg Occup Med. Vol. 5, p. 464, 1952.

11. Marple, V. A. A Fundmaental Study of Inertial Impactors. Ph.D. Thesis, University of Minnesota, December 1970.

12. Pilat, M. J., et al. Source Test Cascade Impactor. Atmos Environ. Vol. 4, p. 617, 1970.

13. McGinn, J. H. and J. T. MacWaters. Ballistic Particle Separator. Rev Sci Instrum. Vol. 31, p. 513, 1960.

14. Hounam, R. F. and R. J. Sherwood. The Cascade Centripeter: A Device for Determining the Concentration and Size Distribution of Aerosols. Am Ind Hyg Assoc J. Vol. 26, p. 122, 1965.

15. Conner, W. D. An Inertial-Type Particle Separator for Collecting Large Samples. J Air Pollut Control Assoc. Vol. 16, p. 35, 1966.

16. Loo, W. B. Letter to the U.S. Environmental Protection Agency. January 10, 1974.

17. Dzubay, T. G., L. E. Hines, and R. R. Stevens. Particle Bounce Errors in Cascade Impactors. Atmos Environ. Vol. 10, p. 229-234, 1976.

18. Priening, O. The Cross Sensitivities of the Royco Aerosol Photometer PC-200. Staub. Vol. 28, p. 29, 1968.

19. Cooper, D. W. Variable Jet Impactor and Aerosol Size Distribution Analysis. Ph.D. Dissertation, Division of Engineering and Applied Physics, Harvard University, 1974.

20. Picknett, R. G. A New Method of Determining Aerosol Size Distributions From Multistage Sampler Data. J Aerosol Sci. Vol. 3, p. 185, 1972.

21. Twomey, S. The Determination of Aerosol Size Distributions From Diffusional Decay Measurements. J Franklin Inst. Vol. 275, p. 121, 1963.

22. Twomey, S. The Application of Numerical Filtering of the Solution of Integral Equation Encountered in Indirect Sensing Methods. J Franklin Inst. Vol. 279, p. 95, 1965.

23. Phillips, D. L. A Technique for the Solution of Certain Integral Equations of the First Kind. J Assoc Comput Mach. Vol. 9, p. 84, 1962.

24. Rust, B. W. and W. R. Burrus. Mathematical Programming and Numerical Solution of Linear Equations. New York, American Edison Company, 1972.

25. Dorsey, J. A. and J. O. Burckle. Particulate Emissions and Process Monitors, Monitors. Chem Eng Prog. Vol. 67, p. 92-96, 1971.

26. Hyland, R. G. The Ikor Continuous Particle Monitor. APCA Conference. Paper Number 72-38. 1972.

27. Prochazka, R. Recording Dust Measurement With the Konitest. Staub. Vol. 26, No. 5, p. 22, 1966.

28. Jones, L., C. Lochboehler, and W. Magee, Jr. Aerosol Filtration by Fibrous Filter Mats. Environ Sci Technol. Vol. 6, p. 821-826, 1972.

29. Stafford, R. G. and H. J. Ettinger. Filter Efficiency as a Function of Particle Size and Velocity. Atmos Environ. Vol. 6, p. 353-362, 1972.

30. Thomas, J. and R. Yoder. Arch Ind Health. 13, 545, 1956.

31. Clarenburg, L. A. A Probabalistic Theory of Aerosol Penetration Through Glass Fiber Filters. Aerosol Science. Vol. 3, p. 461-490, 1972.

32. Anderson, D. P. Unpublished work at NIOSH, Cincinnati. 1971.

33. Miyamoto, S. and H. Bohn. Filtration of Airborne Particulates by Gravel Filters: II. J Air Pollut Control Assoc. Vol. 25, No. 1, 1975.

34. Billings, C. Effects of Particle Accumulation on Aerosol Filter Life. Proc., 9th AEC Air Cleaning Conference. 1966.

35. Happel, J. and H. Brenner. Low Reynolds Number Hydrodynamics. Prentice-Hall, 1965. Chapter 8.

36. Spurny, K. R., et al. Aerosol Filtration by Means of Nucleopore Filters, Filter Pore Clogging. Environ Sci Technol. Vol. 8, No. 8, 1974.

37. Langmead, W. A. and D. T. O'Connor. The Personal Centripeter—A Particle Size-Selective Personal Air Sampler. Ann Occup Hyg. Vol. 12, p. 185-195, 1969.

APPENDIX

TOKEN FLOW CORRECTIONS TO VIRTUAL IMPACTOR DATA COLLECTED IN NEW BEDFORD

Restating the matrix equation as presented in Section 5 of this report which gives E_{ij} values for the coefficients of the linear equations describing aerosol collection for a three stage virtual impactor when token flow is assumed a constant fraction of main flow:

$$\underset{\sim}{E} = \begin{bmatrix} 1 & e & e \\ 0 & 1(1-e) & e(1-e) \\ 0 & 0 & 1(1-e(1-e)-e) \end{bmatrix} \tag{1}$$

which is a close approximation to the actual operating conditions which are described by

$$\underset{\sim}{E} = \begin{bmatrix} 1 & e & e \\ 0 & 1(1-e) & f(1-e) \\ 0 & 0 & 1(1-f(1-e)-e) \end{bmatrix} \tag{2}$$

where token flow is not a constant fraction of main flow.

For the tests run at New Bedford, total flow entering the virtual impactor is equal to 14.15 ℓpm (1/2 cfm) through the backup filter plus 2.08 ℓpm for the second stage token flow plus 2.08 ℓpm for the first stage token flow equals 18.31 ℓpm. Therefore, $e = \frac{2.08}{18.31}$ and $f = \frac{2.08}{18.31-2.08} = \frac{2.08}{16.23}$. Computing values for E_{ij} gives

$$\underset{\sim}{E} = \begin{bmatrix} 1 & 0.1137 & 0.1137 \\ 0 & 0.8863 & 0.1138 \\ 0 & 0 & 0.7725 \end{bmatrix} \tag{3}$$

Choosing the exact approach and applying the method outlined in Section 5 of the report:

$$F_3 = F_3^*/E_{33}$$

$$F_2 = (F_2^* - E_{23}\ F_3)/E_{22}$$

$$F_1 = (F_1^* - E_{12}\ F_2 - F_{13}\ F_3)/E_{11} \qquad (4)$$

where $F_1^* = 12.4$ mg
$F_2^* = 3.5$ mg
$F_3^* = 8.1$ mg

from the data of January 29 in Table 13,

and $E_{11} = 1$
$E_{12} = 0.1137$
$E_{13} = 0.1137$
$E_{22} = 0.8863$
$E_{23} = 0.1138$
$E_{33} = 0.7725$

from matrix (3) above, one obtains the corrected change in weights shown in Table 13.

Alternatively, the inverse matrix, in the report,

$$\vec{F} = \underset{\sim}{E}^{-1}\ \vec{F}^* \qquad (5)$$

may be applied as follows by expanding to

$$\begin{bmatrix} F_1 \\ F_2 \\ F_3 \end{bmatrix} = \begin{bmatrix} E_{11}^{-1} & (-E_{12}/E_{11}E_{22}) & (E_{12}E_{23}E_{22}^{-1} - E_{13})/E_{11}E_{33} \\ 0 & E_{22}^{-1} & -E_{23}/E_{22}E_{33} \\ 0 & 0 & E_{33}^{-1} \end{bmatrix} \begin{bmatrix} F_1^* \\ F_2^* \\ F_3^* \end{bmatrix} \qquad (6)$$

and evaluating by vector multiplication one obtains:

$$F_1 = \frac{F_1^*}{E_{11}} - \frac{F_2^*E_{12}}{E_{11}E_{22}} + F_3^* \; \frac{\left(\frac{E_{12}E_{23}}{E_{22}} - E_{12}\right)}{E_{11}E_{33}} \qquad (7)$$

$$F_2 = 0\ F_1^* + F_2^*E_{22}^{-1} - \frac{F_3^*E_{23}}{E_{22}E_{23}}$$

$$F_3 = 0\ F_1^* + 0\ F_2^* + \frac{F_3^*}{E_{33}}$$

which gives the same result as above.